Analysis Documentation

- Modular coil asm design basis is defined by 5 analysis reports:

  HM Fan, Nonlinear Analysis of Coil and Shell Structure,
  NCSX-CALC-14-001, APPROVED

  HM Fan, Analysis of Integrated Structure,
  NCSX-CALC-14-003, APPROVED

  K Freudenberg, Modular Coil Thermal Analysis,
  NCSX-CALC-14-002, DRAFT

  K Freudenberg, Nonlinear Modular Coil Analysis,
  NCSX-CALC-14-004, DRAFT

  D Williamson, Modular Coil Failure Modes Analysis,
  NCSX-FMEA-14-002, DRAFT

- Additional analysis reports are planned before Design Closeout:

  K Freudenberg, Outboard Bolted Joint Analysis,
  IN PROGRESS

  K Freudenberg, Inboard Welded Shim Analysis,
  IN PROGRESS

  D Williamson, Modular Coil Leads Structural Analysis,
  PLANNED

NCSX
Design Basis Analysis

Nonlinear Analysis of Modular Coil and Shell Structure

NCSX-CALC-14-001-001

February 3, 2006

Prepared by:

_____
Horng-Ming Fan, PPPL

I have reviewed this calculation and, to my professional satisfaction, it is properly performed and correct. I concur with analysis methodology and inputs and with the reasonableness of the results and their interpretation.

Reviewed by:

_____
D. Williamson, ORNL Engineer

Nonlinear Analysis of the NCSX Modular Coil and Shell Structure

1.0 Executive Summary

This report documents the FEA nonlinear analysis approach and its results for the electromagnetic (EM) load due to maximum coil currents and the cooled modular coils. The purpose of the analysis is to evaluate the nonlinear effects on structural responses caused by the surface sliding and separation between a) the modular coil (MC) and the modular coil winding form (MCWF), and b) the MC and clamp assembly. All other contact surfaces are assumed to be bonded. For the vacuum-pressure impregnation (VPI) coils, the relative cooling shrinkage of coil strain has been assumed to be 0.0004 m/m from room temperature to the operating temperature of 85K.

The analysis was updated from the previous linear analysis that considered the coils were bonded to the winding form. This nonlinear analysis reflects a more realistic situation by allowing the contact behavior to deviate from the bonding state. Frictionless unilateral contact elements were used on the contact surfaces. The wing bags were added to support wings on the adjacent shells and a simplified clamp system was added with preloads to simulate the clamp assembly.

The FEA model consists of the modular coils, simplified clamp assembly, and the coil supporting structure, which is an enclosed shell structure including tee-shape coil winding form with wing bags and insulations at the poloidal breaks and the toroidal connection flanges. By taking the advantages of cyclic symmetry in the geometry and loading, the model can be reduced to one field period, a 120-degree sector, to minimize the size of the analytic model and the computer running time.

The peak currents in the MC was selected as the worse case of EM loads from the modular coil current scenarios as shown in Section A.3.2 of Reference [1]. Analytic results are illustrated through a series of graphical plots and tables with some result interpretations. The analyses provide the following results:

- For 2T high beta scenario, the maximum flux density is 4.901 Tesla on the coil type B.
- The net centering EM force Fr in one field period (containing six coils) is 5 MN
- Inside the field period, the same type of coils produce equal force magnitude for the vertical and toroidal EM forces but opposite in the direction in a cylindrical coordinate system
- The maximum axial tensile stress is 253 MPa (22.6-ksi) in the smeared modular coil with a smeared coil modulus of 63GPa. This local stress is conservative because of the large mesh size in a small curvature zone with highly intensive current flow in the local area of the cross-section.
- The coil has a maximum displacement of 2.707 mm.
- The shell structure is made of stainless steel casting. The allowable stress is much large than the maximum stress in the shell. The maximum deflection in the shell is 2.336 mm in the tee of shell type B
- The contact pressures on the wing bags are not uniform. The maximum contact pressure is 136 MPa that could be improved if shape is changed to provide more uniform compression.
- The toroidal connected flange joints are in compression at the inboard regions and change to tension at the outboard regions.
- The shell structure has no bolt connection at the inboard toroidal flange insulation. The force sums (see Tables 4.2.6-1 and 4.2.6-2) show that the shear-compression ratios vary

from 0.123 to 1.003, greater than the hypothetical coefficient of friction of 0.3. If no additional resisting features were provided, the extra shear forces will be transmitted to the first bolt in the inboard regions.

- Distributions of the contact pressure on the poloidal break spacers are more even and in tension. The bolt preload will be designed in opposition to the tensile stresses and shear stresses.
- Stress in the clamp is sensitive to the lateral movement of the modular coil. The deformation tolerance in the clamp assembly including the spring washers shall be checked to accommodate the coil movement.
- Choosing the supports in the mid-span of the shell type C will induce vertical tension in the base support structure. The horizontal reactions are not small. The elimination of the toroidal restraints at the inboard supports will greatly reduce the F_θ at the support reactions.

The results indicate that the weakest link in the structural system for this load case is the toroidal flange joint. Since the EM load is dynamic in nature, the sliding on the joint is not recommended.

2.0 Assumptions

The following assumptions were applied in the analysis:

The contact regions in the shells at poloidal breaks, toroidal connection flanges, and wing bags are bonded, using the surface-to-surface contact elements. The contact surfaces between the winding packs and the MCWF are standard frictionless unilateral contact, also using the surface-to-surface contact elements. Belleville washers in the clamp assembly were simulated using side pads and top pads that were bonded to the clamps, which are then firmly mounted on the tips of tees. The contact behavior between the surfaces of modular coils and the imitating side pads and top pads are frictionless unilateral contact. For surfaces using the bonded option, no sliding or separation between faces or edges will be occurred. It is the frictionless unilateral contact that causes the nonlinear structural response.

The MC material propertied are based on the smeared properties. As the MC conductor test programs have not yet established many of the required data to form a orthotropic property, the model uses isotropic material properties for the winding packs. In reality, the coils should be modeled by the orthotropic property. As the coils are continuous in the axial direction, the isotropic material properties are more suitable to be represented by the test data in the longitudinal direction.

No bolts are simulated in the model and no bolt preloads are applied in the analysis. The normal forces and shear forces across the bolt joints shall be calculated after the analysis for establishing the bolt preloads that will make sure that the bolt joints will not be opened up or sliding.

3.0 Analysis Methodology and Inputs

Methodology

The analysis of the NCSX modular coil system involves coupled-field analysis that uses the same mesh pattern for two fields of applications. This analytic approach can avoid the errors of mapping applied loads from one model to another model. Because of several types of loads are involves, it is more flexible to divide the analysis into two steps. The procedure will first solve the

electromagnetic (EM) analysis and review the results. Then applying the EM loads obtained from the first analysis to the structural analysis for evaluating the stresses and displacements.
Because of cyclic symmetry in the geometry and the loading, the model is formed in a 120-degree sector to minimize the model size and the computer running time. Figure 3.0-1 and 3.0-2 show the models elected for the EM analysis and the structural analysis, respectively. EM model consists of MC, simplified plasma, PF coils, and TF coils while Structural model consists of MC, MCWF, and the coil clamp features. The geometric nonlinearity of the contact behavior, primary caused by the cooled modular coils, was solved using the ANSYS nonlinear method.

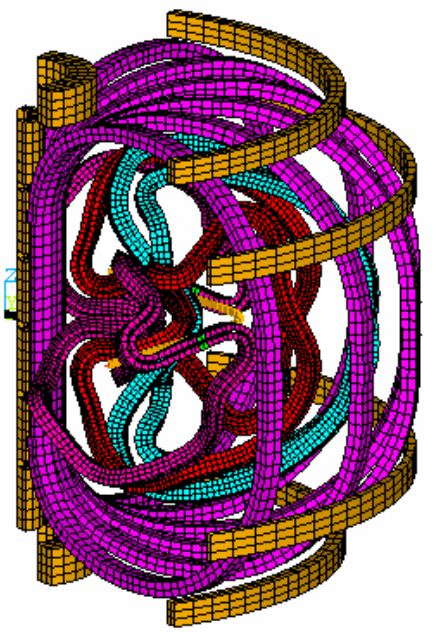

Fig. 3.0-1: EM model consists of MC, simplified plasma, PF coils, and TF coils

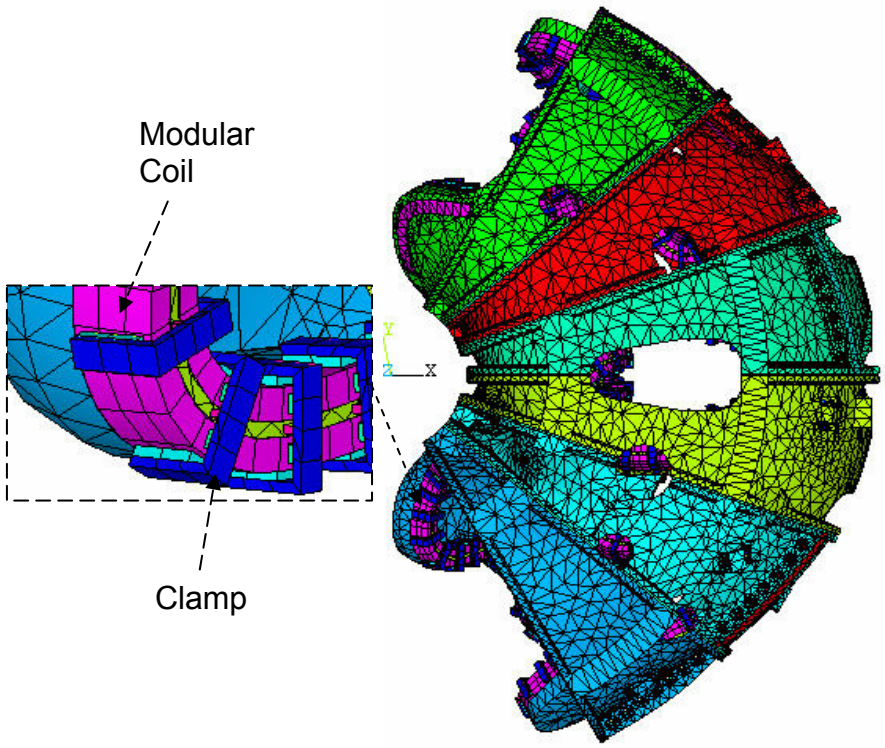

Fig. 3.0-2: Structural model

Inputs of Models

The geometric files of the shell assembly, modular coils, and clamp features were developed by ORNL in the CAD system of Pro/E Wildfire. Some features, such as bolts, bolt holes, chamfers, and fillers in the geometry were removed prior to the meshing for managing the mesh pattern and the model size.

In the EM model, the PF coils, TF coils, and the modular coils are formed by ANSYS 8-node solid element SOLID5. The brick-type PF and TF elements were generated directly from the geometry in the drawings. The MC winding pack was also meshed with SOLID5 element. The plasma current was simplified by SOURE36 current elements located at the center line of the plasma current.

After the EM analysis, the SOLID5 elements for the winding packs were changed to structural 3-D SOLID45 elements, which have the identical nodal points and elements. The finite element model of the shell structure with wind bags and poloidal breaks file was made in the ANSYS Workbench Environment (AWE) by the higher-order tetrahedron elements or if possible, the higher-order brick elements. Bonded option was applied to the contact regions. The half-thickness toroidal flange shims were combined into one thickness in the ANSYS and meshed with higher-order brick elements. The assembly of clamp components, which includes clamp, side pad, and top pad, were formed by the SOLID45 elements. The number of nodes and elements of the model was examined in order to form a final model that can fit into the working memory of the available PC computer. All contact regions used the surface-to-surface contact elements.

The model needs appropriate boundary conditions and support constraints to simulate the structure in a stable and cyclically symmetric condition. This requires cyclic couplings on the boundary nodes and displacement restraints at the base support. To be able to achieve the cyclically coupling condition, the mesh patterns on both end surfaces shall be identical and all nodes on the surfaces shall be rotated into the same global cylindrical coordinate system. At the boundary nodes on θ=+60° and the θ=-60°, couple degrees of freedom were defined for all degrees of freedom as shown in Figure 3.0-3.

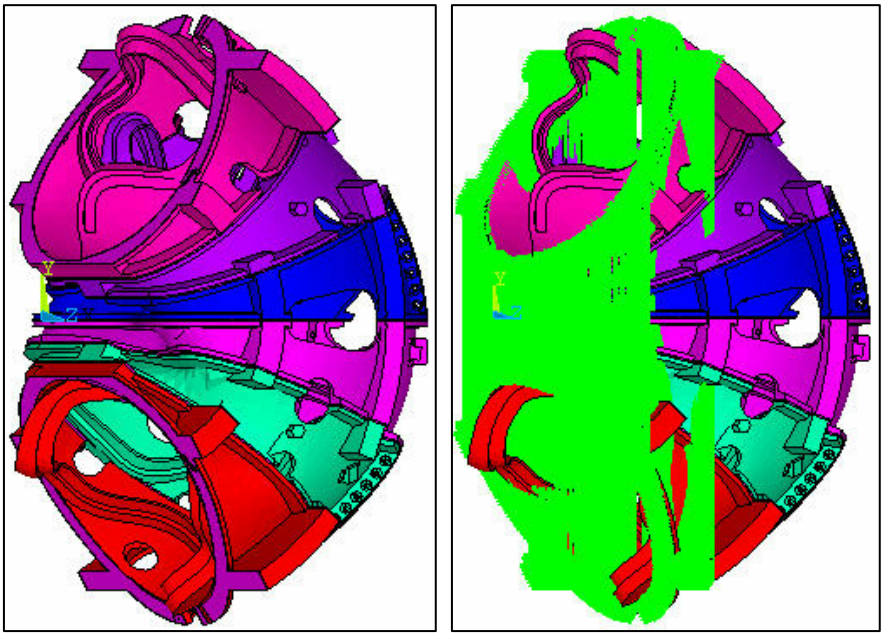

Fig. 3.0-3: Cyclic Symmetry Between θ=-60° and θ=+60°

The cyclically symmetric conditions are also required for the wind bags located outside the end boundaries as they shall be supported on the adjacent shell. To satisfy the requirement, two wing bags outside the field period were given 120º-rotation images at the opposite site of the shell. The wing bag image was then bonded to the shell and coupling to its original as shown in Figure 3.0-4.

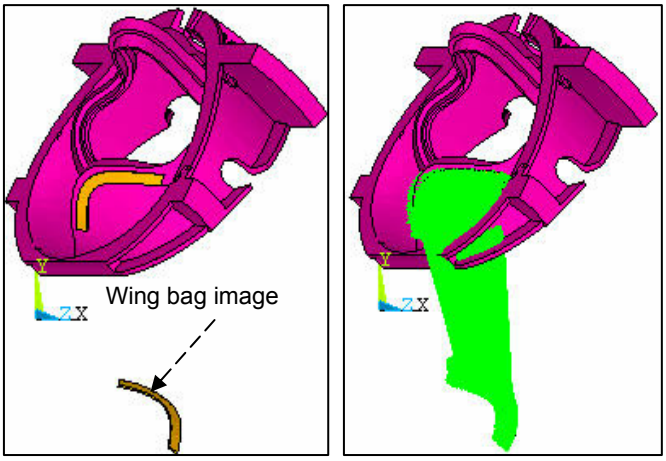

Fig. 3.0-4: Constraint equations for wings outside of the boundary and its image.

As the design of base support structure is not completed yet, assumption was made that the shell structure will be supported at the middle of the bottom stiffeners of shell Type C. The nodes in a four degree zone at the inboard and outboard stiffeners were selected and the displacement constraints were applied to the vertical and toroidal directions. No displacement constraints were placed in the radial direction for minimizing the thermal restraints. All the measuring units are in international MKS system.

Applied Coil Currents for EM Analysis

Reference [1] lists all coil current waveforms and the coil temperature histories at several time steps for all the current operating scenarios. The listed current value indicates the current in each turn, not the current in each conductor. The total modular coil currents will be the currents in Reference [1] multiplied by the number of conductor turns. Table 3.0-1 lists the number of coil turns and turn currents for the 2T high beta scenario that was selected in the analysis. The total currents in the modular coil and the TF coil are equal to the latest revision of the current waveforms (Ref. [2]) but are slight different in the PF coils.

Table 3.0-1: Turn number of each coil set

Coil	M1	M2	M3	PF1	PF2	PF3	PF4	PF5	PF6	TF	Plasma
Turn No.	20	20	18	72	72	72	80	24	14	12	1
Turn Current	40908	41561	40598	-15274	-15274	-5857	-9362	1080	-24	-1030	0

For the current convention system, NCSX utilizes the cylindrical coordinate system with the Z-axis as vertical. A positive PF or plasma current is in the direction, which is counter-clockwise viewed from above. A positive poloidal current, such as TF or modular coil current, flows in the positive Z-direction in the inner leg.

Applied Loads for Structural Analysis

The applied loads are limited to the modular coil EM load, cooling strain, as well as the preloads from clamps. The cooling strain is due to temperature changes during the coil VPI process and the initial cooling to the operating temperature of 85K. R & D test has indicated that the winding pack cure shrinkage is very small and negligible. The other test result shows that the CTE of the winging pack is slightly higher than the winding form and when the modular coil is cooled to 85K, the relative thermal strain between the modular coil and the winding form is about -0.04%. As the coil contracts more than the winding form, gaps may occur in some parts of coils. The gravity loads were not included in the analysis.

In order to achieve a uniform shrinkage during the initial cooling stage that produces no restraints at the supports, it requires that the elevations of structural supports within the cryogenic boundary shall be placed on the same elevations and the supports shall be free to move in the radial direction. This model is constrained at the inboard and outboard bottom flange surfaces, whose elevations are at slightly different. A uniform temperature change in the shell will produce additional stresses from the support constraints of different elevations, which in fact do not exist. To simulate a load case of uniform temperature change in the model, the equivalent temperature drop of 23.26K that is equivalent to coil strain of 0.04%, should be applied to the WP only while keeping the temperature on MCWF unchanged.

The pressure developed from the thermal expansion of the side pad and top pad was used for the imitation of the Belleville washer preloads. The initial preloads produced for the side pads and the top pads are 556N (125 lbs) and 92.6N (20.8 lbs), respectively.

Material Properties

The modular coil consisted of copper strands impregnated with resin to form a rectangular section. R & D test results [3] illustrate the flexural modulus of elasticity of the winding pact at 77K varies from 11.08Msi (76.4GPa) for bare Cu specimens to 7.37Msi (50.8GPa) for glass wrapped specimens. The longitudinal compressive test at room temperature [4] shows the modulus of elasticity at an average value of 9.11Msi (62.8GPa). The modulus of elasticity in the transverse direction is lower at 5.4Msi (37.0GPa) [5]. As the test program has not yet established all of the required data for forming an orthotropic property, the analysis employed the smeared isotropic material property for the WP. The flange shim insulations placed between toroidal flange joints are formed with a 3/8-in SS covered by 2 layers of 1/16-in G11. The equivalent isotropic properties were calculated for their material properties. To preserve the accuracy of the model rigidity, the modulus of elasticity for the additional wing bag image was set to 5% of the wing bag. Table 3.0-2 summarizes the material properties of all components.

Table 3.0-2: Material properties of components

	E (MPa)	CTE (m/m°C)	Poisson's Ratio
Tee/shell	145,000.00	1.70E 05	0.31
Modular coil	63,000.00	1.72E-05	0.20
Toroidal spacer	150,000.00	1.70E-05	0.27
poloidal spacer	163,000.00	1.70E-05	0.31
Wing beg	13,750.00	3.00E-05	0.32
Wing beg Image	689.00	3.00E-05	0.32
Clamp	163,000.00	1.70E-05	0.31
Top pad	21 28	1.25E-03	0.00
Side pad	6.96	1.25E-03	0.00

4.0 Results and Interpretations

4.1 EM Analysis

The maximum current scenario at 2T high beta at t=0.0sec was selected for the EM model as shown in Fig. 3.0-1. Figure 4.1-1 demonstrates the flux density contour plot of three coil types, in which the coil type B has the maximum flux density of 4.901 Tesla.

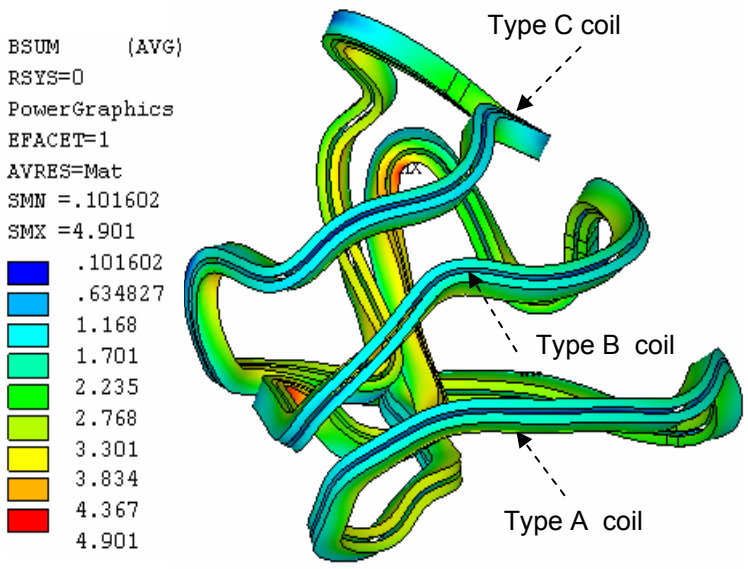

Flux density unit in Tesla

Fig. 4.1-1: Flux density at modular coils

Figure 4.1-2 displays the element vector forces for three coil types on the right-hand side. Table 4.1-1 summarizes the net force components of all six modular coils in the cylindrical coordinate system. The values of EM loads show that net force components Fθ and Fz of the same coil type are equal in magnitude and opposite in direction in the cylindrical coordinate system. The Fr is in

the same radial direction. The six coils induce 5 MN net EM forces acting toward the center and zero net forces in the vertical and toroidal directions. The net vertical forces are downward in the right-hand-side coils and upward in the left-hand-side coils.

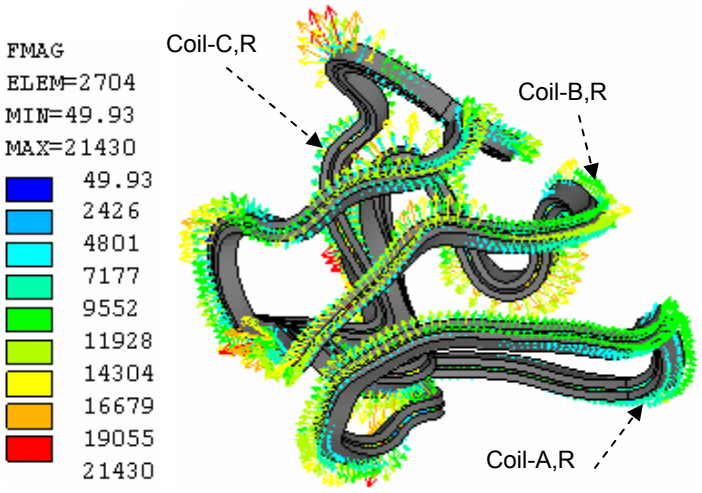

Fig. 4.1-2: Element vector forces of Type B modular coils

Table 4.1-1: Net forces on the modular coils

	Fr, N	Fθ, N	Fz,N
Coil-A,R	-859495	-58278	-38550
Coil-A,L	-859495	58278	38550
Coil-B,R	-1343701	-152699	-459628
Coil-B,L	-1343701	152699	459628
Coil-C,R	-298928	27737	-463462
Coil-C,L	-298928	-27737	463462
Total	-5004250	0	0

4.2 Nonlinear Structural Analyses

The following sections present the results of all model components. More details of graphical plots are demonstrated and discussed in the PowerPoint files (see References [6] and [7])

4.2.1 Shell Structure

Figure 4.2-1-1 shows two displacement plots, in which the maximum total displacement and the maximum vertical displacement is 2.336-mm and 1.240-mm, respectively. Both of them occur at tee in the wing of the shell type B. The maximum displacement occurs on the tee mostly due to the lateral deformation of web caused by the lateral forces of the modular coil. Because of net vertical forces are equal and opposite with respect to the mid-span, the deformation at bottom of the mid-span is small. The deformations are smaller at the inboard regions than the outboard regions because of the higher shell stiffness in the inboard.

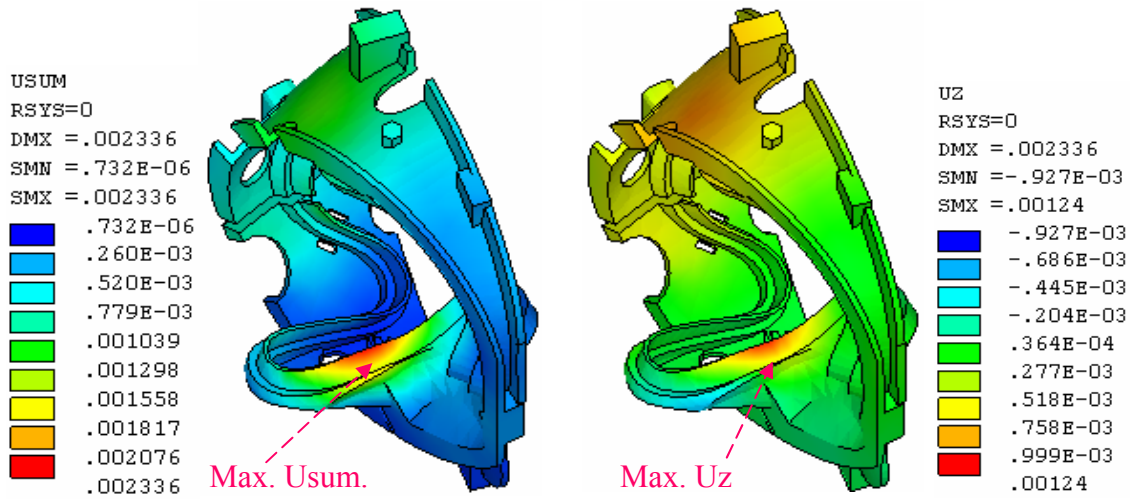

Fig. 4.2.1-1: Maximum displacements occur at wing of shell Type B

Figure 4.2.1-2 illustrates the von Mises stresses of the shell structure with a local area near the lead opening of the shell type B, in which the maximum local von Mises is 265-MPa (38.4-ksi). The model was built without chamfers at the lead openings. If chamfers were built in the model, the local stress should be greatly reduced. Departing from the peak local stress area in the shell Type B, the high stress was found at the root of the wing cantilever, near the location of the maximum displacement. At that location, the flange of tee is thin and the maximum Seqv is about 210 MPa. The stress plot shows that most parts of the shell have stress lower than 118 MPa (17.1 ksi). Table 4.2.1-1 summarizes the maximum stresses and displacements of the shell types A, B, and C.

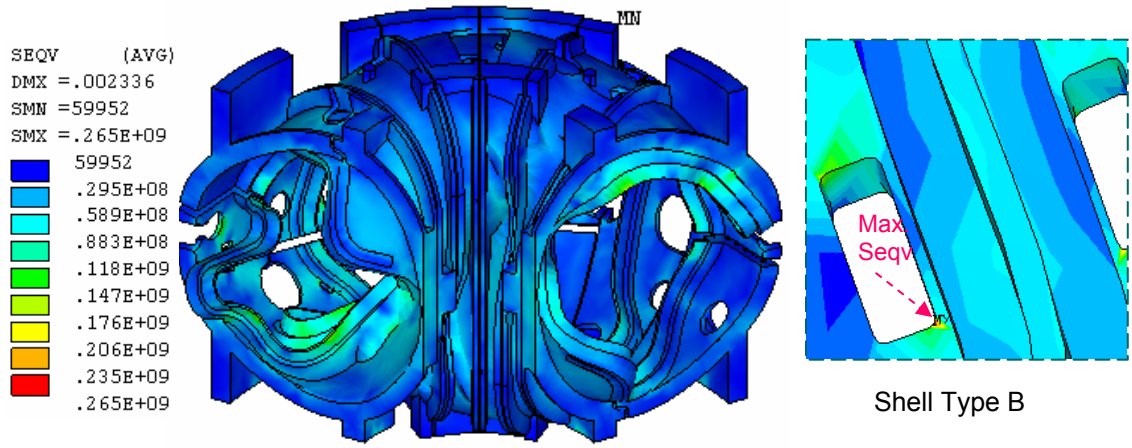

Fig. 4.2.1-2: Stress plot for shell Type B

Table 4.1.2-1: Maximum displacements and stresses of shell structure

	E (GPa)	Max Displacement (mm)	Max von Mises stress (MPa)
Shell Type A	145	1.124	161
Shell Type B	145	2.336	210*
Shell Type C	145	1.395	180*
* Note – By neglecting the local peak stress at the corner of the lead opening			

Product specification of casting shell (see Reference [8]) states the minimum 0.2% yield strength and the tensile strength to be 496.4 GPa and 655 GPa, respectively. The allowable is the less of 1/2 tensile strength or 2/3 yield strength. Using the lower value in the specification, the allowable stress would be 322.5 MPa, which is higher than the maximum von Mises stress.

4.2.2 Modular Coil

On the base of the selected material properties, the assumed contact properties, and the designated base support locations, the axial stresses and displacements of the modular coils are summarized and listed in Table 4.2.2-1. The contour plots of the axial stresses of three coil types are shown in Fig. 4.2.2-1.

Table 4.2.2-1 Maximum displacements and axial stresses of shell structure

	E (GPa)	Max Displacement (mm)	Max axial stress (MPa)
Coil Type A	63	1.589	253
Coil Type B	63	2.493	144
Coil Type C	63	2.707	156

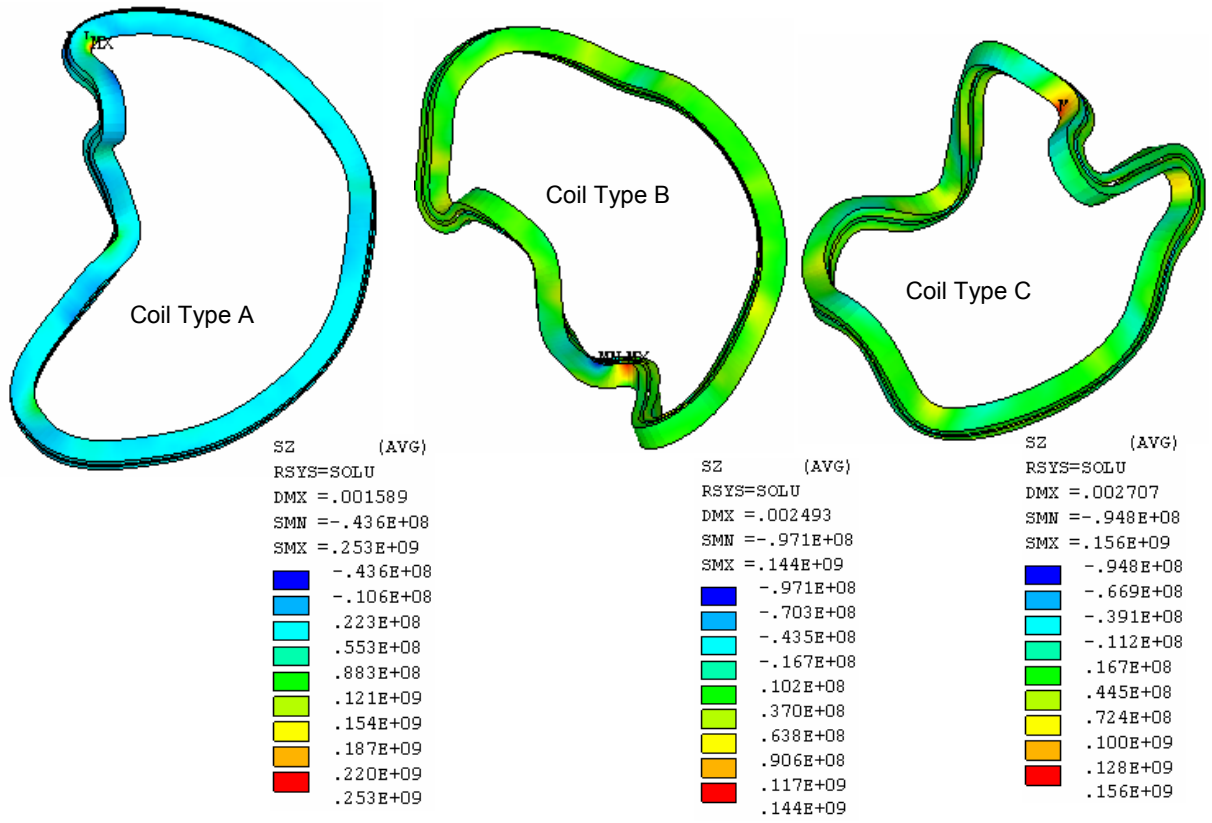

Figure 4.2.2-1: Axial stresses on the modular coils

Peak local axial stress, Sz, locates at coil type A at where the coil winding extend beyond the edge of shell type A and the radius of winding curvature is small. The coil shrinkage and the position on the wing are the primary contribution to the bending stress. The non-homogeneous current flow and large mesh size also contribute to higher stress. Away from the peak stress area, the stress is all below 140 MPa.

The maximum displacement is 2.707 mm in the coil type C. The contour plot of the type C coil displacement is illustrated in Fig. 4.2.2-2. Because of cool-down shrinkage, when winding at one side of tee develops gap, the other side of winding is in contact with the tee.

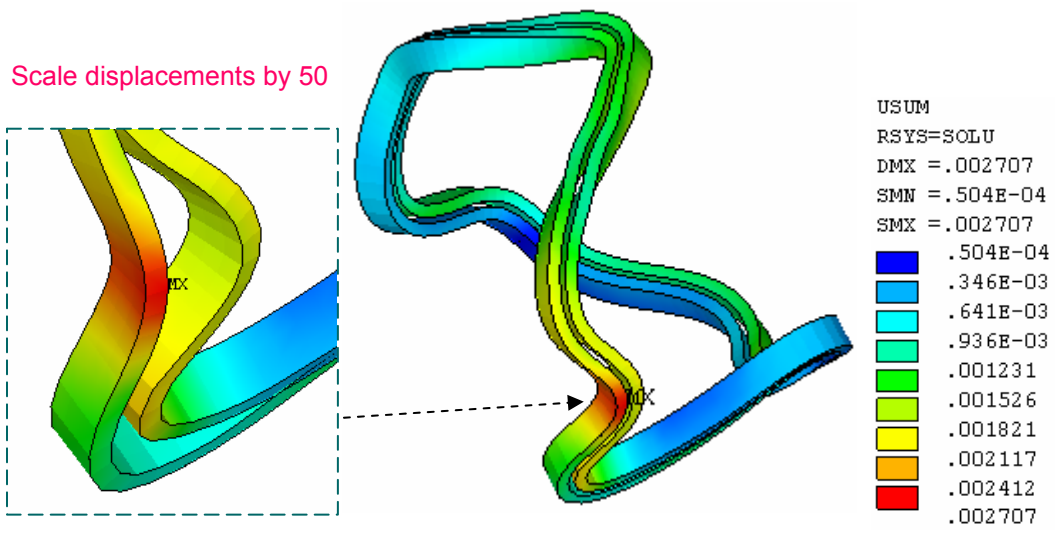

Figure 4.2.2-2: Contour plot of total displacement of type C coil

Figure 4.2.2-3 shows the gap distances between the modular coils and tees. The value of gap distance is the sum of the initial gap and the deformation gap. The gap distances in general are very small (red color in CONTGAP plot). The local large gaps are caused by geometry errors in tee as shown in Fig.4.2.2-4. However, the small areas without contact should have negligible effects on the results.

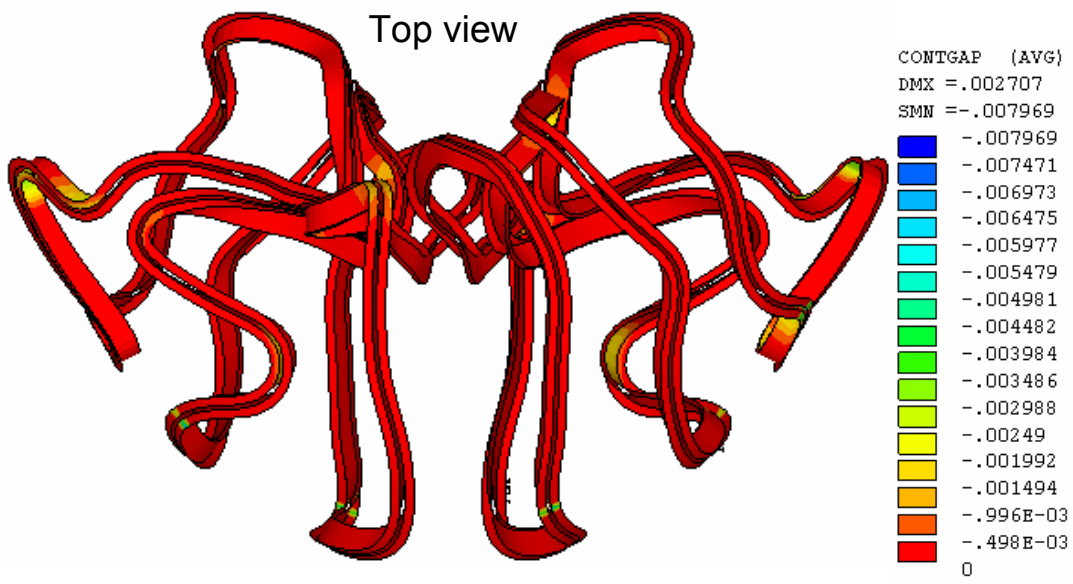

Figure 4.2.2-3: Gap distance between modular coils and tees

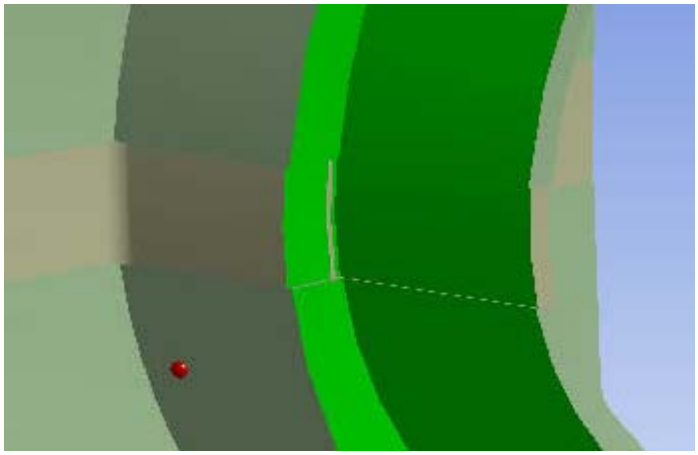

Figure 4.2.2-4: Surfaces of winding form are not continuous at poloidal breaks

4.2.3 Clamps

The clamps are used to hold the coil in position. Higher stress in the clamp was expected at where the coil moves away from the winding form. Although the model could not exactly simulate the behavior of Belleville washers and the complexity of joint construction, the results provide some thoughts of the higher stress locations.

Figure 4.2.3-1 displays the von Mises contour plot of the coil type C. High stresses are found at the interfaces of clamps and tees because of the rigid connection. High stresses are primarily caused by the bending moments and the shear forces that are primarily induced by the lateral movement of the coils. The maximum von Mises stress is 283 MPa at the clamp-tee interface. The actual stresses should be much smaller if sliding and rotation are allowed at the clamp assembly.

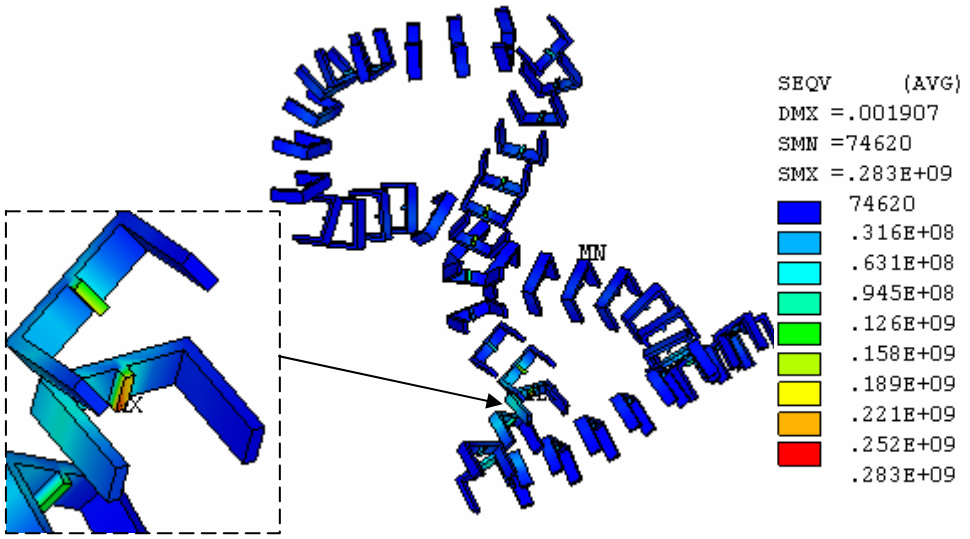

Figure 4.2.3-1: Von Mises stress plot of clamp for coil type C

4.2.4 Wing Bags

Wing bag was designed to carry the loads from the wing to the next shell segment. The amount of load transfer depends on the stiffness of the wing bag and the contact behavior. The analysis presumed that the wing bag modulus of elasticity was 13,750 MPa and was bonded to the shells.

Figure 4.2.4-1 shows the contour plot of the wing bag contact pressure at the shell type A. The unit of contact pressure is Pascal. Positive pressure indicates load toward the surface and therefore is in compression. The distribution of the contact pressure is not very uniform on the contact surface. Most effective spot on the wing bag locates near the cantilever end of the wing. The areas with tensile contact pressure (negative sign) are not effective to transfer loads. The maximum value of the contact pressure occurs on the wing bag between shell types B and C as shown in Figure 4.2.4-2. The maximum pressure is 136 MPa (19.73 ksi). If the actual wing bags are not bonded to the shell, the contact surface behavior in the model should be modified. The load transfer through the wind bag is more or less proportional to its stiffness.

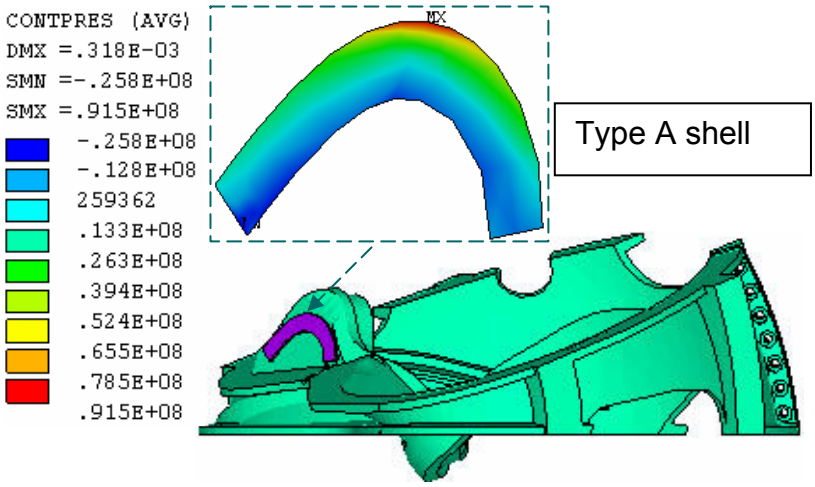

Figure 4.2.4-1: Contact pressure on wing bag at shell type A

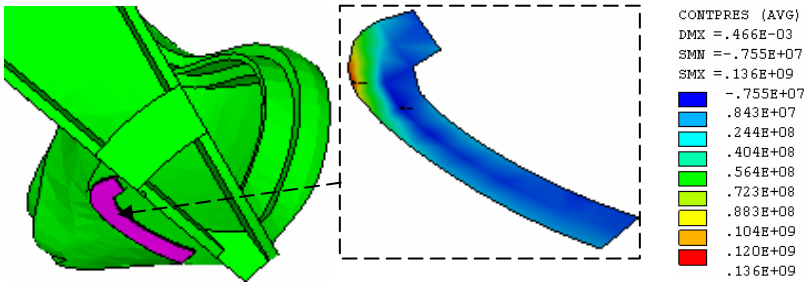

Figure 4.2.4-2: Contact pressure on wing bag between shell types B and C

4.2.5 Poloidal Break Joints

No bolts or any bolt preloads were included in the poloidal break joints. The poloidal break insulations were bonded to the shells at the contact surfaces. Figures 4.2.5-1 and 4.2.5-2 illustrate the plots of contact pressures and the contact shear stresses in the poloidal breaks. In the contact pressure plot, negative pressure is in tension. The stress distributions in the poloidal breaks are not uniform and the net normal forces are in tension. The tension in the joint should be overcome by the bolt preload. The net compression provided by the bolt preload shall also produce enough friction force to withstand the shear force in each poloidal break. The maximum compressive pressure appears at tee because of joint eccentricity with respect to the middle plane of the shell.

.

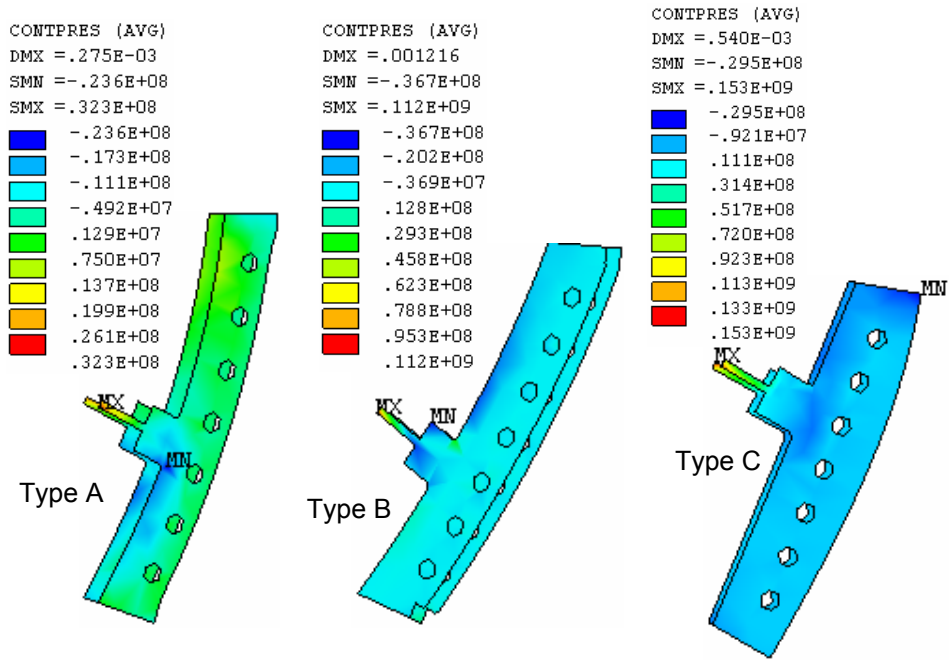

Figure 4.2.5-1: Contact pressures on poloidal break insulation

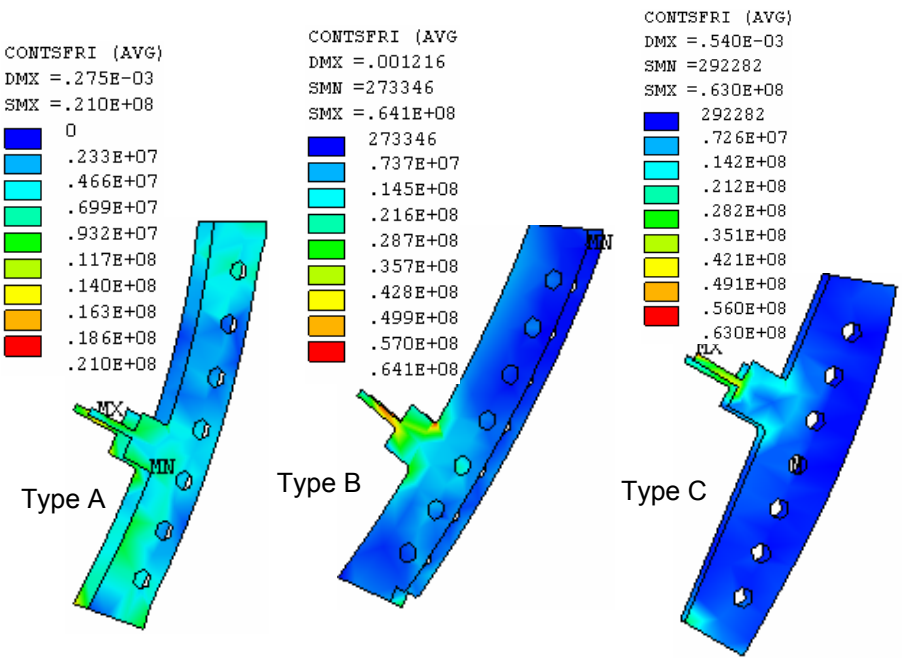

Figure 4.2.5-2: Contact shear stresses on poloidal break insulation

4.2.6 Toroidal Flange Joints

The model did not include bolts or any bolt preloads in the toroidal flange joints. The flange insulations were assumed bonding to the flanges at the contact surfaces in the analysis. In the real structure, bolts and screws are used in the flange joint design. The nominal diameter of the bolt or screw is 1.375 inches. Because of the tight flange spacing at the inboard flange regions, they are no spaces available to provide bolts. The total number of bolts and screws used at the shell flanges are as follow:

18 bolts and 2 screws at shell joint A-A
24 bolts and 3 screws at shell joint A-B
17 bolts and 12 screws at shell joint B-C, and
24 bolts and 8 screws at shell joint C-C

For viewing clarity, Figure 4.2.2-6 demonstrates the contour plots of toroidal stresses in the range from -80-MPa to 10-MPa at the inboard region of the toroidal shims. The gray color indicates that the stress is outside of the stress range. The red color demonstrates that the area is in tension and the other colors are in compression. The inboard regions without bolt connections were also pointed out. Because of the net EM loads acting toward the machine center, wedge action will produce net compression at the inboard. The plots clearly demonstrate that the average stress in the region is in compression.

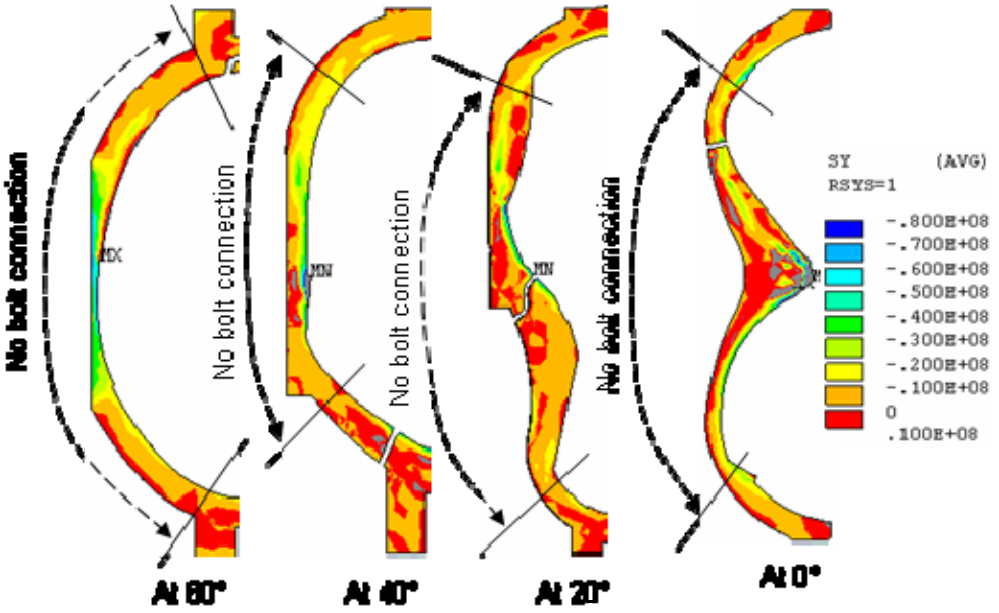

Figure 4.2.6-1: Normal stresses at the inboard regions of flange insulation elements

To prevent the joint sliding in the areas without bolt connection, the friction forces produced from the compressive forces shall be more than the shear forces. Therefore, the ratio of the shear force to the compressive force should be smaller than the coefficient of friction on the contact surfaces if no fasteners were provided.

Local coordinates were defined on the flange surfaces to evaluate the normal and shear forces at the no bolt zones. The net forces in the toroidal flange joints, in Newton, are shown in Table 4.2.6-1

for joint regions above the mid-plane and Table 4.2.6-2 for joint regions below the mid-plane. In the Tables, the total shear force is the vector sum of the horizontal shear and the vertical shear. The resulting shear-compression ratios range from 0.123 to 1.003. When the shear-compression ratio is greater than the coefficient of friction and no shear resisting features, such as shear keys or shear studs, are provided, the excessive shear loads will be transmitted to the first bolt or screw near the inboard region.

Table 4.2.6-1: Net forces in the inboard no bolt zone above the mid-plane

	Jiont A-A	Joint A-B	Joint B-C	Joint C-C
Horizontal Shear	471,544	564,467	193,878	-455,543
Vertical Shear	-343,918	-26,772	-10,660	150,214
Total Shear	583,638	565,101	194,171	479,670
Compression	1,130,981	1,230,928	1,582,631	1,160,683
Shear-Comp. Ratio	0.516	0.459	0.123	0.413

Table 4.2.6-2: Net forces in the inboard no bolt zone below the mid-plane

	Jiont A-A	Joint A-B	Joint B-C	Joint C-C
Horizontal Shear	-468,620	-376,206	598,869	365,042
Vertical Shear	-383,967	-479,818	-52,266	190,812
Total Shear	605,834	609,718	601,146	411,904
Compression	1,165,284	925,483	599,342	1,121,274
Shear-Comp. Ratio	0.520	0.659	1.003	0.367

While the wedge action of EM load produces net compression at the inboard, the net forces at the outboard are more and less in tension due to in-plane EM loads. Figure 4.2.6-2 illustrates the normal stress Sy and the shear stresses Sxy, Syz for the toroidal flange insulation elements at 0°, 20°, 40°, and 60°. Three stress components Sy, Sxy, and Syz are displayed in the cylindrical coordinate system. For viewing clarity, the contour plots only show the stress range within -80 MPa to 10 MPa for the normal stress and -16 MPa to 16 MPa for the shear stresses. Stresses outside of the range are in grey color. High local stresses were found in the flange shims at the corners of the cut-out out, such as high compression in the inboard region of shim at 40º. Smoothing the shapes of flange shims at cut-out areas will minimize those peak local stresses.

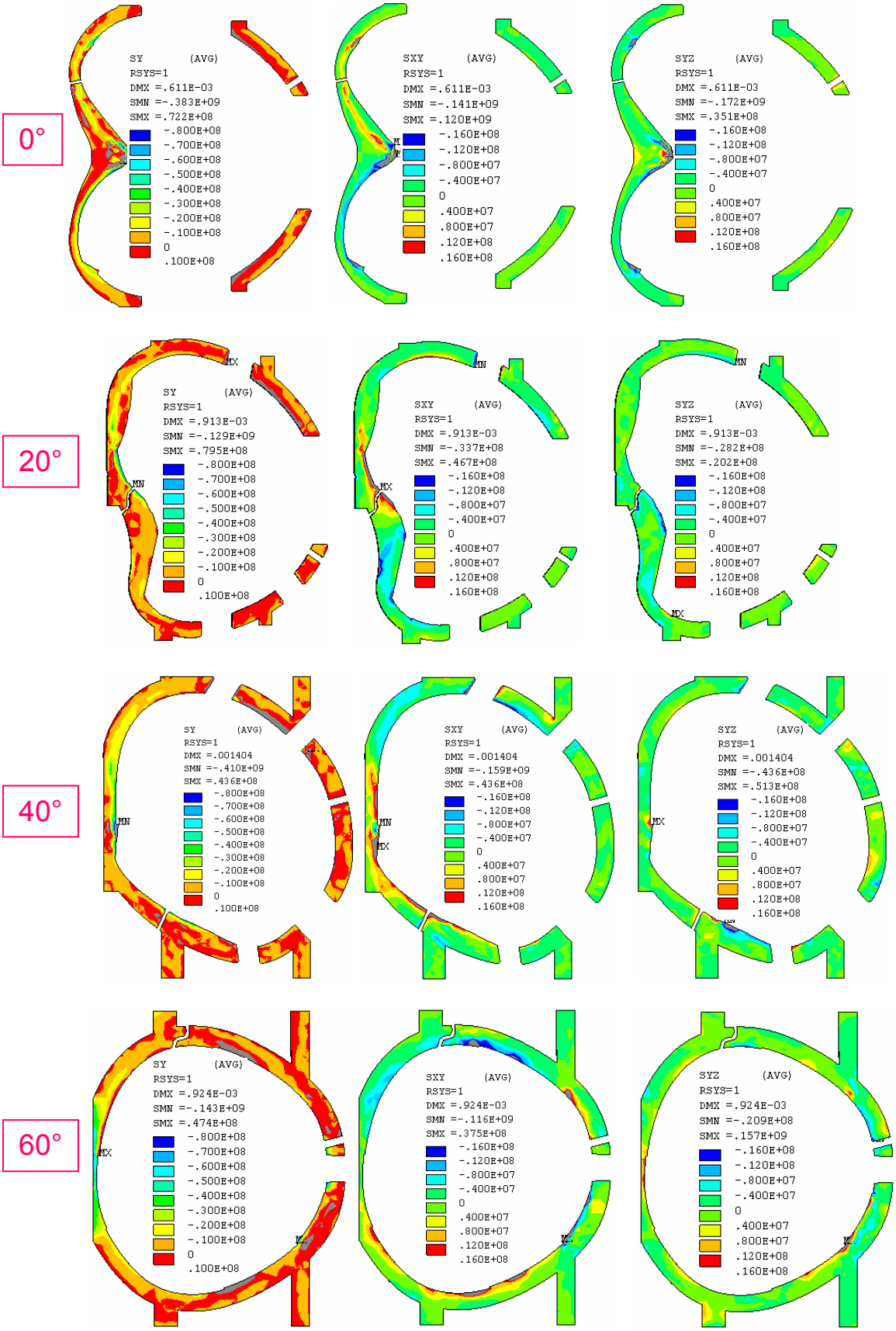

Fig. 4.2.6-2: Normal stresses and shear stresses for toroidal flange insulation elements

Being no bolt pretension including in the analysis, the required bolt preloads shall be able to withstand the tensions and produce sufficiently frictional forces to resist the shear forces in the contact surfaces. For evaluation of bolt loads in the bolt joint, the shear force and normal force may be evaluated in a small area for a group of bolts along the flange insulation, instead of at the nodal point of each bolt location. The calculation will first selects a group of elements belonging to a group of bolts and then obtains the associated nodal points on the surface of the selected elements. A rectangular coordinate system parallel to the selected surface is defined and the nodal force components on the selected nodes are summarized. Fig. 4.2.6-3 demonstrates of nodal force sums along the flange between shell types B and C of the toroidal flange insulation elements. In the plots, Fx and Fz are the components of the net shear forces in the radial and vertical directions, respectively. The Fy is the net normal force across the joints. Positive Fz indicates that the force is out of the element and therefore is in tension. The force unit is Newton.

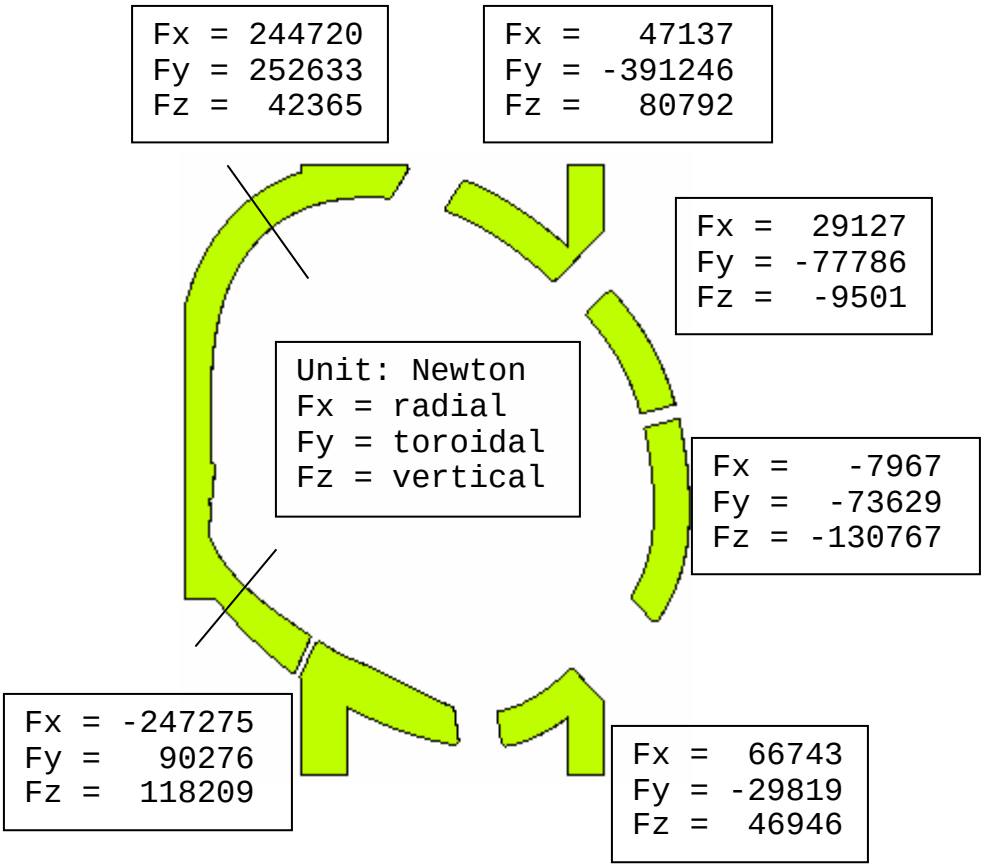

Fig. 4.2.6-3: Forces along the flange between shell types B and C

4.2.7 Effects of Flange Shim Geometry

Two nonlinear runs filen9.db and filen9b.db were performed with slightly shape variation at the flange inboard insulation between flange joint A-A. Using the cylindrical coordinate system, Figure 4.2.7-1 shows the stress contour plots with the same contour values for elements of the original and the revised insulation shapes. In the plot, Sy is the normal stress while Sxy and Syz are the shear stress components in two perpendicular directions. Local stresses are sensitive to the shape of

flange insulation at the inboard areas. A small protrusion in the insulation ends up yielding higher maximum local stresses.

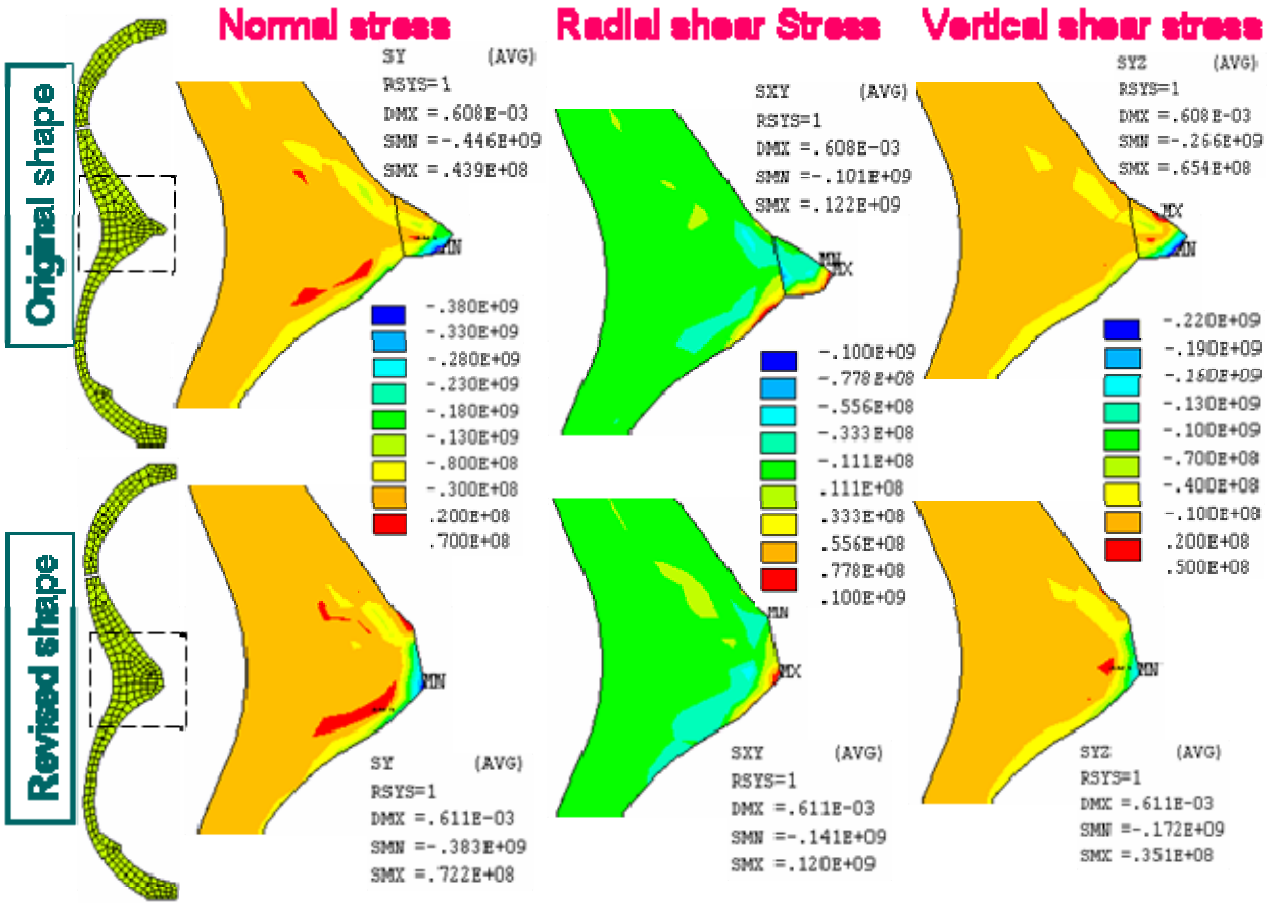

Figure 4.2.7-1: Stress distributions due to shape variations in the inboard flange insulation

4.2.8 Reactions at Supports

The nodal reactions at the inboard and outboard support locations are summed up and shown in Fig. 4.2.8-1 under the cylindrical coordinate system. The unit is Newton. There are no radial reactions on the supports due to no displacement restraints in that direction. The total reactions on the right-hand side supports are -96,553 N for F_θ and -347,540 N for Fz. The total reactions on the left-hand side supports are –149,280 N for F_θ and 347,540 N for Fz. Thus the total support reactions become –2.458E+6 N for F_θ and zero net reaction for Fz.

Idealistically, if the support was placed on a single point, there would be zero support reactions because of the balance in the toroidal and vertical EM forces. Adding more supports will produce displacement restraints against the movement of the shell structure and thus induce reactions on the support locations. The structure will become more rigid and the deformations will become smaller. They can also carry some loadings directly to the base floor instead of balancing the loads through the toroidal flange joints. Placing the inboard and outboard supports will be more stable under the seismic loading condition. However, it produces large horizontal reactions due to the horizontal constraints. If the toroidal restraints at the inboard supports are eliminated, the horizontal reaction F_θ will be greatly reduced. Large toroidal reaction F_θ is not desirable since it will increase the difficulty in the design of the base support structure.

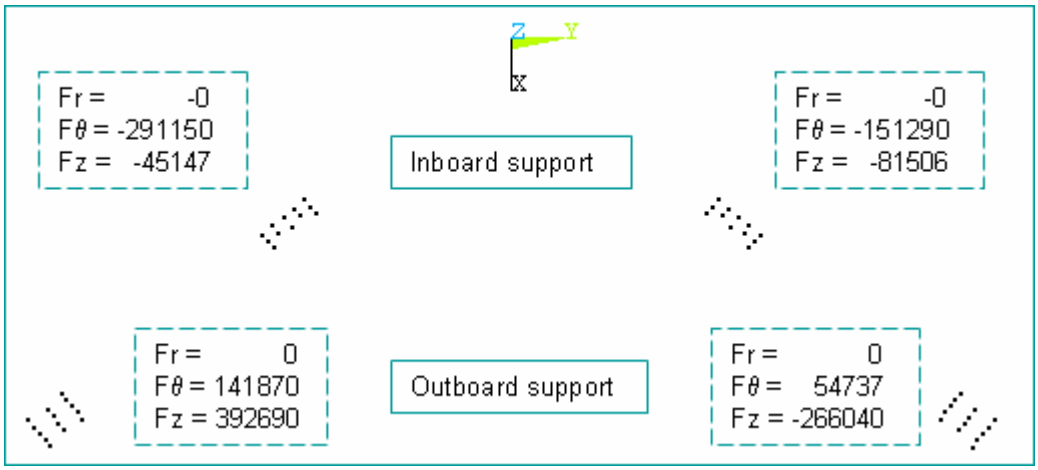

Figure 4.2.8-1: Reactions at inboard and outboard supports

4.2.9 Contact Status of Top Pads and Side Pads

Figure 4.2.9-1 shows the contact status of the top pads and the side pads with MC. Examining the contact status of top pads on the modular coil surfaces illustrate that most of top pads are in near contact condition. This indicates the initial expansion of the top pad is too low and suggests that a higher temperature increase or higher CTE is needed if contact is desired. The side pads are under sliding and near contact condition. Sliding contacts on the side pads are results of the sliding between coils and tees as the pads are bonded to the clamps.

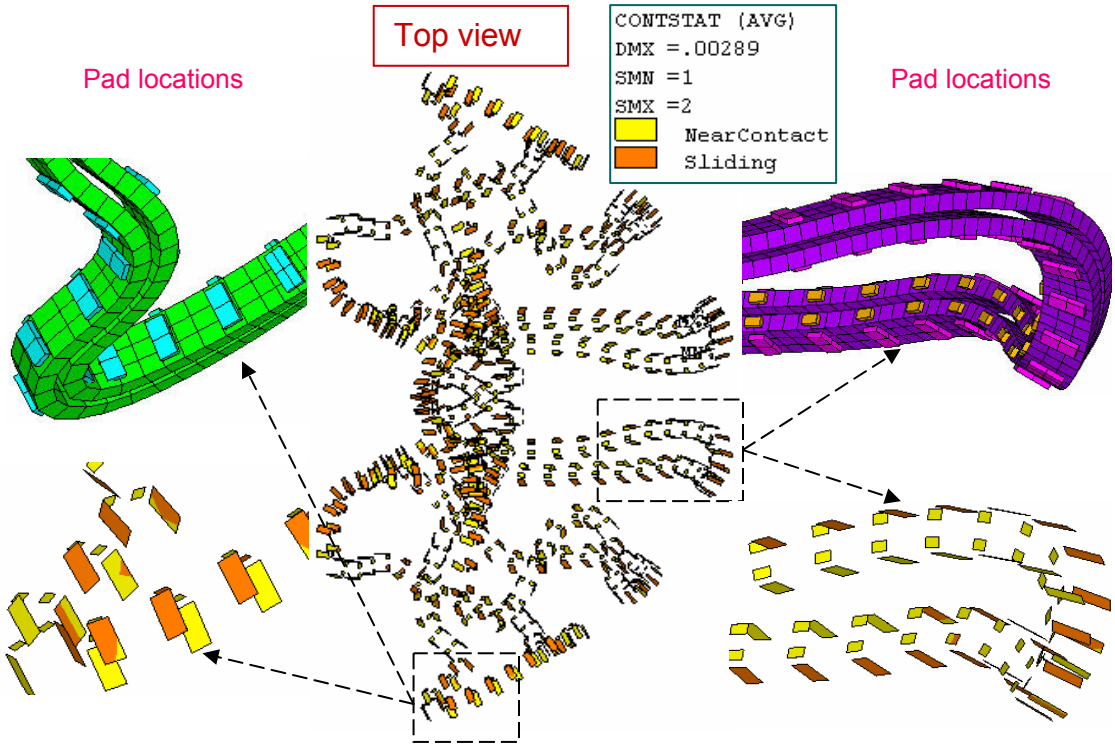

Figure 4.2.8-1: Contact status of top pads and side pads on modular coils

5.0 Summary & Commentary

The analysis is for modular coil with cool-down and EM load. An initial shrinkage of coil strain 0.0004 m/m and the maximum coil current scenario of 2T high beta at t=0.0 second were selected as load input. The model assumed all surfaces in the shell structure were bonded and no bolt preloads were applied at the toroidal flanges and the poloidal breaks. The main nonlinear effect comes from the frictionless contact behavior between the winding and the winding form and between the winding and clamp assembly.

There are 5MN of net radial EM forces induced by the modular coils in one field period. The vertical forces Fz and the toroidal forces Fθ are equal and opposite in direction for the coils in the right-hand side and the left-hand side, resulting in zero net forces. The EM load produces wedge action at the inboard leg region. Out side the region, the net forces in the shell are generally in tension.

The shell structure is made of stainless steel casting. According to the NCSX design criteria (see Ref. [9]), the allowable stress for the membrane plus bending will be 322.5 MPa or 46.78 ksi, which is larger than the maximum stress. The maximum deflection in the shell is 2.336 mm in the tee of the shell type B.

Maximum axial stress in the modular coil is 253 MPa, located locally at coil type A at where the coil winding extend beyond the edge of shell and the radius of winding curvature is small. The value is conservative because of non-homogeneous current flow and large mesh size. Away from the local stress area, all stresses are below 140 MPa. The maximum displacement is 2.707 mm in the coil type C.

The peak von Mises stress in the clamp is 283 MPa, based on the rigid mount of clamp to the tee. If sliding and rotation are allowed in the clamp assembly, the maximum stress will be much lower. If the Belleville washers in the clamp could handle the coil movements, the stress in the clamp should be relatively constant. As the clamp assembly may not be able to confine the movement of the modular coil, an option is to remove the particular clamp when the displacement of coil is too large for the clamp.

The contact pressures on the wing bags are far from uniform. The contact surfaces are assumed to be bonded to the shells. The maximum contact pressure on the wind bag is 136 MPa (19.7 ksi), which is more or less proportional to its stiffness. The tensile stress area in the wing bag is not effective for the load transfer. A shape change to minimized the tensile region will result in a more even stress distribution and lower compression. If the actual wing bags are not bonded to the shell, the contact surface behavior should be modified.

The distributions of contact pressure on the poloidal break spacers are more even, except the narrow section in the tee. The net force in the poloidal break is in tension. The bolt preload will be designed to overcome the tensile stresses and shear stresses.

There are no bolts available in the inboard regions of the toroidal flange shims. The calculations show the shear-compression ratios range from 0.123 to 1.003, greater than the hypothetical coefficient of friction, said 0.3. The coefficient of friction between two surfaces relates to the surface preparation and contact materials. If there are no additional shear resisting features, some shearing forces may transmit to the first bolt or screw in the inboard regions. To simulate this condition appropriately, the contact behavior should be changed from bonding to standard contact.

High local stresses were found in the flange shims at the corners of the cut-out such as compression in the inboard region at 40º (see Fig. 4.2.6-2). Smoothing the shapes of flange shimrs will minimize those peak local stresses.

Choosing the supports in the mid-span of the shell type C will induce tensile reactions in the support structure. The elimination of the toroidal restraints at the inboard supports will greatly reduce the horizontal reaction in the supports.

As the coil shrinkage during cool-down is the main factor of the nonlinear behavior, the assumption that the initial coil shrinkage strain of 0.0004 m/m should be verified and confirmed. Finally this analysis is only for a governing load case with modular coil cool-down and EM load. The complete analysis shall include all possible load conditions.

5.0 References

[1] C08R00_c3.XLS, dated 1/13/2004, PPPL web site
ncsx.pppl.gov/NCSX_Engineering/Requirements/Specs/GRD/Rev1/TDS_XL_C08R00_c3.pdf

[2] C08R00_C7.xls, dated 9/1/2005, PPPL web site
ncsx.pppl.gov/NCSX_Engineering/Requirements/Specs/GRD/Rev3/C08R00_C7.pdf

[3] T. Kozub, "NCSX Composite Coil Tests", March 15, 2004, PPPL web site
ncsx.pppl.gov//NCSX_Engineering/Meetings/CY-2004/March/040315_MatlTest/

[4] T. Kozub, "NCSX Composite Coil Tests", April 5, 2004, PPPL web site
ncsx.pppl.gov//NCSX_Engineering/Meetings/CY-2004/March/040405_MatlTest/

[5] L. Myatt, "Transverse Compression of Modular Coil Conductor from ANSYS", April 13, 2004, PPPL web site:
ncsx.pppl.gov/NCSX_Engineering/Meetings/CY-2004/April/040412_MatlTest/

[6] H. Fan, "Nonlinear Analysis of Modular Coils and Shell Structure for Coil Cool-down and EM Loads, Part 1 – Results of Shell Structure and Modular Coils", September 28, 2005, E-mail attachment.

[7] H. Fan, "Nonlinear Analysis of Modular Coils and Shell Structure for Coil Cool-down and EM Loads, Part 2 – Results of Clamp Assembly, Wing Bags, Poloidal Break Joint, and Flange Spacer Joints", November 15, 2005, E-mail attachment.

[8] NCSX Product Specification, "Modular Coil Windings Forms", NCSX-CSPEC-141-03-10, November 15, 2005

[9] I. Zatz, Editor, "NCSX Structural Design Criteria, Draft E", May 10, 2004, PPPL web site:
ncsx.pppl.gov//Meetings/FDR_2004/FDR_docs/Postings/NCSX-CRIT-CRYO-00-dE.pdf/

NCSX
Design Basis Analysis

Analysis of NCSX Integrated Structure

NCSX-CALC-14-003-00

November 2, 2006

Prepared by:

H. M. Fan, PPPL

☐

I have reviewed this calculation and, to my professional satisfaction, it is properly performed and correct. I concur with analysis methodology and inputs and with the reasonableness of the results and their interpretation.

☐ **Reviewed by:**

A. Brooks, PPPL

Analysis of the NCSX Integrated Structure

1.0 Executive Summary

This report documents a nonlinear FEA model for NCSX coil support structure and its analytic results for the four loading cases, representing four stages during NCSX operation. The four stages are dead load (DL) only at room temperature, dead loads plus cool-down to 85° K, dead loads plus cool-down and electromagnetic (EM) loads at 85° K, and dead loads and EM loads. The last load case assumes the thermal strain during pulse will cancel the cool-down strain. The analyses do not consist of seismic loads, the interacting loads from other components, and the TF coil preloads.

As the previous nonlinear analysis [1] for the modular coil (MC) and the modular coil winding form (MCWF) indicated the trouble areas at the MCWF joints for the cool-down and EM loads, it is important to make analyses with a model that includes the TF structure and loadings that consider all governing load cases. Due to the physical memory of the existing PC (32 bits with 1.5GB), the modeling efforts required to keep the model size within a acceptable limit. Therefore, the element size for most parts do not have fine mesh pattern. The parts that have few contributions to the stiffness of the integrated system, such as the vacuum vessel and the center stack, were disregarded in the model. However, the load impact from those parts should be considered in the analysis. The model did not contain the modular coil clamp assembly because of its modeling complexity and less input to the modeling stiffness. Alternatively, the modular coils were bonded to the winding forms for stability. The model consists of MCWF system, TF structure system, and all modular coils, TF coils, PF4, PF5 and PF6 in one field period, which is a 120-degree sector.

The FEA model was formed using contact elements among all connecting parts. All the contact surfaces are assumed to be bonded except the MCWF wing interfaces that have frictionless unilateral contact behaviors. The nonlinear property at the wing interfaces offers more rational assessment of the forces across the MCWF toroidal joints. Using less nonlinear elements will utilize less disk memory, reduce running time, and minimize the difficulty for the solution convergence.

The highest MC conductor currents of the current waveforms at full operating capability as shown in Section A.2.3.2 of Reference [2] were selected as the governing case of EM loads. Additional load cases may be run to verify whether the present case is the worst case or not. For the vacuum-pressure impregnation (VPI) modular coils, the relative cooling shrinkage of coil strain has been assumed to be 0.0004 m/m from the room temperature to the operating temperature of 85K.

The NCSX structure will be supported at three locations, 120 degrees apart at the C-C joints [3] to keep the EM loads from the support. Each support offers only the vertical and toroidal restraints and let the structure move freely in the radial direction. The design of base support is not complete yet. For convenience, the base support was located below the outboard stiffening leg.

The exact simulation of the integrated structure, which involves bolt preloads, partial-bolted joints, sliding interfaces, and indefinite orthotropic material properties of the modular coils, was very tedious and may have difficulty of nonlinear convergence. This model shall be treated as a basic model that provides the capability for further modifications of the modeling assumptions. Because of time limit, no further adjustments have been run. In order to obtain conservative answers for particular areas, it is recommended that additional runs should be carried out by modifying some

contact surface behaviors or the material properties. The following results are derived from the current modeling assumptions.

- For 2T high beta scenario, the maximum flux density is 4.901 Tesla on the MC Type B.
- The net centering EM force Fr in one field period from MC is 5 MN.
- Radial preloads for the TF coils is not considering in the analysis. Current design concept indicates that the preloads will be counter balanced by the ring tension of the inboard TF structure.
- The impact of EM loads on the MCWF is much greater than the dead weight and the cooldown thermal strain.
- The maxim displacement is 2.604 mm, occurred at the modular coil Type B from the DL and EM loads. The maximum displacement in the MCWF is 2.371 mm, located near the maximum coil displacement in the shell Type B.
- The maximum von Mises stress in MCWF is 220 MPa (31.9 ksi), found at the inboard location of the shell Type A for dead load plus EM load. The allowable stress of stainless steel casting [15] for the membrane plus bending is 322.5 MPa (46.78 ksi).
- The highest longitudinal stresses of the modular coil is 139MPa (20.1 ksi) in coil Type A from the load case of DL and EM with cool-down effects.
- The PF4, PF5, and PF6 are constrained by the TF structure. Displacements of the integrated structure, especially the vertical displacements, have some impact on their stresses.
- TF and PF currents are not the highest currents. The stresses in this EM load case do not stand for the critical load case for the TF and PF coils and possibly the TF structure.
- No EM loads enter into the base support. All four load cases post the same vertical support reactions, which is 339.4 KN (76.3 kips).
- The contact pressures on the wing bags are not very uniform. With modulus of elasticity at 13,750 MPa, the maximum contact pressure is 128 MPa (18.6 ksi.), occurred on the wing bag Type B. The pressure could be improved if shape is changed to provide more uniform compression.
- The TF structure will help carrying some loads to the base support, if the TF structure sections are fully bonded at the shim joints.
- The thermal strain from the cool-down has only small impact on loads at flange joints in comparison with the EM loads.
- Based on the net bolt preload of 45797 lbs for the 1 3/8” bolt, several locations along the toroidal flange joints have shear forces far exceeds the allowable value. That might cause the joints to slip.
- In evaluating the bolt joint capacity, the selected areas for the bolt group shall be small enough that the centers of bolt groups match closely with the centers of bolt loads.
- The worst location for the joint slip in the MCWF is at the inboard flanges joint B-C.
- A complete design of the bolt joint should also consider the impact of preload change due to thermal variation and the creep of the insulation materials.
- The model assumed all contact surfaces were bonded except for the wing interfaces that used frictionless contact elements through the wing bag shims. In the real case, the modular coils, TF coils, and PF coils are not exactly bonded to the structure. Some bolt joints may not be firmly connected. It is recommended that additional runs by changing contact behaviors or modifying the material properties shall be performed to assess the impact of modeling assumptions.

2.0 Assumptions

The following assumptions were applied in the analysis:

The model was built on the Pro/E model. All the part contact surfaces are assumed to be bonded except the MCWF wing interfaces. The wing bag shim was bonded to shell on one side and had frictionless contact behaviour to the adjacent shell on the other side. With primary interest in the forces on the MCWF joints, the frictionless contact elements properly imitate the forces that transfer through flange joints at wings.

All material properties of coil conductors are based on the smeared properties. As the MC conductor test programs have not yet established many of the required data to form an orthotropic property, the model utilized isotropic material properties for the winding packs. As the coils are continuous in the axial direction, the isotropic material properties are more suitable to be represented by the test data in the longitudinal direction. The isotropic properties are also used for the TF and PF coils.

The model did not contain the modular coil clamp assembly because of its modeling complexity and less stiffness contribution. To ensure the stability of the modular coils in the model, they were bonded to the winding forms. Two longitudinal shear moduli in the coils were reduced to limit the shear impact on the contact surfaces and lower the composite action with the MCWF. The shear rigidities of shims for the TF and PF coils are decreased for the intention of less resistance to the coil movements. A description of the FEA model was given in a PowerPoint document [4].

To minimize the size of the model, the model disregarded the parts that have few contributions to the stiffness of the integrated system, such as vacuum vessel and center stack. However, their load impacts were added in the solution phase. For conservative reason, the weight of center stack was supported at the upper TF structure and the weight of vacuum vessel assemble was hung from the upper side of the shell Type A.

To make sure an adequate wedge action for the TF coil, all TF coils will be preloaded by pulling in the radial direction against the TF structure. As this assembling procedure will be carried out before the TF structure is tied down to the MCWF, these preloads will not transfer to MCWF and will not be considered in the analysis.

No bolt holes and bolt connections were simulated in the model and no bolt preloads were applied in the analysis. The normal forces and shear forces across the bolt joints shall be calculated after the analysis for establishing the required bolt preloads that will make sure that the bolt joints will not be opened up or sliding.

At the discussion meeting [3] of the stellarator support structure, the notes showed that the structure will be supported at three locations, 120 degrees apart at the C-C joints. The supports offer cyclically symmetric restraints of weight and seismic loads, but no EM loads. For this purpose, only the vertical and toroidal restraints exist on each support.

As the design of base support structure is not completed yet, fictitious base support blocks were added beneath the integrated model to keep high local stress and deformation away from the structure.

3.0 Analysis Methodology and Inputs

3.1 Methodology

The analysis uses the same mesh pattern for EM and stress analyses so that it is able to avoid the errors of mapping applied loads from one model to another model. The procedure will first solve the electromagnetic (EM) analysis and review the results. Then applying the EM loads obtained from the first analysis to the structural analysis for evaluating the stresses and displacements.

Because of cyclic symmetry in the geometry and the loading, the model is formed in a 120-degree sector to minimize the model size and the computer running time. Figure 3.1.1 and 3.1.2 show the models elected for the EM analysis and the structural analysis, respectively. The geometric nonlinearity of the contact behavior, caused by the wing interfaces, was solved using the ANSYS nonlinear method.

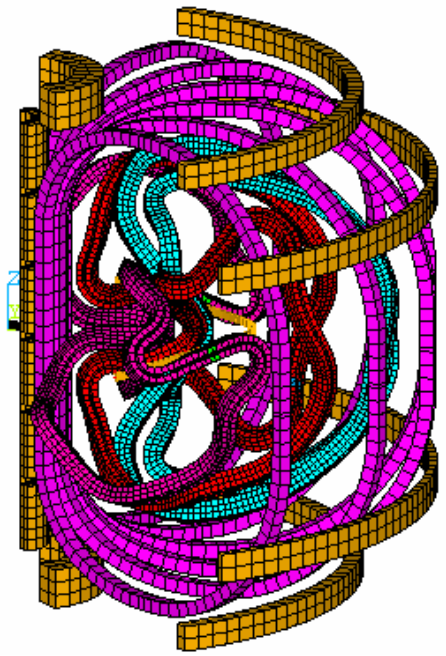

Fig. 3.1.1: EM model consists of MC, simplified plasma, PF coils, and TF coils

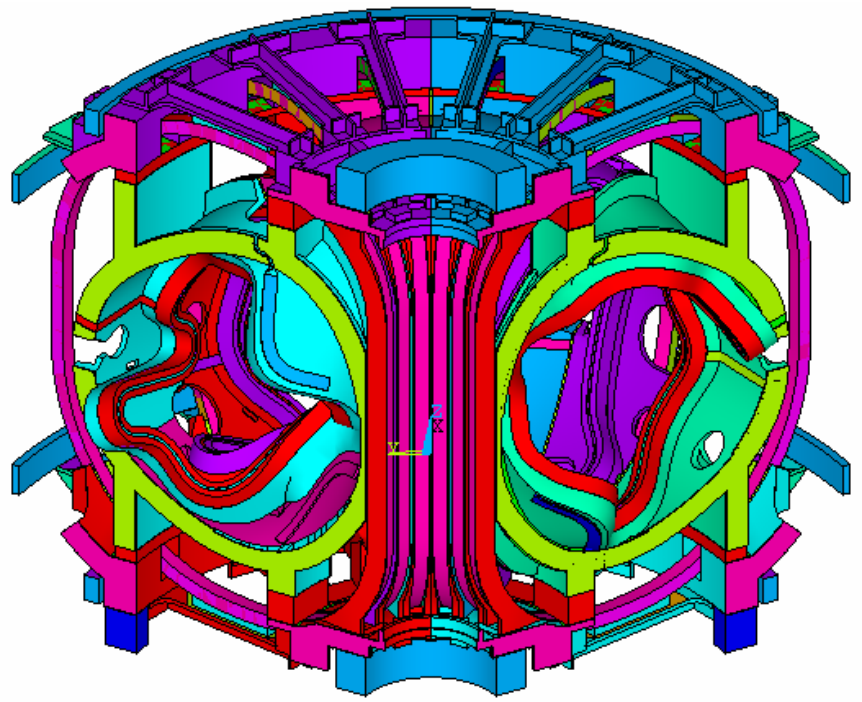

Fig. 3.1.2: Integrated structural model

3.2 Inputs of Models

The geometric files of the MCWF and modular coils were developed by ORNL while the geometric files of the TF structure and TF and PF coils were provided by PPPL. Some small features, such as bolts, bolt holes, chamfers, and fillers in the geometry were removed prior to the meshing.

In the EM model, the PF coils, TF coils, and the modular coils are formed by ANSYS 8-node solid element SOLID5. For the current input, the modular coils and TF coils were cut near the mid-height at the outboard legs. The plasma current was simplified by SOURE36 current elements along the center line of the plasma current.

After the EM analysis, the SOLID5 elements for the winding packs were shifted to structural 3-D SOLID45 elements with identical number for the nodal points and elements. The final structural model consists of the following components:

1) Modular coils
2) MC winding form (MCWF)
3) MCWF poloidal breaks
4) MCWF toroidal shims
5) MCWF wing bag shims
6) PF coils No.4 to No.6
7) PF coil brackets and shims
8) TF coils
9) TF coil shims at inboard, outboard, top and bottom
10) TF inboard wedge spacers
11) Inboard TF structure
12) Outboard TF structure

13) Tie bars for (11) and (12)
14) TF structure toroidal shims
15) Connecting blocks between TF structure and MCWF
16) Fictitious base support blocks

The number of nodes and elements of the model was examined in order to form a final model that can fit into the 3.2 bit PC with 1.5GB total physical memory. All contact regions used the surface-to-surface contact elements. Even with a total number of 163,090 elements and 283,750 nodes, the model does not have fine mesh size.

The model needs appropriate boundary conditions and support constraints to simulate the structure in a stable and cyclically symmetric condition. For parts with identical boundary nodes on θ=+60° and the θ=-60°, such like MCWF and PF coils, coupled degrees of freedom were defined for all degrees of freedom. For those without identical boundary nodes in the TF wedges and TF structure, the constraint equations were generated. Figure3.2.1 shows the model with boundary condition, in which the green color and the pink color indicated the coupling and constraint equation, respectively. To be able to achieve the cyclically boundary condition, all nodes on the boundary surfaces shall be rotated into the same global cylindrical coordinate system. The cyclically symmetric conditions were also required for the wind bags located outside the end boundaries on the shell Type C. The detail arrangement has been explained in the previous report [1].

Fictitious base support blocks were added beneath the integrated model to keep high local stress and deformation away from the structure. The model was restrained by one-nodal support that has vertical and toroidal constraints on the fictitious block. All the measuring units in the model are in international MKS system.

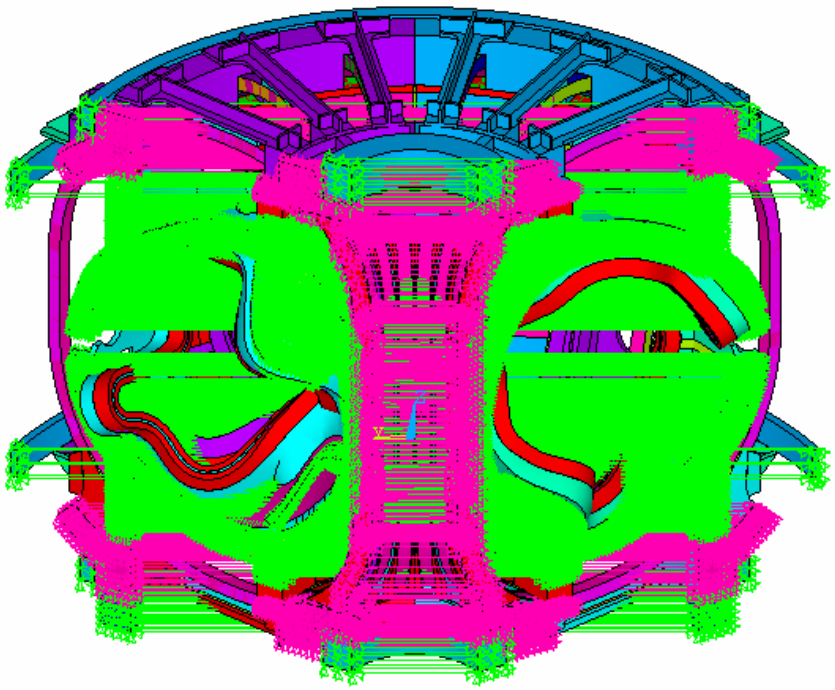

Fig. 3.2.1: Cyclic Symmetry Between θ=-60° and θ=+60°

3.3 Applied Coil Currents for EM Analysis

Reference [2] presents coil operating capability including turn per coil and all current waveforms. The listed current is the current in each turn, not the current in each conductor. Therefore, the modular coil currents will be the currents multiplied by the number of conductor turns. Table 3.3.1 lists the number of coil turns and turn currents at the full operation capability for the 2T high beta scenario that was selected in the EM analysis.

Table 3.3.1: Turn number of each coil set

Coil	M1	M2	M3	PF1	PF2	PF3	PF4	PF5	PF6	TF	Plasma
Turn No.	22	22	20	72	72	72	80	24	14	12	1
Turn Current	37190	37783	36538	-14615	-14615	-9054	-7498	460	453	-1301	0

For the current convention system, NCSX utilizes the cylindrical coordinate system with the Z-axis as vertical. A positive PF or plasma current is in the direction, which is counter-clockwise viewed from above. A positive poloidal current, such as TF or modular coil current, flows in the positive Z-direction in the inner leg.

3.4 Applied Loads for Structural Analysis

The individual loads are EM loads, cooling strain, and deal loads that including interface dead load from vacuum vessel and center stack. The cooling strain is the relative strain between modular coils and MCWF due to temperature changes during the modular coil VPI process and the initial cooling to the operating temperature of 85K. R & D test has indicated that the winding pack cure shrinkage is very small and negligible. The other test result shows that the CTE of the winging pack is slightly higher than the winding form and when the modular coil is cooled to 85K, the relative thermal strain between the modular coil and the winding form is about -0.04%.

To simulate the load case of cool-down of the modular coils, the equivalent temperature drop of 23.26K that is equivalent to coil strain of 0.04%, should be applied to the WP only. The temperatures on the other parts were kept unchanged.

To apply gravity load, specify gravity acceleration in a positive Z direction by using ACEL command. As the model does not contain vacuum vessel and center stack, the appropriate weight shall be added at the part interfaces. One third of center stack weight [5] is 1288.4 lbs (5731 N) and one third of vacuum vessel weight [6] is 4912.5 lbs. The weight of inside vessel components was estimated about 2000 lbs.

The structural analysis shall consider all possible loading combinations to determine the governing load case. Four load cases were defined in the analysis. They are (1) dead load only at room temperature, (2) dead loads plus cool-down to 85° K, (3) dead loads plus cool-down and EM loads at 85° K, and (4) dead loads and EM loads. The last load case assumes that the thermal strain during pulse will cancel cool-down strain.

Radial preloads for the TF coils was not considering in the analysis. Current design concept indicates that the preloads will be counter balanced by the ring tension of the inboard TF structure.

To accomplish this condition, the TF coils shall be preloaded before the TF structure attached to the MCWF.

3.5 Material Properties

The material properties are represented by isotropic materials with some modifications on the shear modulus of elasticity to consider the parts that are formed by the composite materials or possible surface sliding. The modular coil R & D test results [7] illustrate the flexural modulus of elasticity of the winding pact at 77K varies from 11.08Msi (76.4GPa) for bare Cu specimens to 7.37Msi (50.8GPa) for glass wrapped specimens. The longitudinal compressive test at room temperature [8] shows the modulus of elasticity at an average value of 9.11Msi (62.8GPa). As the test program has not yet established all of the required data for forming an orthotropic property, the analysis employed the smeared isotropic material property with a reduced longitudinal shear modulus of elasticity to consider the impact of possible contact sliding from the winding form.

The elastic modulus of MCWF casting alloy shall meet 145GPa at 77° K [9]. The flange shim insulations placed between toroidal flange joints are formed with a 3/8-in SS covered by 2 layers of 1/16-in G11. The equivalent isotropic properties were calculated for their material properties. The casting TF structure has not completed the design yet. Its elastic modulus was assumed to be the same as the MCWF. Table 3.5.1 summarizes the material properties of all components. In the Table, the shear modulus G with a sign of "*" is calculated from the isotropic material relationship. The shear rigidities of shims for the TF and PF coils are decreased for the intention of less resistance to the coil expansion movements. For the modular coils, the longitudinal direction is Z for the element coordinate system. The 1st shear modulus is for Gxy and the 2nd shear modulus is for Gyz and Gxz. The much small values for the Gyz and Gxz intend to limit the shear impact on the contact surfaces and lower the composite action with the MCWF.

Table 3.5.1: Material properties of components

	E (MPa)	G (MPa)	CTE (m/m/°K)	Density (kg/m^3)	Poisson's Ratio
MCWF	145,000	*	1.700E-05	7750	0.31
Modular coil	63,000	26250 / 525	1.720E-05	8500	0.20
MCWF toroidal shim	150,000	*	1.700E-05	7750	0.27
MCWF poloidal shim	193,000	*	1.700E-05	7750	0.31
MCWF wing bag	13,750	*	3.000E-05	1820	0.32
Wing bag image	6,894	*	3.000E-05	0.1	0.32
PF coil	120,000	*	1.600E-05	8300	0.33
PF6 coil bracket	193,000	*	1.700E-05	7750	0.31
PF coil support shim	22,000	440	1.720E-05	1900	0.21
TF coil	120,000	*	1.600E-05	8300	0.33
TF coil side shim	22,000	440	1.720E-05	1900	0.21
TF coil top/bot shim	95,000	950	1.700E-05	7750	0.31
TF coil wedge spacer	145,000	*	1.700E-05	7750	0.31
TF structure	145,000	*	1.700E-05	7750	0.31
TF structure tie bar	145,000	*	1.700E-05	7750	0.31
TF structure shim	22,000	*	1.720E-05	1900	0.21
Connecting block	145,000	*	1.700E-05	7750	0.31
Base support block	193,000	*	1.700E-05	7750	0.31

4.0 Results and Interpretations

4.1 EM Analysis

Figure 4.1-1 demonstrates the flux density contour plot, in which the maximum flux density is 4.901 Tesla in the modular coil. The maximum flux density equals to the value of the previous analysis [1] which has same currents in the modular coils and the TF coils. The currents in the PF coils have some variations.

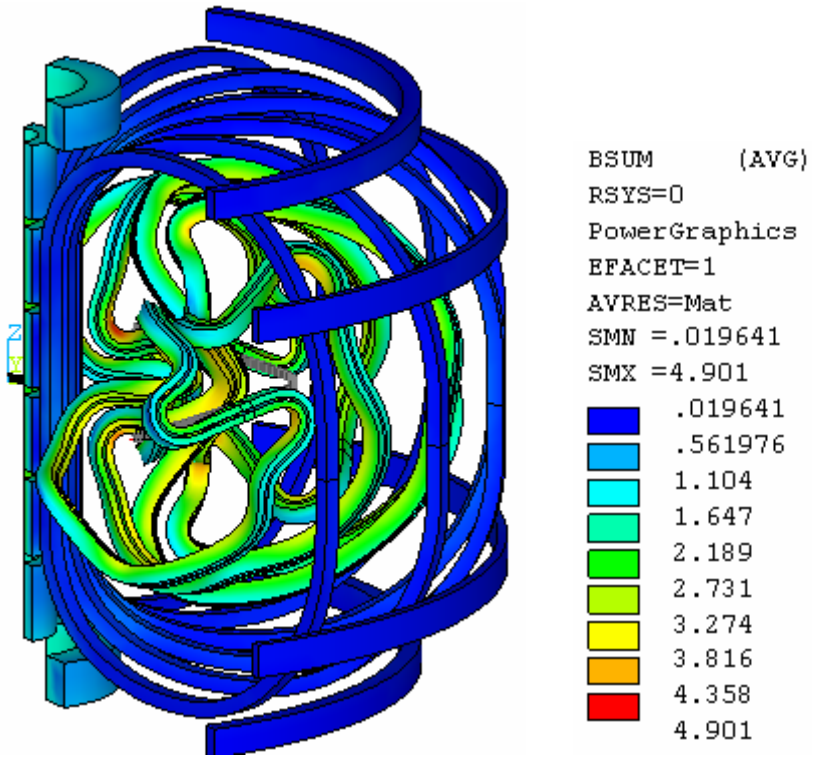

Fig. 4.1-1: Flux density contour plot

Figure 4.1-2 displays the magnetic forces that show the magnetic forces in the TF, PF5, and PF6 coils are very small in comparison with the forces in the modular coils. Because of the stellarator stmmetry, the net EM force components in the vertical and toroidal directions are equal and opposite for the three right-hand-side modular coils and the three left-hand-side modular coils that result in net zero forces.

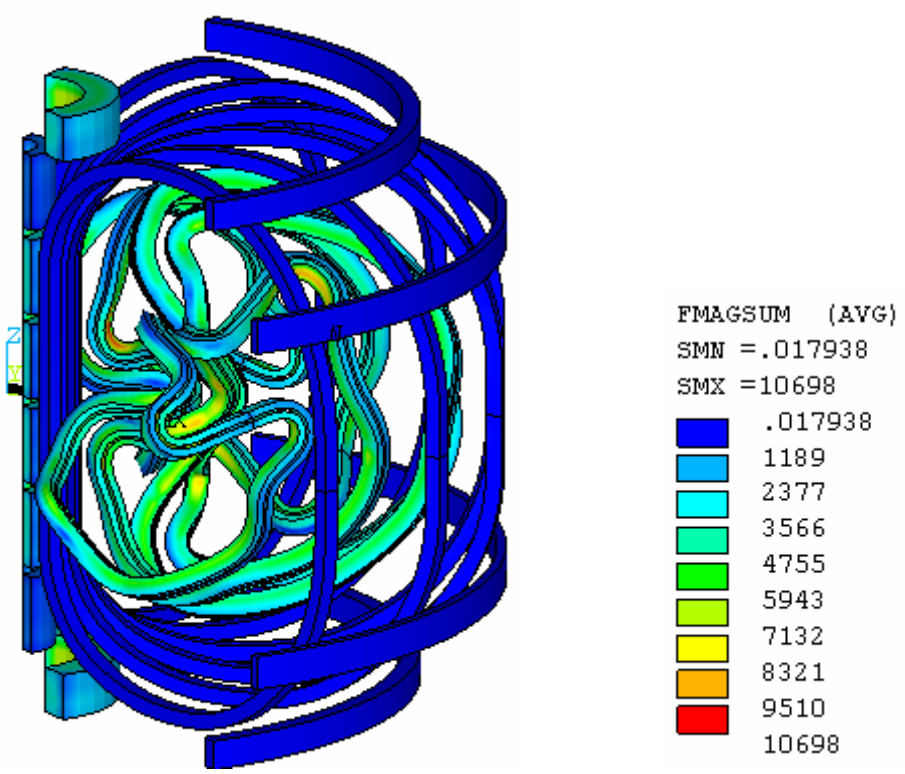

Fig. 4.1-2: Element vector forces of Type B modular coils

4.2 Structural Analyses

Four load combination cases representing four stages during operation as shown in Section 3.4 were run in the analyses. As the interest in the analysis will be focus on the MCWF joints, the results will put emphasis on the MCWF structure and the toroidal flange joints.

4.2.1 Displacements

The cool-down displacement calculation was based on the relatively thermal strain between the modular coil and the winding form, from which the thermal stresses were induced. The free thermal displacement from the room temperature to the 85K that does not generate thermal stresses in the structure did not include in the analysis and the following displacement values.

The integrated structure is supported at the edge of the outboard leg with vertical and toroidal constraints. The maximum displacements of the four load cases are illustrated in Table 4.2.1.1. For the dead load, the maximum displacement occurs at the mid-section between supports. During the cool-down, modular coils shrink more than the MCWF that causes bending moments in the combined section of MC and MCWF and yields greatest displacement on the wings of MCWF. With the DL and EM loads, the maxim displacement is 2.604 mm, occurred at the modular coil Type B. The maximum displacement in the MCWF is 2.371 mm, located near the maximum coil displacement in the shell Type B.

Table 4.2.1.1: Structural Displacements of Four Load Cases

	Dmax (mm)	Uz-max (mm)	Uz-min (mm)
Dead load	0.384	0	-0.384
DL + Cooldown	0.595	0	-0.517
DL + Cooldown + EM	2.559	1.104	-1.318
DL + EM	2.604	1.091	-1.285

The vertical displacement contour plots for the dead load only and the dead loads plus EM loads are illustrated in Fig. 4.2.1.1 and Fig. 4.2.1.2, respectively. The unit of displacement is meter. In the case of only the dead loads (Fig. 4.2.1.1), the vertical displacements are greater in the inboard region than the outboard region. If more evenly distributed displacement is preferred, the location of the supports shall be moved toward the inboard leg. In Fig. 4.2.1.2, the vertical displacements in the right-hand side are opposite to the left-hand side mainly due to stellarator symmetry of the EM loads.

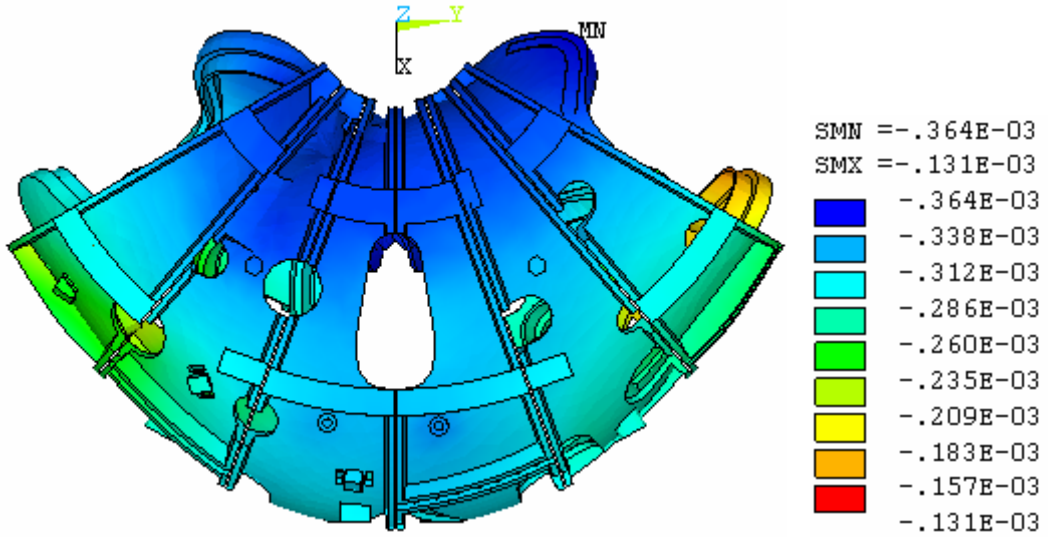

Fig. 4.2.1.1: Vertical displacement (Uz) for dead loads

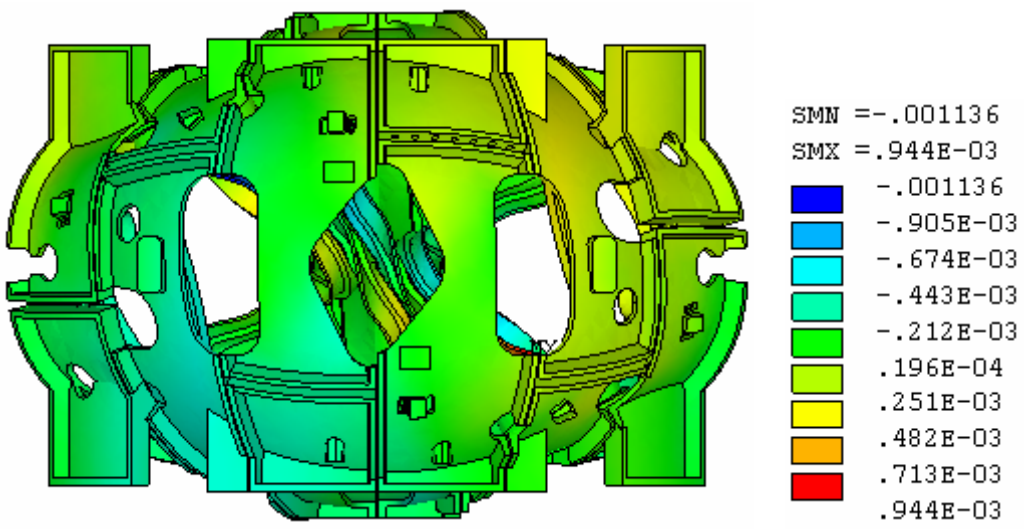

Fig. 4.2.1.2: Vertical displacement (Uz) for DL plus EM loads

4.2.2 Stress in MCWF

A review of the stress results demonstrates the Load Cases 3 and 4 are the leading cases for the structural responses primarily due to the EM loads. Examining stresses on all parts show that the maximum stress takes place at the MCWF toroidal shim AA for the Load Case 4, as shown in Fig. 4.2.2.1. The peak stress is confined locally at the corner of an element and therefore it is not a great concern.

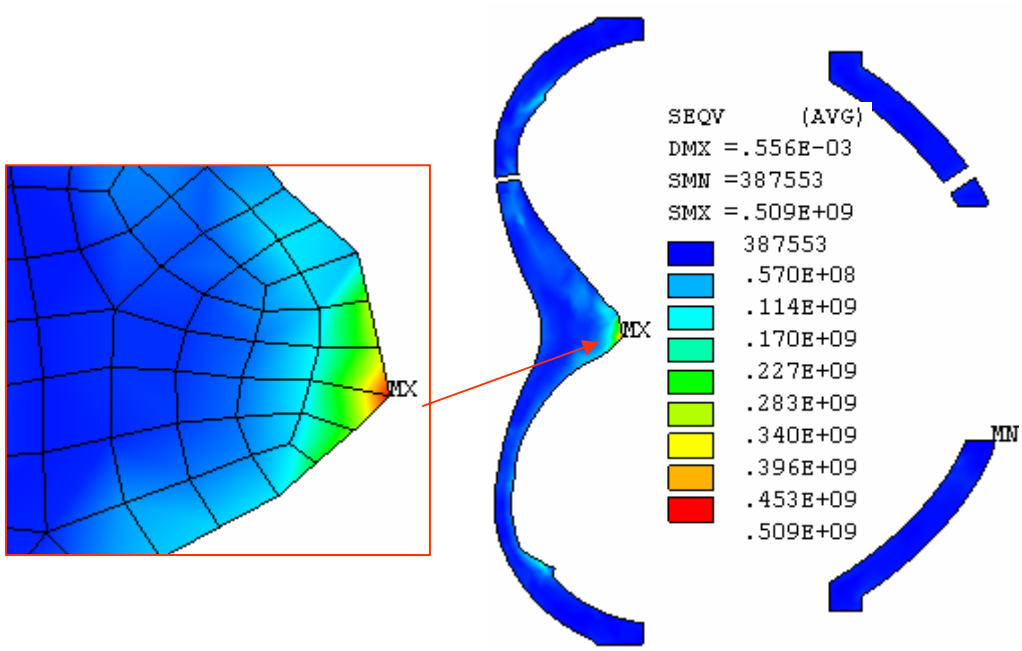

Fig. 4.2.2.1: Peak local stress from DL plus EM loads

For the dead load plus EM load, the von Mises contour stress of the MCWF, which is the major load-carrying element, is shown in Fig.4.2.2.2. The maximum stress of 220 MPa (31.9 ksi) was found at the inboard location of the shell Type A, as shown in the Fig. 4.2.2.3. The peak stress is

limited to a small area, near the maximum stress spot on the toroidal shim AA displayed in Fig. 4.2.2.1. The stresses in the other areas are much smaller than the maximum value.

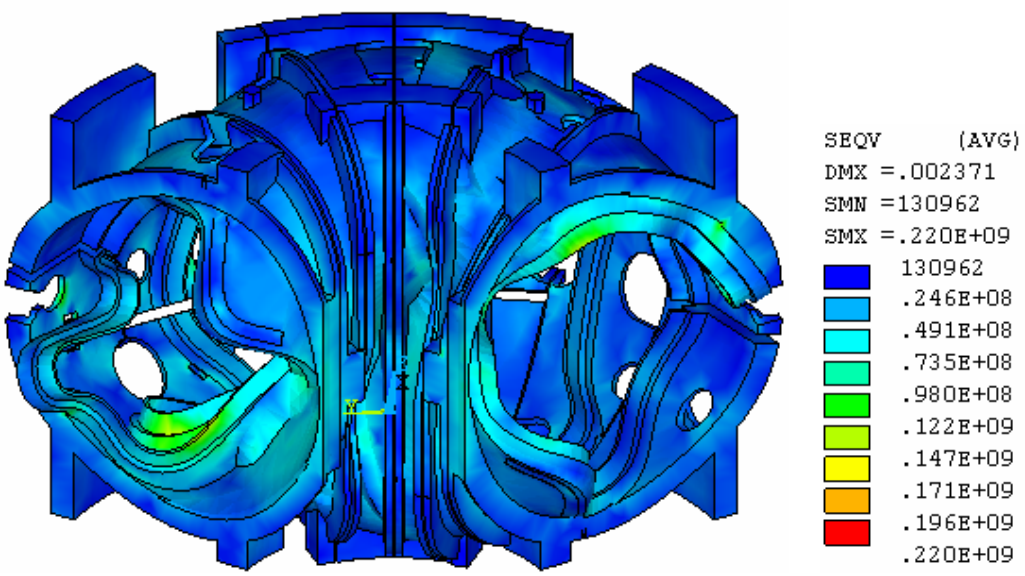

Fig. 4.2.2.2: MCWF von Mises stress from DL plus EM loads

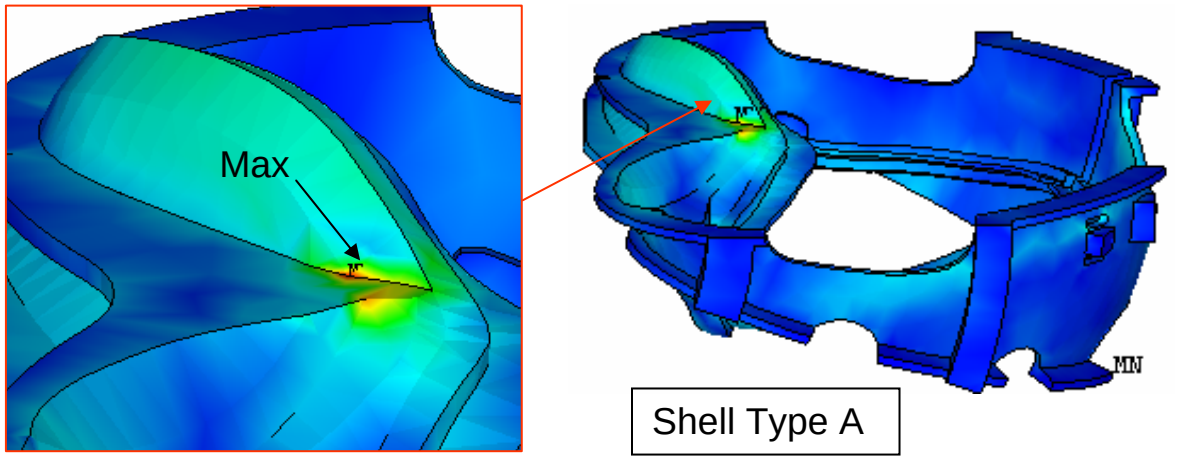

Fig. 4.2.2.3: Maximum von Mises stress from DL plus EM loads

The shell structure is made of stainless steel casting. According to the NCSX design criteria (see Ref. [12]), the allowable stress for the membrane plus bending will be 322.5 MPa or 46.78 ksi [15], which is larger than the maximum stress.

4.2.3 Stress in Coils and TF Structure

On the base of the selected material properties and the assumed bonding contact behavior, the longitudinal stresses contour plot for the modular coil Type A, which have the highest stress, is illustrated in Fig. 4.2.3.1 from DL and EM with and without cool-down effects. The load case with

cooldown yields more tension in the coils than the load case without cool-down because of additional shrinkage in the modular coils than the winding form.

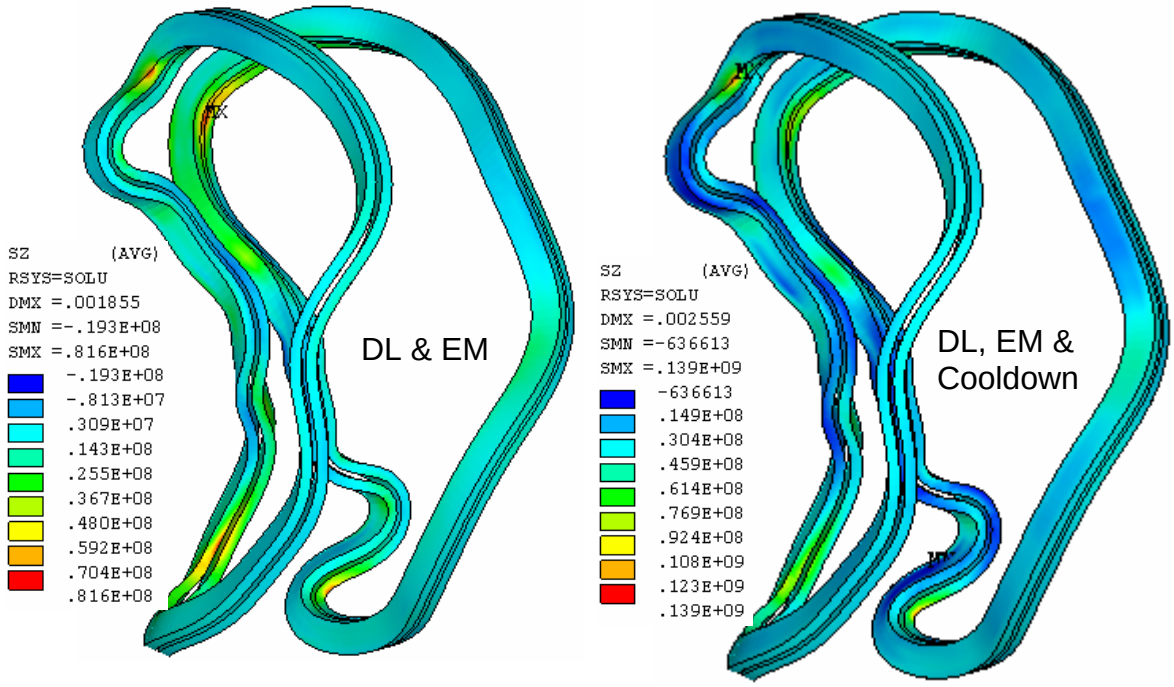

Fig. 4.2.3.1: Axial stress of coil Type A from DL and EM with and without Cool-down

The currents used in the analysis for the PF coils and TF coils do not represent the highest currents in the coils and, therefore, the stresses in those coils are not considered to be the critical stresses. It is noted that the PF coils are constrained on the TF structure. The displacements of the integrated structure, especially the vertical displacements, have more impact on the stresses in the PF5 and PF6. Figure 4.2.3.2 exhibits the axial stress contour for the PF5 and PF6.

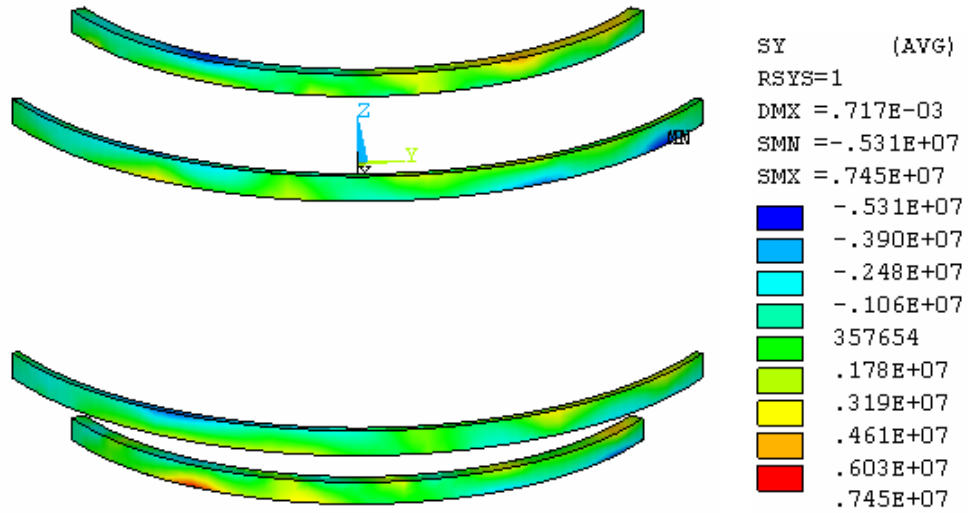

Fig. 4.2.3.2 Axial stress of PF5 and PF6 from DL plus EM loads

The design of TF structure has not completed yet. From the applied DL and EM load, stress contours of the lower TF structure are given in Fig.4.2.3.3. The toroidal stresses are shown on the left side and the von Mises stresses are shown on the right side. The results are not necessary represent the critical load condition due to the input currents. However, it indicated two structural behaviors: (1) the outer TF structure subjected to bending in the toroidal direction under the vertical deformation of the integrated structure, and (2) the maximum stress will be at the lower TF structure near the base support.

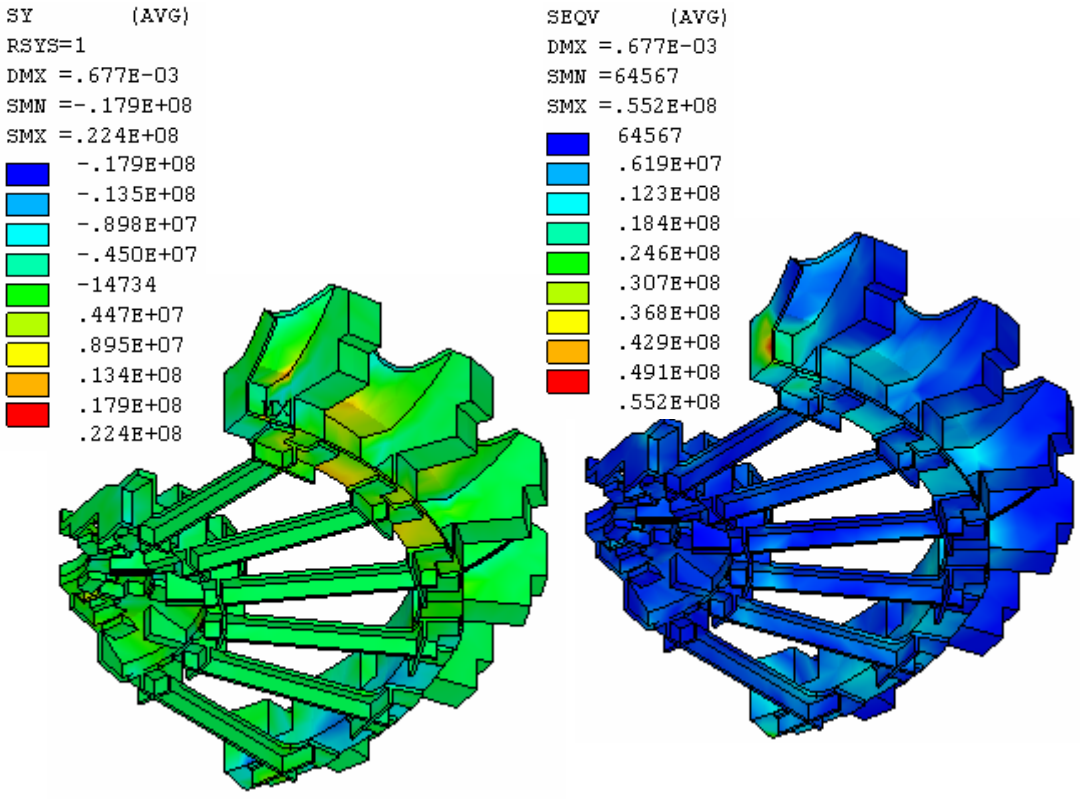

Fig. 4.2.3.3: Axial stress of PF5 and PF6 from DL plus EM loads

4.2.4 Base Support Reactions

The support reactions from the four combined load cases are listed in Table 4.2.4.1. They are only vertical and toroidal restraints at the support. Because of the stellarator symmetry, the EM loads do not transfer to the support. Neither the thermal strain from the cool-down produces loading on the support. The only loading that transfers to the support is the dead load, resulting a vertical reaction of 339.4 KN (76.3 kips).

All four load cases post almost the same reactions. The small force variations in the toroidal direction are caused by nonlinear convergence and FEA model. The nodal points and elements in

the model are not totally symmetric with respect to the middle of the cross section, although the CAD geometries are symmetry.

Table 4.2.4.1: Support Reactions for Four Load Cases

	Fr (KN)	Fθ (KN)	Fz (KN)
Dead load	0	0.074	339.4
DL + Cooldown	0	0.077	339.4
DL + Cooldown + EM	0	0.280	339.4
DL + EM	0	0.283	339.4

4.2.5 MCWF Toroidal flange Joints

The model did not include any bolts or any bolt preloads in the toroidal flange joints. An investigation of MCWF bolt joints [10] was performed by A. Brooks based on the net bolt preload of 45797 lbs for the 1 3/8" bolt. The flange was divided by several regions as shown in Figure 4.2.5.1 in according with the discontinuation in the flanges and at inboard regions without bolt connection (green color). In each region, the normal force and the shear force were evaluated from the FEA results. The required coefficients of friction to prevent slip were then calculated and plotted for all the flange regions.

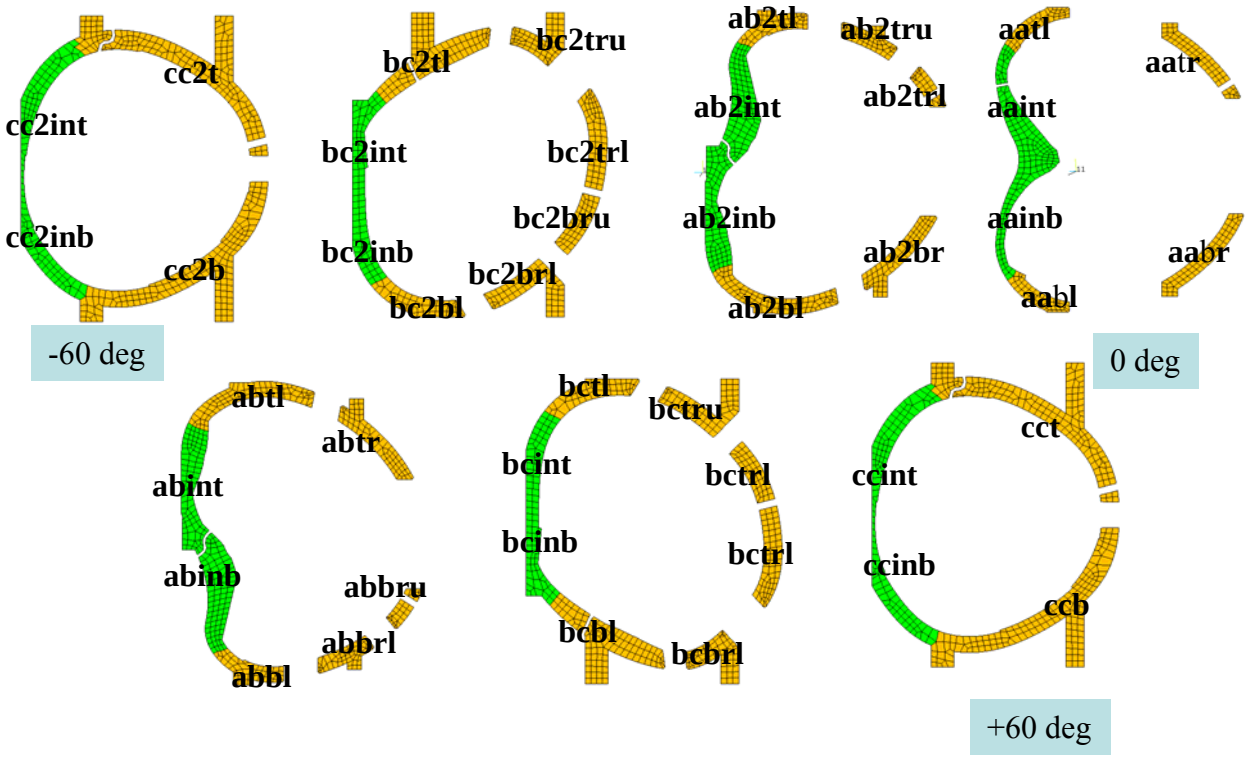

Fig. 4.2.5.1 Designated names in flange regions for selected bolt groups

Figure 4.2.5.2 illustrates the coefficients of friction needed [11] to prevent slips for EM load at the MCWF toroidal flange joints from two FEA models, one with MCWF only (red color) and the other with integrated model (blue color). The side-by-side result comparison shows the influence of adding TF structure in the model. Some improvements are found in most of regions. However, the shear forces in many regions are much higher than the allowable coefficient of friction, 0.15, prescribed by the design criteria [12]. The results indicate that the TF structure can assist in carrying loads to the base support, if the TF structure shim joints are fully bonded and good enough to maintain the bending, torsional and shearing stiffness along the longitudinal direction as assumed in the integrated model.

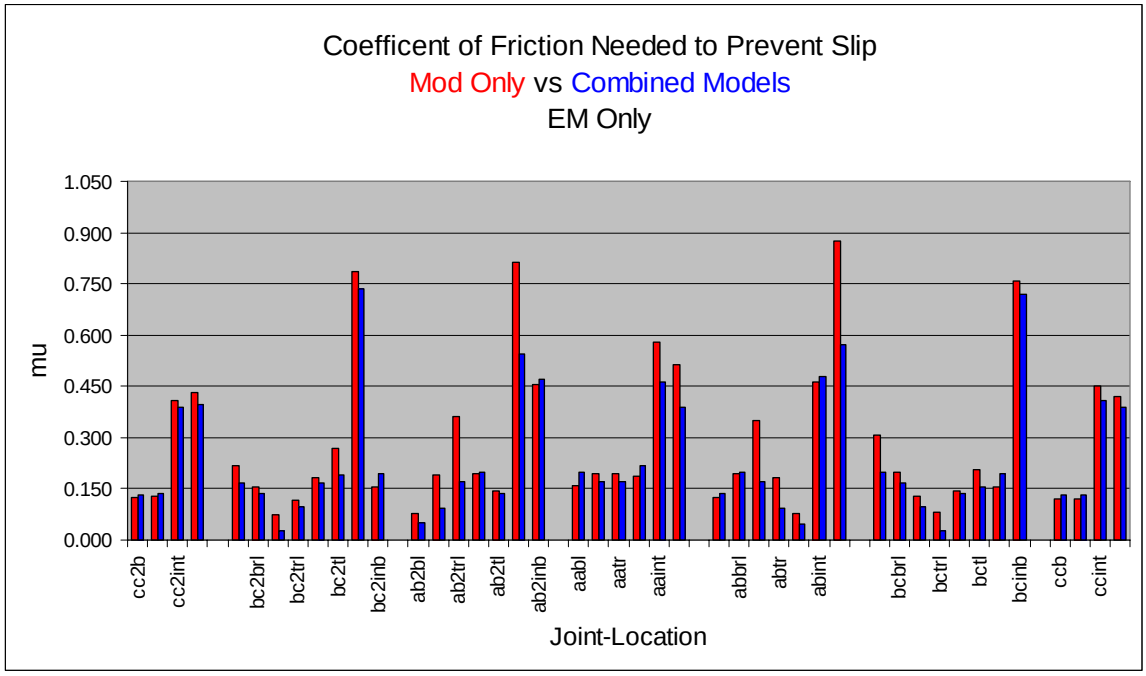

Fig. 4.2.5.2 Comparison of required coefficient of friction at bolt joints for two models with EM only load case

Figure 4.2.5.3 [11] illustrates the coefficient of friction needed to prevent slips on the integrated model that subjected to the dead loads and EM loads with or without cool-down strain. A comparison of the required coefficients of friction shows that the thermal strain from the cool-down has only small effects at flange joints. The worst location for the joint slip is at the inboard flange joint B-C.

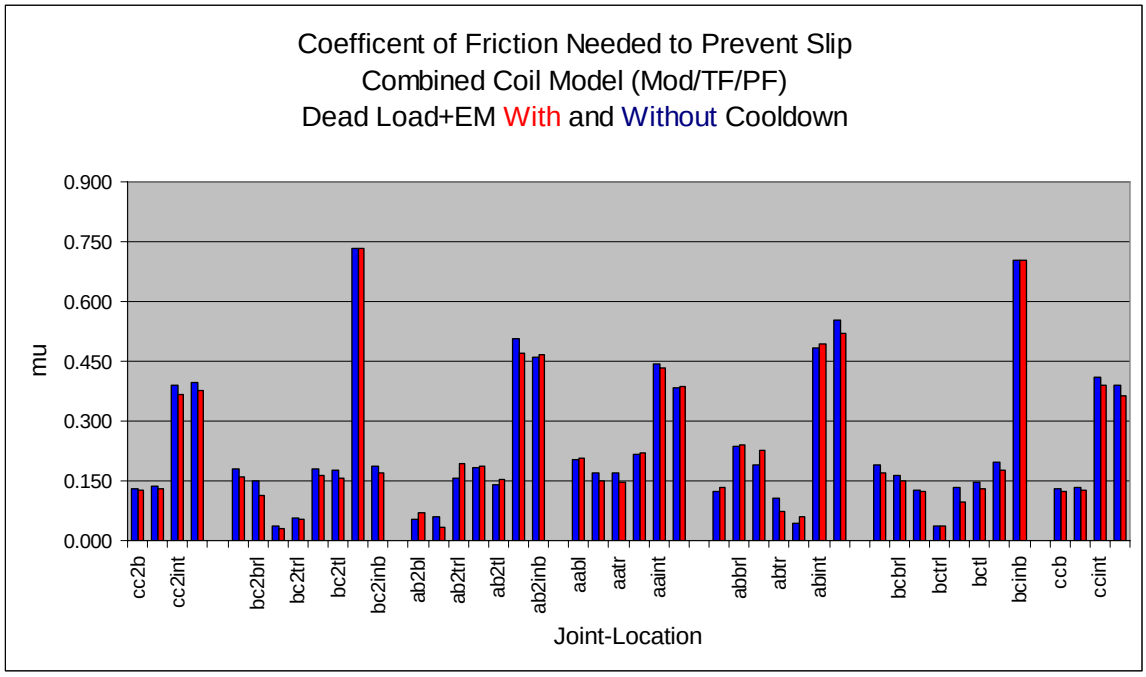

Fig. 4.2.5.3 Comparison of required coefficient of friction for DL and EM load with and without cooldowm.

The approach for calculating required coefficients of friction yields accurate results only when the center of load matches the center of the bolt group in each region. As the joint loads are not uniform along the flanges, the resulting load centers and the bolt group centers, in general, will not be coincident. To avoid obvious discrepancy, it is suggested that some regions should be subdivided into smaller areas, such as regions CCB, CC2B, CCT, and CC2T.

4.2.6 Wing Bags

Wing bag was designed to carry the loads from the wing to the next shell segment. The amount of load transfer depends on the stiffness of the wing bag, the contact behavior and the stiffness of wing. The model assumed wing bag shim was bonded to shell on one side and had frictionless contact behaviour to the adjacent shell on the other side. This is the only nonlinear action in the model in order to predict more appropriate load-transferring mechanism. The analysis presumed that the modulus of elasticity of wing bag was 13,750 MPa.

Figure 4.2.6.1 shows a contour plot of the wing bag contact pressure at the shell Type A for the DL and EM loads. The unit of contact pressure is Pascal. Positive pressure indicates load toward the surface and therefore is in compression. The distribution of the contact pressure is not very uniform on the contact surface. Most effective spot on the wing bag locates near the cantilever end of the wing. The maximum contact pressure is 128 MPa (18.6 ksi.), occurred on the wing bag at shell Types B.

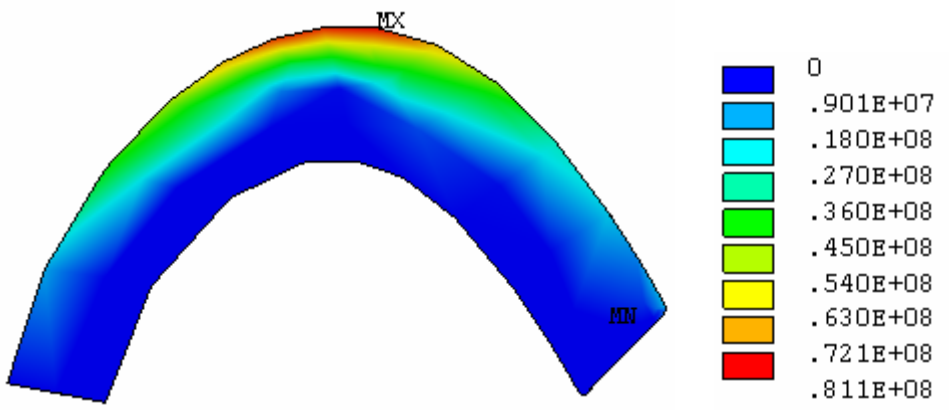

Figure 4.2.6.1: Contact pressure on wing bag at shell Types A

4.2.7 Commands in Solution Phase

The integrated FEA model database file "file6.db" includes the support constraints and the EM loads for 2T high beta scenario at 0 seconds. When the support location or the EM load changes, the corresponding nodal constraints or the nodal forces should be removed and replaced.

The inputs of dead loads make use of the ANSYS acceleration command "acel' and add in the proper weights from PF coil center stack [13] and vacuum vessel [14]. For conservative, these additional weights are supported on the upper structure. The input commands are:

```
acel,,,9.806
csw=-3865*4.448/6          ! center stack weight/6
f,278757,fz,csw
f,299941,fz,csw
esel,s,mat,,90             ! vacuum vessel
nsle
nsel,r,loc,z,nz(261533),nz(261533)
f,all,fz,-6900*4.448/32
allsel
```

The relative thermal strain between the modular coils and the winding form is about 0.04% when they are cooled to 85K. By setting up the reference temperature at 0° K, the equivalent modular coil temperature becomes -23.2558° K. The input commands are:

```
tref,0
esel,s,mat,,1,3       ! MC
nsle
bf,all,temp,-23.2558
allsel
```

The displacement criterion was used for the nonlinear convergence criteria. As the load case including EM load was more difficult to converge due to coarse elements, a separate convergence tolerance value was selected depending on the load case with or without EM loads

```
    cnvtol,u,,0.05              ! without EM loads
or
    cnvtol,u,,0.05*2.1          ! with EM loads
```

5.0 Discussions

A FEA model of integrated structure was created with the main interest in studying the MCWF joints during the operation stages. As previous model did not include the TF structure, it is essential to understand what will be the impact on the MCWF joints by adding the TF structure.

In order to run the ANSYS model in a PC with 32 bits and 1.5 GB memory, it is necessary to keep the model within a proper size. For this, fillers and chamfers in the Pro/E geometry were removed. Most of the element sizes are not fine and those parts that have few contributions to the model stiffness were eliminated, such as the PF coil center stack and the vacuum vessel assembly. The complex clamp system for the modular coil was removed, and instead, the modular coils were bonded to the MCWF to assure a stable condition.

The model assumed all contact surfaces were bonded except for the wing interfaces that used frictionless contact elements through the wing bag shims. In the real case, the modular coils, TF coils, and PF coils are not exactly bonded to the structure. Some bolt joints may not be firmly connected on contact surfaces. It is recommended that additional runs by changing contact behavior or by modifying the material properties shall be performed to assess the impact of modeling assumptions.

Stress in the coil is derived from the displacement and the material property. If the accurate stresses of coils are wanted, suitable orthotropic material properties shall be provided and correct contact assumptions shall be presented. To simulate the sliding condition on the MC contact surfaces, an approximate approach may be used by distorting the shear moduli of one of contact part to a very small value without changing the bonded contact behavior. This may be useful for the TF coil shims too.

The currents in the TF and PF coils do not have the highest currents. The stresses in this EM load case do not stand for the critical load case for the TF and PF coils and possibly the TF structure.

Bolt joint contact was assumed to be always bonded. If there was a possibility of partial opening at the joint due to insufficient or unevenly distributed bolts, a standard contact element shall be used.

The stellarator symmetry of the support system makes certain that there are no EM loads transferring to the base support. The analysis did not cover the seismic loads and some interacting forces from the attached components. Therefore, the main load on the support is the dead weight. The support location can be modified to test the best support location.

The selected EM loads from currents at 2T high beta current scenario have the highest currents in the modular coils. Additional load cases may be run to verify the present case is the worst case.

The investigation of the bolt joint was based on the net bolt preload of 45797 lbs. It considered neither the impact of preload variations due to the temperate change, nor the loss of preload due to the creep of insulation materials.

6.0 References

[1] H. Fan, "Nonlinear Analysis of Modular Coil and Shell Structure", NCSX-CALC-14-001-001, February 3, 2006

[2] Engineering Technical Data "C08R00_C8_Ultimate.xls", January 14, 2006, PPPL NCSX web site

[3] B. Nelson, "Requirements for stellarator core support", March 14, 2006

[4] H. Fan, "Descriptions of the NCSX Integrated Model – file6,db", PPPL Email, July 18, 2006

[5] Drawing No. SE132-001 "Centerstack Assembly PF Coils 1, 2, & 3",

[6] F. Dahlgren, Nastran FEA model "model21bbe2a.dat"

[7] T. Kozub, "NCSX Composite Coil Tests", March 15, 2004, PPPL NCSX web site

[8] T. Kozub, "NCSX Composite Coil Tests", April 5, 2004, PPPL NCSX web site

[9] P. Heitzenroeder, "NCSX Product Specification Modular Coil Winding Forms", NCSX-CSPEC-141-03, February, 7, 2006

[10] A. Brooks, "MCWF Toroidal Joint Concerns", PowerPoint presentation attached in the email dated February 28, 2006

[11] A. Brooks, "Analysis of Coil Structure", PowerPoint presentation attached in the email dated July 12, 2006

[12] I. Zatz, Editor, "NCSX Structural Design Criteria, Draft E", May 10, 2004, PPPL web site

[13] NCSX Drawing No. SE132-001 "Centerstack Assembly PF Coils 1, 2, & 3",

[14] F. Dahlgren, Nastran FEA model "model21bbe2a.dat"

[15] P. Heitzenroeder, "FEA Analyses Results of the A1 Casting with Thin Wall Regions", E-Mail attachment, August 8, 2005

NCSX

Design Basis Analysis

Modular Coil Thermal Analysis

NCSX-CALC-14-002-00

Draft A

13 July 2004

Prepared by:

_____

K. Freudenberg, ORNL

I have reviewed this calculation and, to my professional satisfaction, it is properly performed and correct. I concur with analysis methodology and inputs and with the reasonableness of the results and their interpretation.

Reviewed by:

_____

B. Nelson, ORNL Engineer

Table Of Contents

I. Executive Summary

The purpose of this analysis is to examine the heat transfer characteristics of a local model of a 10 turn modular coil during and after an operational pulse. Each pulse generates a tremendous amount of heat in the winding coils that must be removed by cooling tubes such that the coil packs return to a baseline cryogenic temperature of about 85 K within 15 minutes. Also, the conduction path is varied by removing and/or adding copper cladding at several corners to determine the most financially and thermally economical option.

II. Assumptions

- Initially temperature of all components = 80 K (cryogenic)
- Heat from the pulse is imposed as a uniform volumetric heat generation (7.58E7 W/m^3 for 1 sec) and is applied to the Cu/epoxy winding pack only.
- Cooling from the fluid in the tubing is imposed as constant temperature of 80 K throughout the 15 minute cycle.
- Radiation exchange with other surroundings is negligible.
- Material properties are temperature dependent (see table below in material property section)

III. Analysis Methodology and Inputs

For this study, the maximum temperature of the coil must return to approximately the same starting temperature of 80 K after 15 minutes. Although, there is no definitive temperature limit defined, it is generally accepted that the temperature should reach steady state equilibrium of less than 95 K when considering ratcheting temperatures after each successive pulse. This ensures that the liquid Nitrogen in the cooling tubes will not see a large delta T across its outer boundary and thus boiling will not occur. The model is a representative straight 3d section of the modulator coil pack and is not an actual section of a production coil form that has twists and turns.

Software and data files

The model is constructed in Ansys 8.0 and all of the preprocessing and post processing is done within the Ansys environment.

Drawings and models

No drawings have been referenced in this study. All models have been created as Ansys files.

Material properties

The temperature dependent material properties are listed in Table 1. For clarification, the insulation is the material that surrounds the winding cable and the glue is the material that is used to connect the copper cladding layers together and used in the "crimp" joints. Also, for modeling and meshing purposes it is necessary to model the glue as thicker than it is in reality, otherwise an extremely large mesh will result. The glue is 0.2" thick in the model and is approximately 0.05" in reality, thus the conductivity has been multiplied by 4 to account for this scaling factor.

Table 1: Material property data

Cp (J/kg K)	80 K	100 K	150 K	200 K
Winding cable	171.4	212.3	270.1	300.7
Cu Cooling Plate	205.1	255.3	324.1	359
Insulation	348.9	413.7	537	626.8
SS Tee	215.3	275.5	362.1	416.4
glue	348.9	413.7	537	626.8
K (W/m K)	80 K	100 K	150 K	200 K
Winding cable (x, y direction)	7.5	7.5	7.5	7.5
Winding cable (z direction)	300	300	300	300
Cu Cooling Plate	529.3	461.5	418.1	407
Insulation	0.227	0.252	0.396	0.322
glue (4 * insulation)	0.91	1.01	1.58	1.29
SS Tee	8.114	9.224	11.17	12.63
Density (kg/m^3)	80 K -200K			
Winding cable	7028			
Cu Cooling Plate	8900			
Insulation	1200			
SS Tee	8030			
glue	1200			

Model setup

The model has been meshed with Solid 90 elements for the thermal analysis. Only half of the coil is measured as it is symmetric about its central axis. A detailed view of the elements and model are shown below in Figure 1, with the corresponding material color guide. Several cladding connecting scenarios were examined and detailed in Figure 2 and in Table 2. In addition, the effect of thermal conductivity and the presence of the tee (which acts as a heat sink) are also studied to determine a range of plausible temperature values. The connections between the cladding pieces and the crimp joints have been modeled using blocks of material with conductivity values documented above in material properties. These blocks conventionally represent contact resistance in heat transfer.

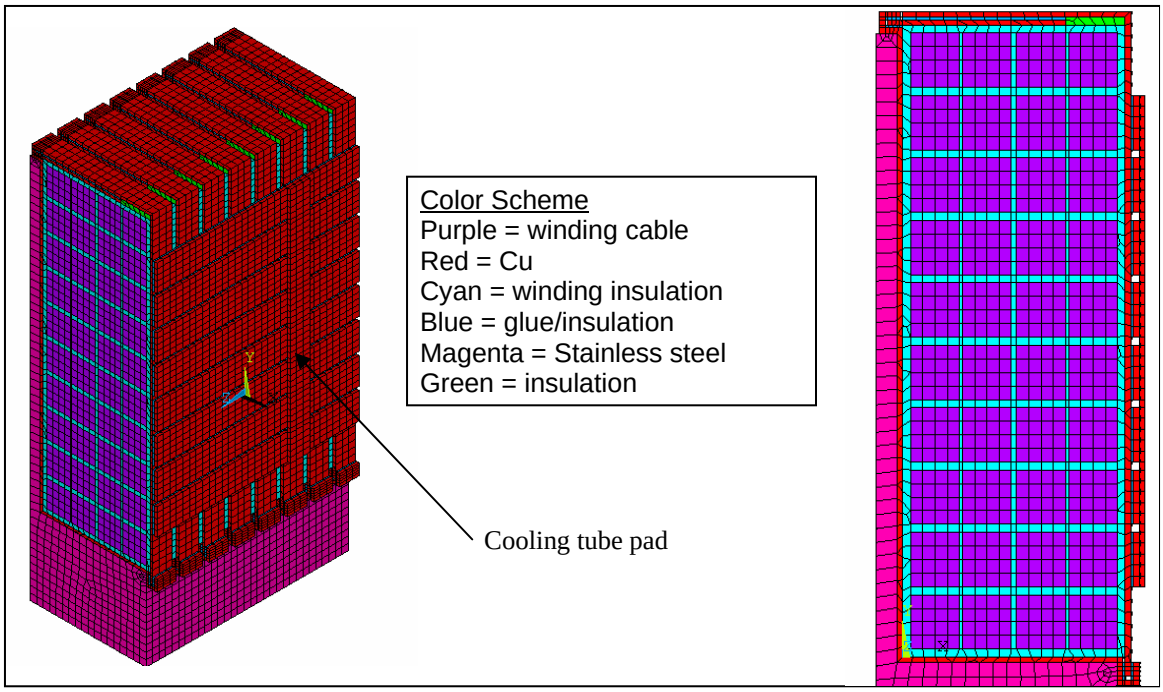

Figure 1: Mesh used to model winding pack section

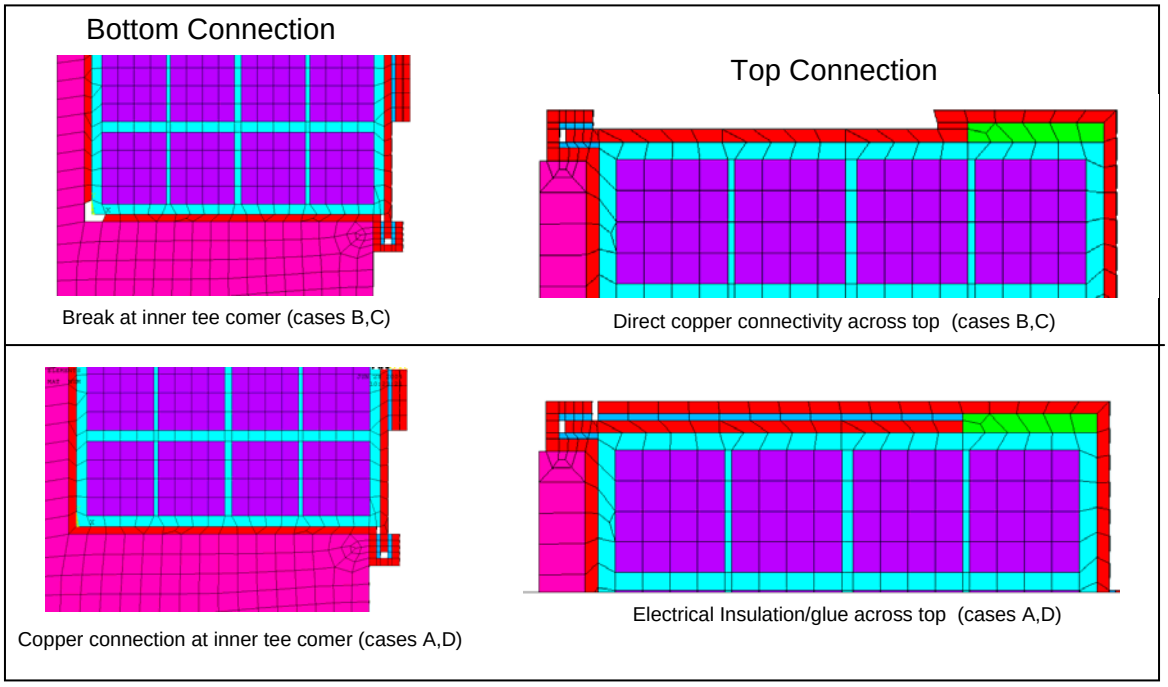

Figure 2: Cladding connection configurations, upper insulation alternatives.

Placing a break at the inner corner of the tee cladding connection (top image in Figure 2) will allow the removal of a piece of electrical insulation from the top connection and provide an easier construction method to ensure electrical isolation. The lower image in Figure 2 is the default baseline from which all comparisons in this document are based.

Table 2: Description of cases considered in Ansys

	baseline (A)	B	C	D	E (no Tee)	F (no Tee)
Break at inner tee corner of Cu clading	no	yes	yes	no	no	yes
Direct Cu Connection across top	no	yes	yes	no	no	yes
glue/insulation conductivity (W/mK)	0.91	0.91	100	100	0.91	0.91

The chosen glue conductivity values in this study are intended to illustrate a range of plausible maximum temperature values as the minimum conductivity value is perhaps too conservative and the maximum value of 100 W/m-K is most likely unachievable.

Thermal analysis setup

A transient thermal analysis was run on the representative modular coil shown above. Initially, all temperatures are set to 80 K, cryogenic conditions. The heat generation term of 7.58E7 W/m^3 is applied to the winding cables for one second and then the model is allowed to cool by means of a constant temperature of 80 K applied to the cooling tube pad, indicted in Figure 1, for 15 minutes. The process is then repeated with the final nodal set temperature from the previous 15 minute cycle used as the beginning temperature set of the next cycle. This process is generally carried out at least 5 cycles so that a steady state equilibrium can be reached and the effect of ratcheting is known.

IV. Results

Cladding configuration comparisons

The contour plots after the first 15 minute cycle are shown below in Figure 3 for cases A and D. These two cases are grouped together to show the effect of changing the glue/crimp conductivity form 0.91 W/mK to 100 W/mK. The max temperature for the baseline case is 88.452 K where as the max temperature for the higher conductivity case is 85.251 a difference of about 3.2 degrees. Thus for geometric situation where a direct cladding connection is used at the inner tee corner and an insulation pad is placed at the top connection to ensure electrical isolation the max temperature after 15 minutes will fall between 85.2 K and 88.5 K.

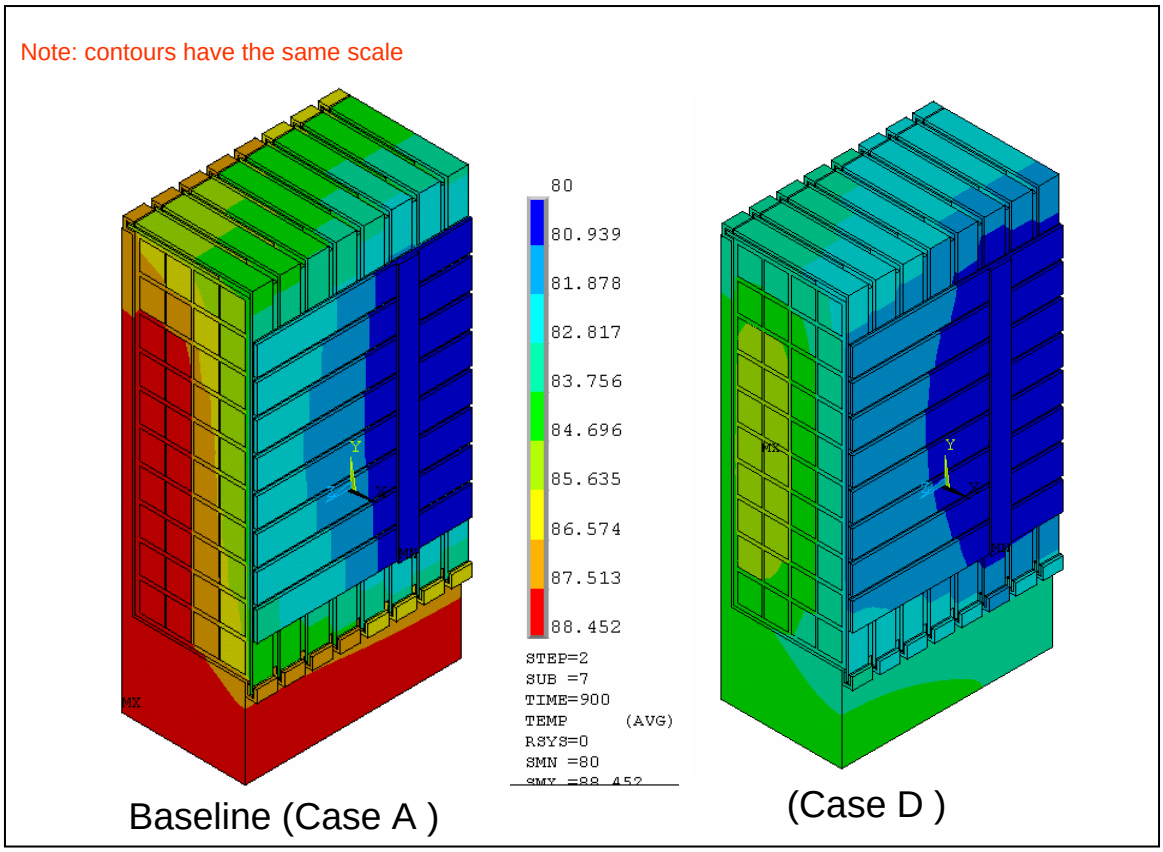

Figure 4: Temperature distribution after the first pulse (Different glue/crimp conductivities)

Figure 5 illustrates the second geometric case where the cladding junction corner with the tee has been split into two pieces and the top cladding connection no longer requires electrical insulation. Case B has the lower conductivity value of 0.91 W/m-K and case C has the upper conductivity of 100 W/m-K. The maximum temperatures for both cases are 88.79 and 86.074 respectively.

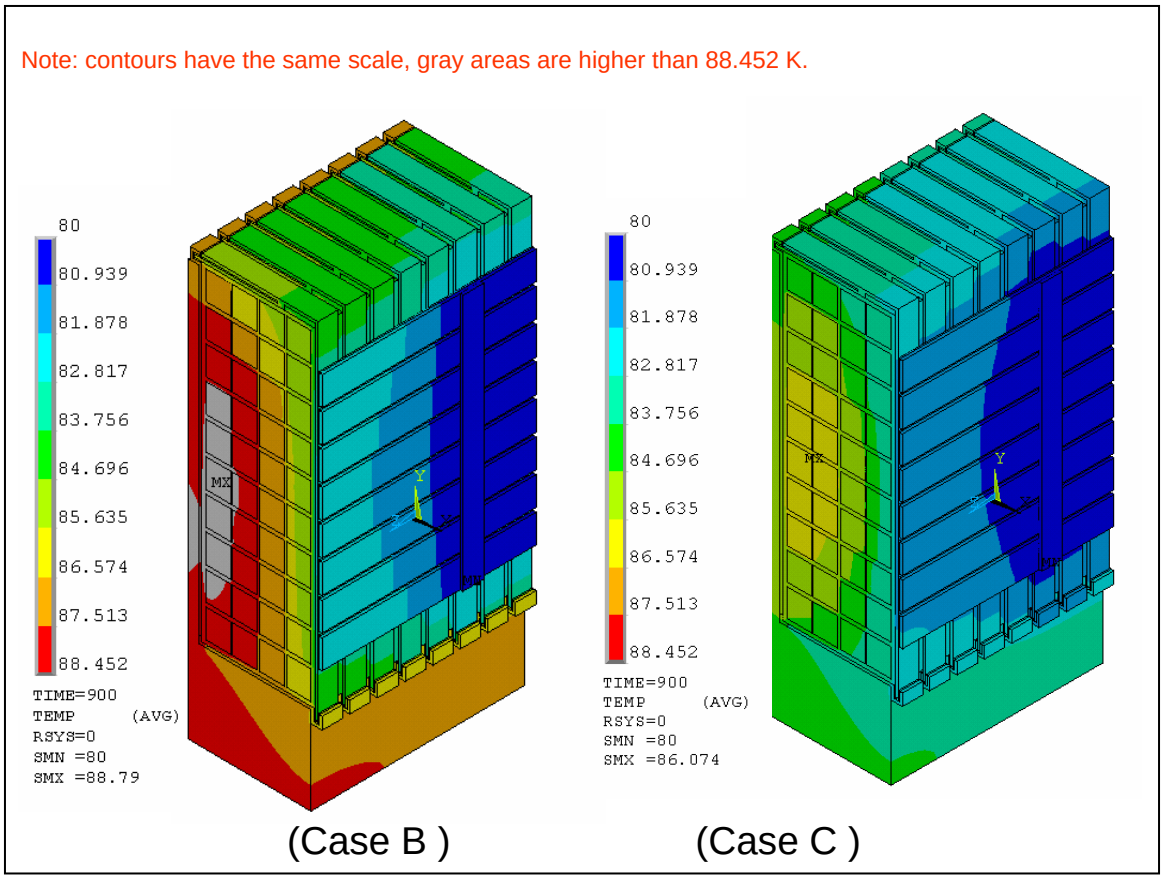

Figure 5: Temperature distribution after the first pulse (Different glue/crimp conductivities, cladding tee corner connection broken)

Effect of tee heat sink

The effect of the tee as a heat sink has also been considered and is shown below in Figures 6 and 7. Figure 6 compares the baseline case to the situation where the tee has been removed from the analysis. The removal of the tee would correspond to a case where there is sufficient insulation between the tee and the winding pack that no heat crosses the boundary. This may also be the case if the winding shrinks away from the tee as it is heated up doing an operational pulse. The max temperature for the case without the tee is only marginally higher than the baseline case at 88.623 K as opposed to 88.452 K.

Figure 7 displays a similar comparison between the second geometric configuration where there is a break in the cladding at the inner tee corner and the identical case except with the tee removed. The max temperature for case without the tee is only slightly higher than that without at 89.644 K as opposed to

88.79 K. The comparison of the tee without the heat sink demonstrates that its removal only marginally increases the max temperature of the coil by generally less than a degree. However, an important observation is that if the tee is in intimate contact with the winding pack, it will absorb some of the heat from the pulse and thus will experience a temperature rise. The max temperature of the tee and the winding pack are within in a degree for all of the cases where the tee acts as a heat sink. Table 4 shows all of the max temperatures for both the tee and the inner winding pack.

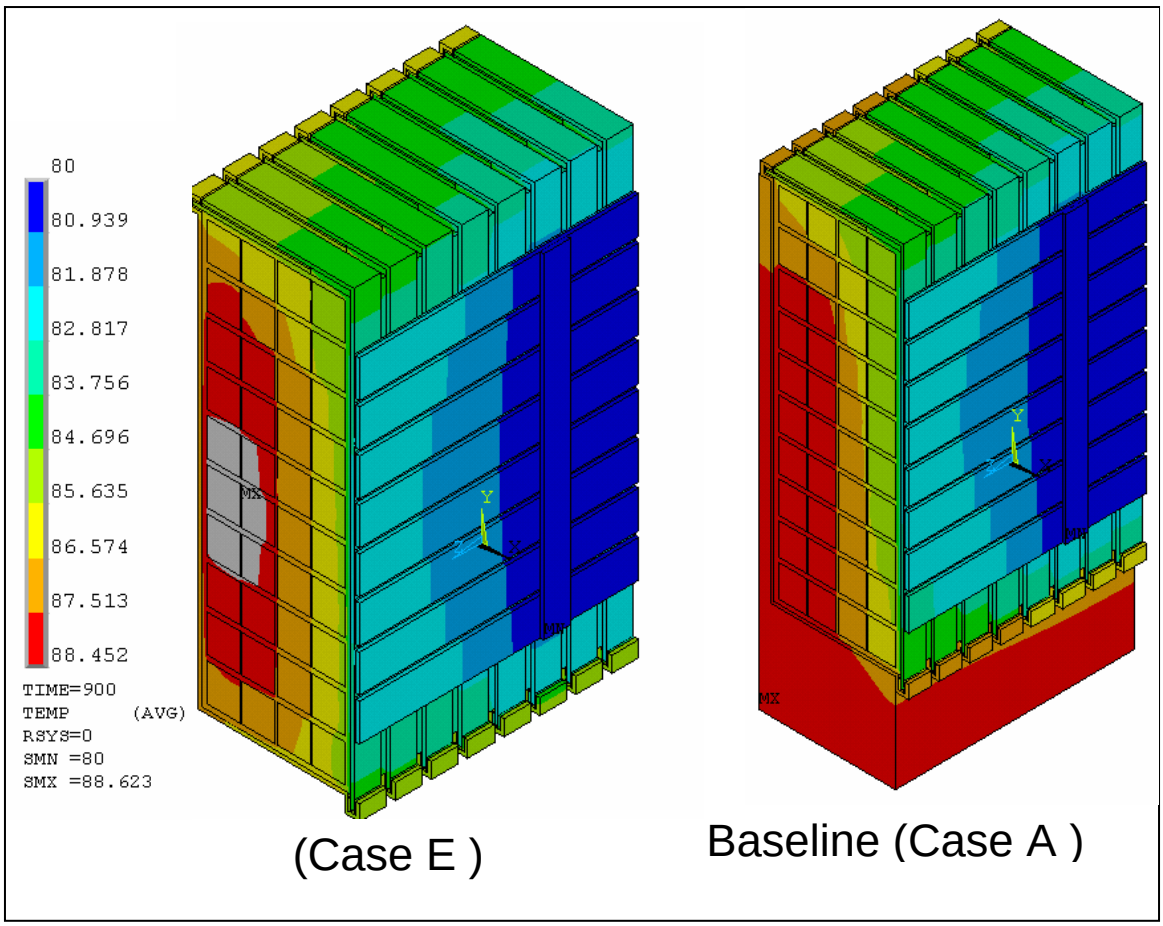

Figure 6: Temperature distribution after the first pulse (with and without tee)

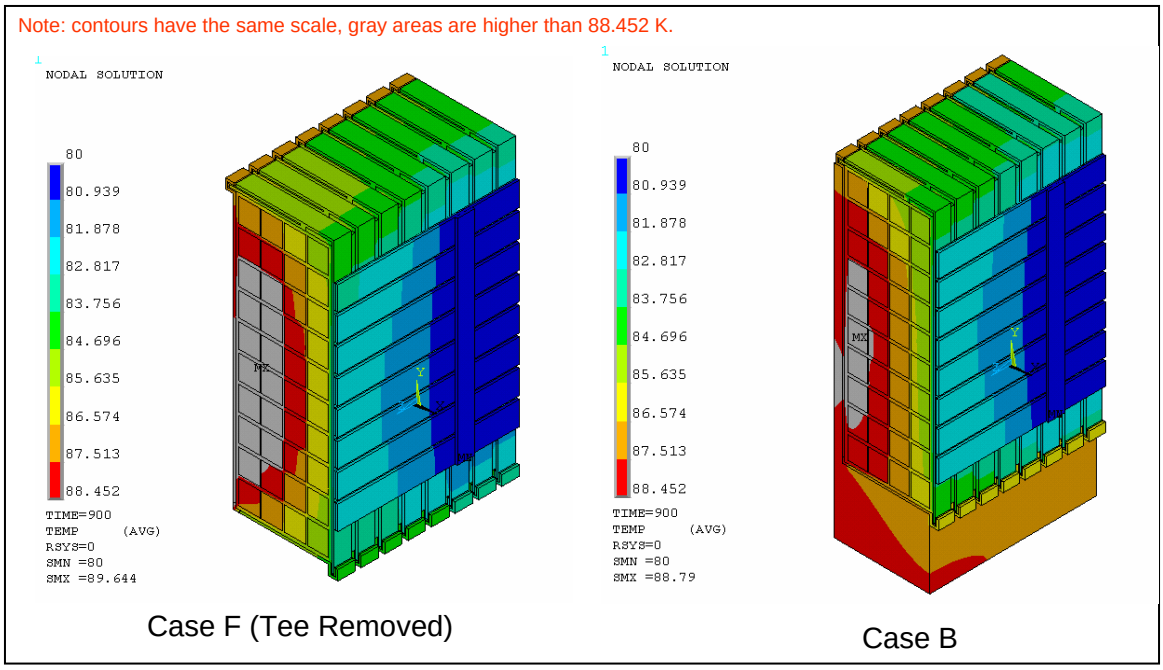

Figure 7: Temperature distribution after the first pulse (with and without tee, cladding tee corner connection broken)

Table 4: Summary of max temperature results

	Max temp in coils (K)	Max temp in tee (K)
Case A	88.415	88.452
Case B	88.79	88.49
Case C	86.074	85.337
Case D	85.251	84.4
Case E	88.623	N/A
Case F	89.64	N/A

Ratcheting of nodal temperatures

Figures 8 and 9 illustrate the effect of ratcheting temperatures over time. Case A was run out over ten cycles and reached a steady state equilibrium temperature of around 94 K after the third cycle. Case B was run out only 5 cycles but managed to reach equilibrium at 93.3 K after the third cycle also. Thus, the maximum steady state temperature is only marginally affected by the cladding connection scenarios studied in this report as there is less than a degree difference between the two cases.

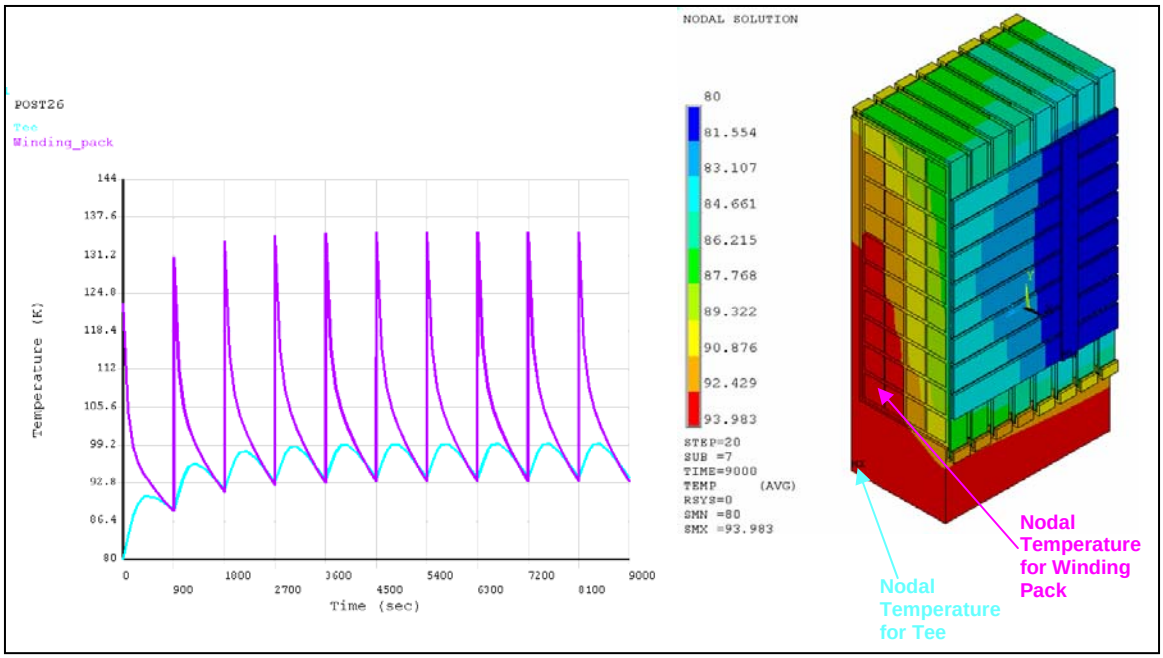

Figure 8: Ratcheting node temperature for tee and winding pack (case A).

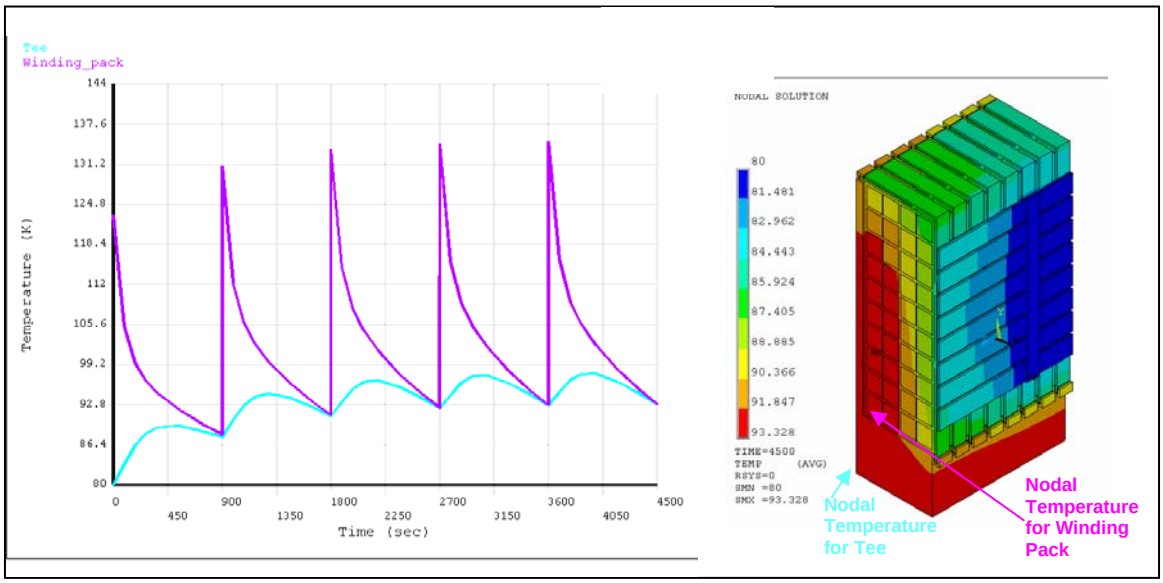

Figure 9: Ratcheting node temperature for tee and winding pack (case B).

The ratcheting profile is affected by changing the conductivity of the glue as shown in Figure 10. Not surprisingly, the higher conductivity produces a lower steady state temperature of 87 K. Also, the nodal temperatures approach steady state more quickly (after the second cycle) than the lower conductivity cases (A and B). This suggests that a realistic expectation for the max temperature of the winding pack is for it to fall somewhere in the range of 87 K and 94 K, depending on the glue conductivity and the contact resistance (conductivity) of the crimp connection.

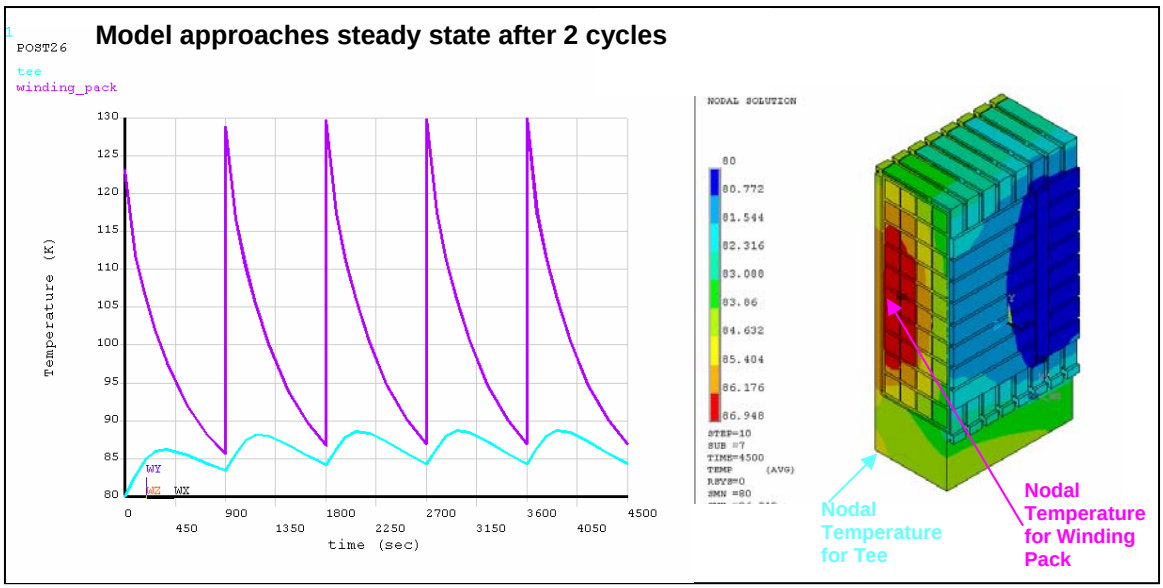

Figure 10: Ratcheting node temperature for tee and winding pack (case C, higher glue/crimp conductivity).

Temperature variation along the length of the coil

Due to the relatively high conductivity of the winding pack along the length of the coil (300 W/m-K), there is little variation in the temperature of the winding pack even at locations far from the cooling tube. This is shown in Figure 11 where the image on the right depicts the temperature distribution of the cross section of the pack at the location of the cooling tube connection. The two temperature distributions of the coil pack are almost identical and this as typical for all cases studied. There is some variation in the tee and the cladding along the length of the coil but the winding pack temperature distribution appears independent of location along its length.

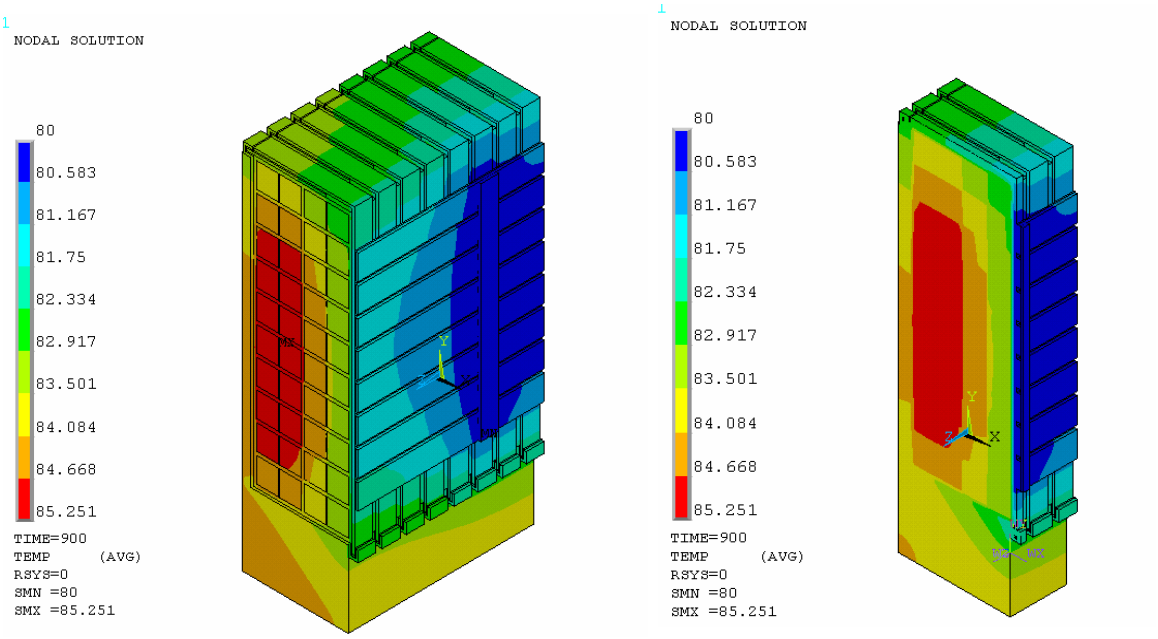

Figure 11: thermal variation along length of conductor (case D, typical for all cases)

Crimp/glue conductivity independence

Until now both the glue that holds the cladding vertical and horizontal pieces together and the crimp joints have had the same value of conductivity (contact resistance) applied to them in each case studied. The dependency was broken to determine which value (crimp or glue) was the dominant factor in determining the overall temperature distribution. Figure 12 illustrates the effect that the glue/crimp conductivity values have on the max temperature of the coil. The blue curve is indicative of the case where the glue and crimp conductivities are equal, the red curve is indicative of the case where the glue conductivity is set to its maximum (best achievable) value of 100 W/m-K and the crimp conductivity is allowed to vary and finally, the green curve is for when the crimp conductivity is set to its maximum (best achievable) value of 100 W/m-K and the glue conductivity is allowed to vary. The blue curve can be considered a worst case boundary as it is not possible to obtain values to the right or above that curve.

Figure 12 illustrates that crimp conductivity has less an effect than does the glue conductivity. That is, when the glue conductivity is set to 100 W/m-K and the crimp conductivity is allowed to vary, the resulting max temperatures are a few degrees lower from the default case where the conductivity values are equal. In contrast, the green line shown on the graph, where the crimp conductivity is set to its max value, indicates that the temperature is only slightly lower than the default case. This suggests that care should be taken to ensure that the most conductive glue is chosen for adhering the cladding pieces to each other.

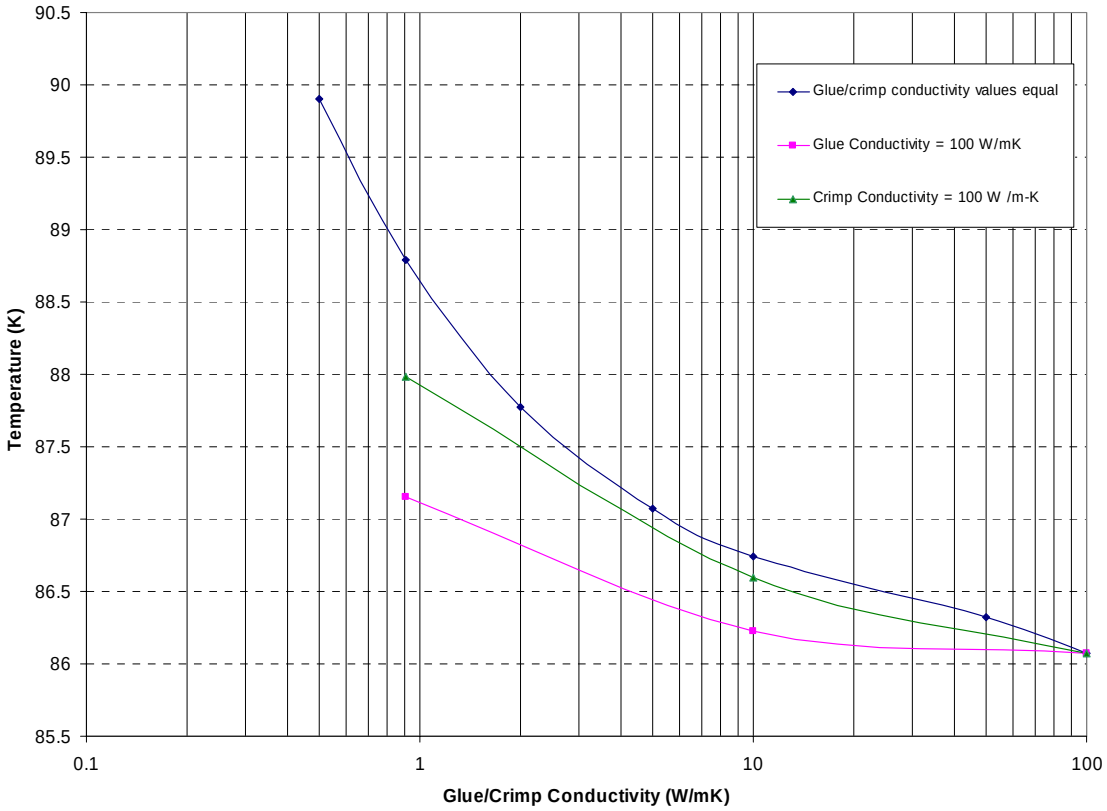

Figure 12: Crimp/glue conductivity dependency on log scale

V. Summary and Recommendations

- For low conductivity glue/insulation, expect steady state at around 93-94 K. If glue/crimp joints can be more conductive (i.e. less contact resistance) the value can be dropped to around 84-85 K.
- Breaking the cladding at the lower corner of the tee does not have an appreciable effect on the temperature profile as shown by cases B and C. It raised the winding pack temperature slightly (1 degree).
- Removing the tee (i.e. floating winding pack) tends to cause slightly (1 degree or so) higher winding pack temperatures at least during the first pulse/cool down.
- All cases studied thus far achieve a steady state within 4 cycles.
- Due to the relatively high conductivity of the coil in the winding direction, the temperature profile of the winding pack remains relatively constant along its length.
- The glue (connecting the cladding plates together) conductivity is a more dominate factor in reducing the max temperature of the winding pack than the crimp conductivity.

Based on these findings, *it is recommended that case B should be selected as the target configuration for the cladding. This case breaks the cladding connection at the inner corner of the tee and allows for the removal of the electrical insulation at the top of the winding pack.* This method of construction is a little easier to assemble as the cladding no longer has to be bent into the relief groove in the tee doing assembly and the connection at the top of the tee becomes more straight forward when removing the extra piece of insulation. It was found that this geometric case experienced only a slight (less than a degree) increase in the max temperature and thus, it is considered a robust and viable option for assembling the cladding.

Additionally, care should be taken to ensure that the cladding is held together by highly conductive glue. This analysis has shown that depending on how mush loss there is across the glue and crimp joints the max temperature will fall in the range of 85-94 K. The upper value of 94 K is associated with using an epoxy/insulator conductor value of 0.91 W/m-K. Conductive glue conductivity vales are usually approximately ten times better than a straight insulator (although in certain cases, they can be significantly be better than that) which would put the max temperature around 86-87 K according to Figure 12. The crimping connections are also important in terms of ensuring a good conductive path but they are less of a factor than the glue.

NCSX

Design Basis Analysis

Non-Linear Modular Coil Analysis

NCSX-CALC-###_dA

Draft A

21 July 2007

Prepared by:

_____

K. Freudenberg, ORNL

I have reviewed this calculation and, to my professional satisfaction, it is properly performed and correct. I concur with analysis methodology and inputs and with the reasonableness of the results and their interpretation.

Reviewed by:

_____

D Williamson, ORNL Engineer

Table Of Contents

I. Executive Summary

The purpose of this analysis is to examine the structural characteristics of the NCSX modular coil shell and windings. A non-linear FEA study has been performed on the modular coils of the National Compact Stellarator Experiment (NCSX). The modular coils provide the primary magnetic field within NCSX and consist of flexible cable conductor wound on a cast and machined winding form and vacuum impregnated with epoxy. Eighteen coils and associated winding forms are connected at assembly into a toroidal shell structure. The ANSYS® model, includes the complete shell structure of all three coils and contact regions allow the winding to slide and detach form the shell structure. The winding pack is thus restrained only by the clamps. The purpose of this study was to evaluate the structural response of the windings and shell structure during cooldown and normal operation.

II. Introduction

The function of the NCSX modular coil system is 1) to provide specified quasi-axisymmetric magnetic field configurations, 2) to provide access for tangential neutral beam injection (NBI), radio frequency (RF) heating, and diagnostics, and 3) to provide a robust mechanical structure that minimizes non-symmetric field errors. The coil set consists of three field periods with six coils per period, for a total of 18 coils. Due to stellarator symmetry, only three different coil shapes are needed to make up the complete coil set. The coils are connected electrically in three circuits according to type, and as such can produce alternate magnetic configurations by independently varying the current for each type.

The modular coils are wound onto stainless steel castings that are then bolted together to form a structural shell. As shown in Fig. 1, the winding cavity is a "tee" structure that is located on and integral with the plasma side of the shell. During operation, electromagnetic forces push the windings outward against the shell and laterally toward the "tee", so that only intermittent clamps are required for structural support.

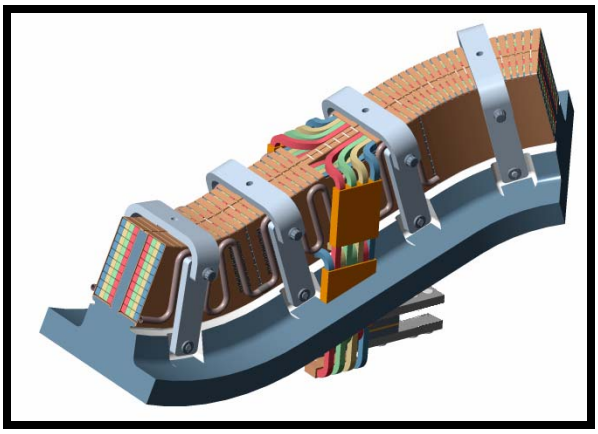

Fig. 1. Mod Coil Schematic showing the winding cavity (tee), winding and clamps

This primary focus of this analysis is to acquire a proper understanding of how the coil set will react structurally when loaded with the magnetic field. In contrast to the linear analysis, as documented in Myatt [1], this analysis allows the winding packs to slide on the coil via frictionless contact surfaces. The stresses, strains and potential winding/shell gap

displacements are central in determining whether the structure is within the design criteria as stated in by Reiersen [2]. The deformed winding coil shape calculated by the analysis will also be used as a physics tool to verify that the magnetic field

III. ANALYSIS APPROACH

The geometry of the shell and modular coil structures renders any global stress analysis performed by hand as a virtual impossibility. Thus, the approach taken in this report was to perform a series of finite element models and compare and contrast the answers for both the linear and non-linear cases where the winding slips along the tee..

II.A. Assumptions

1. Material properties evaluated at 77 K.
2. Winding packs are modeled with isotropic material properties.
3. 60 - degree "anti-cyclic symmetry" on edge flange faces based on the 3 coil shell model (A,B,C).
4. Non-linear sliding between tee and winding pack is frictionless.
5. Clamps are only used on winding packs that are free to move against the shell.

II.B. Material Properties

The properties used assumed that the shell is made of stainless steel and the coil windings consist of a homogeneous copper/epoxy mixture. The properties are listed in Table 1. The thermal properties are shown in Table 2. These values are used where when the thermal loading from a localized modular coil model is applied to the shell and the winding form.

TABLE I: Material Properties.

	E (Mpa)	CTE /K	Poisson's Ratio
Tee/shell	151,000.00	0.00E+00	0.31
Modular Coil	58,600.00	1.00E-05	0.3
Toroidal Spacer	151,000.00	0.00E+00	0.31
poloidal spacer	151,000.00	0.00E+00	0.31
Wing bag	1,100.00	2.30E-04	0.42
Wing bag	1,100.00	2.30E-04	0.32
Clamp	151,000.00	0.00E+00	0.31
Top pad	21.28	1.25E-03	0

TABLE II: Material Properties.

Cp (J/kg K)	80 K	100 K	150 K	200 K
Winding cable	171.4	212.3	270.1	300.7
Cu Cooling Plate	205.1	255.3	324.1	359
Insulation	348.9	413.7	537	626.8
SS Tee	215.3	275.5	362.1	416.4
glue	348.9	413.7	537	626.8

K (W/m K)	80 K	100 K	150 K	200 K
Winding cable (x, y direction)	7.5	7.5	7.5	7.5
Winding cable (z direction)	300	300	300	300
Cu Cooling Plate	529.3	461.5	418.1	407
Insulation	0.227	0.252	0.396	0.322
glue (4 * insulation)	0.91	1.01	1.58	1.29
SS Tee	8.114	9.224	11.17	12.63

Density (kg/m^3)	80 K -200K
Winding cable	7028
Cu Cooling Plate	8900
Insulation	1200
SS Tee	8030
glue	1200

II.C Magnetic Loading

Calculations to determine the fields and forces acting on all of the stellarator core magnets have been completed for seven reference operating scenarios. The worst case for determining forces in the modular coils appears to be the 2T high beta scenario at time=0.197-s. Two independent field calculations have been performed, one with the ANSYS [3] code and the other with MAGFOR [4]. A comparison of magnetic flux density at 2-T indicates that the models are in good agreement, with only a 4% difference in peak field due primarily to mesh and integration differences. TF loads are also applied to the global model on the support legs of the modular coil winding form (See Appendix A).

II.D. Analysis Methodology

The conductor experiences about 0.04 % shrinkage more than the shell when being cooled down to 85 K. This differential strain value was utilized through the coefficient of thermal expansion and a known temperature change. Example: strain = -400με , arbitrary temp difference = 72 F. Therefore, Winging cte = -400με /72 F = = 5.55E-6 /^{o}F, Tee cte = 0 /^{o}F. Thus, by applying a global temperature change to the model, an imposed strain was exerted between the winding and the tee. The preload on the clamp pads was imposed in a similar manner.

The complete shell structure of all three coils, was studied with the FEA program ANSYS. The model uses stellerator symmetry and constant equations for the edge flange restraints (shown below in Fig.3). One node on the B shell is restrained

in the vertical direction (z) to complete the required DOF constraints. The magnetic forces are calculated directly as nodal forces in the Ansys Electromagnetic Solver. Thus, the averaging errors derived from converting MAGFOR Electromagnetic load output to discrete pressure areas have been eliminated. Contact regions defined in ANSYS allow the winding to slide and detach from the shell structure. A prototypical clamp has been placed over the clamp pads attached to the top of the tee, which more closely models the real world behavior of the clamp.

The ANSYS model runs three coils at a time with only one coil free to slide. Thus, for each run, only one set of clamps is needed to solve. By running the coils "in-turn", the models are able to converge to a solution in a reasonable amount of time. Running a multiple contact problem with all three coils sliding is not currently solvable. Other components have been included in the Ansys solution. These include, wing shims, (modeled as an epoxy/glass composite) which brace the wings against their opposing shell and edge flange shims which connect the three shell types together. The wing shims on the CC and AA flanges were not included. In a separate linear analysis by Len Myatt, he showed that there was little benefit to adding the wing shims given the complexity involved relating to writing the constraint equations and adjacent contact elements. In general, the supported C-wing configuration reduces the maximum stress and deformation in the coil C WP (83MPa vs. 70 MPa for unrestrained and restrained respectively), but has minimal effect on the MCWP maximum stress .

Figure 2 shows the hierarchy of how the eventual non-linear solution is derived. The ProE models are first simplified by removing obvious mesh consuming features such as bolt holes and rounds in some places. Next, the model is fed into Mechanica so that the winding packs can be broken into regions which can be sweep meshed for the Ansys magnetic solver. The model is then transferred into workbench where it is meshed and the material properties are defined. This is also where the contact regions are defined between the windings and the shell structure. The model is then transferred to classical Ansys and the associatively with the ProE is lost. Here, only nodes, elements material properties, components and any loading are transferred to Ansys classical. The solid CAD data, i.e. volumes areas, lines and key-points, is not currently transferred from workbench to ANSYS classic.

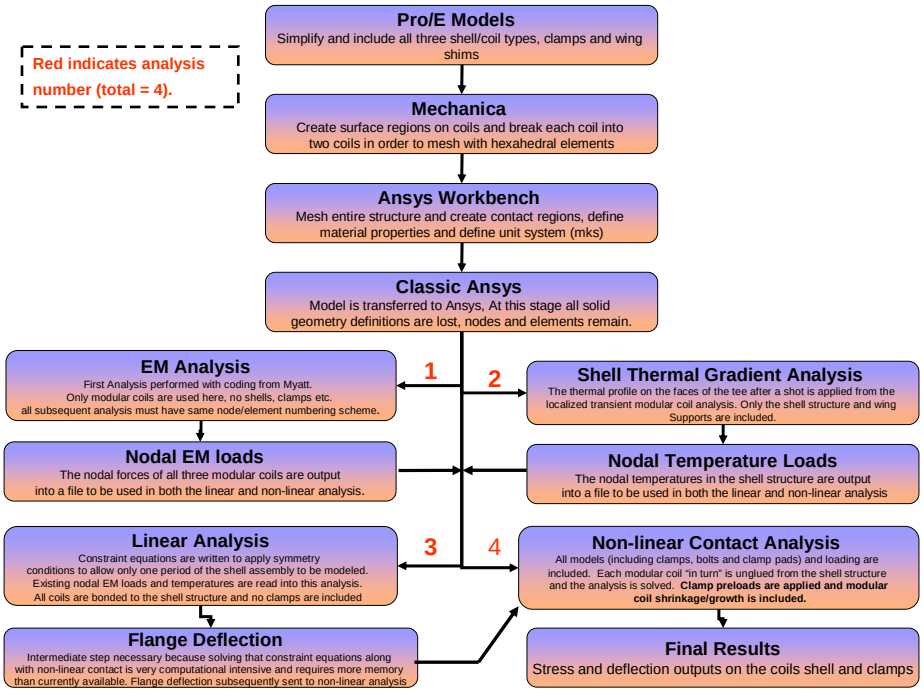

Fig 2: Hierarchy for solving the non-linear contact analysis for the NCSX half period assembly

II.E. ANSYS Mesh

The ANSYS Mesh (shown in Fig. 3) consists of both tetrahedral shell elements and hexahedral coil elements. Bonded contact surfaces are used to join all parts together. The contact surfaces between the windings and the shell structure are set to a frictionless option so that the coil may be "slippery" and slide along the length of the coil, as well as open up gaps from the shell. Although some features have been suppressed in the shell, namely bolts holes on the flanges, there are many intricate details that are incorporated in the shell structure. These include the tee relief grove, port holes, poloidal break and various other chamfers, rounds and cuts which provide for a very robust model and mesh. The winding pack mesh consists of a 2 X 6 element formulation with an average element length of 2.3 cm. Latter revisions have included the bolt holes to determine the stress on each individual bolted joint region and the shear loading over the flange face.. Originally, the three coil structure was meshed as one body encompassing the three coils and four shims. Today, each has its own material properties, real constants and key-opts.

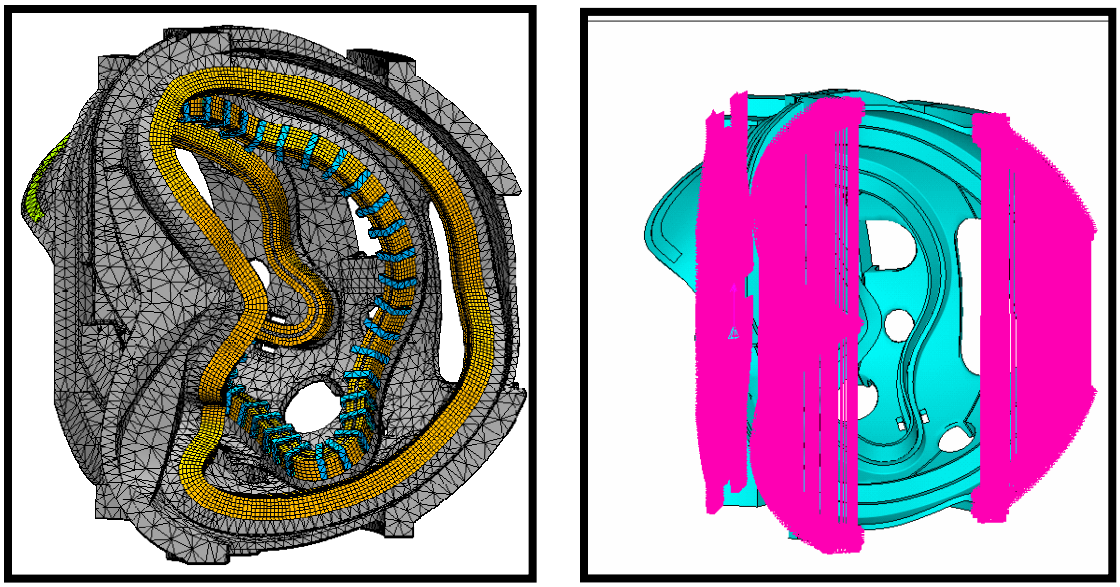

Fig. 3. Right) Mesh of the overall assembly model including clamps on Coil B. Left) Constraint equations connecting the top and bottom of the AA and CC flanges.

II.F. NCSX Modular Coil Analysis Capabilities

- 4 Different Magnetic Loading Scenarios (0.5 T,1.7T Ohmic/t=0.0s, or 2.0T HighBeta/t=0.0s, or 320kAOhmic/t=0.206s, or 2.0T HighBeta/t=0.197s). Fig.4 shows the EM model and corresponding forces.
- Thermal shrinkage/growth of winding pack as the winding pack will shrink away during curing and during pulse.
- Thermal gradient in shell due to heating of winding pack during/after pulse. This is shown in Fig 5. and Fig 6. below. A transient thermal model of a simple winding pack (straight) was run with full detail of the conductors and turn wrap insulation, which illustrated the thermal contours of the shell after a 15 minute cool down period. These thermal restraints were then placed on the global model and Fig 6. shows excellent agreement between the two models near the tee region. Finally, Fig 7 shows the thermal load applied to the entire 3 coil shell model as a steady state solution. This illustrates the predicted thermal distribution between 15 minute shots. These thermal loads are then superimposed and read into the structural model when it runs. It was found that they have a minimal effect on the results.
- Non-linear contact as the coils can “in turn” separate and slide along the shell structure. This requires three separate runs of the analysis code for each coil.
- Clamps are included in the non-linear model and are modeled according to the current clamp design.
- Preloads using ANSYS pretension elements can be applied to both the clamps bolts (a few at a time)
- Preloads can be applied to the Belleville washers in the clamp assembly using the cte of the washer material to push against the clamp and winding.
- Symmetry conditions are applied via constraint equations on the outer flanges in the linear model. This allows only one half period of the model to be analyzed (six coils and three shells)

- Magnetic loading accounts for all EM sources in the assembly, e.g. PF, TF coils, plasma, solenoid and modular coils.

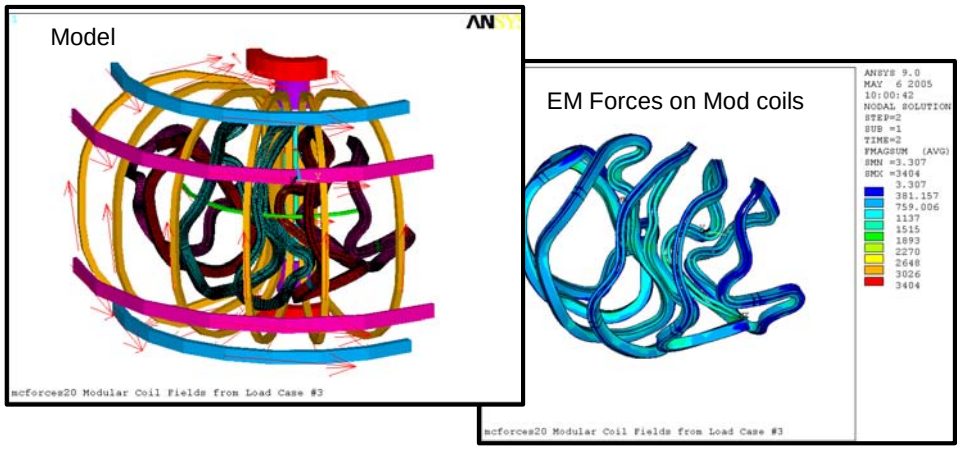

Fig 4: Electromagnetic model and resultant forces on the modular coils

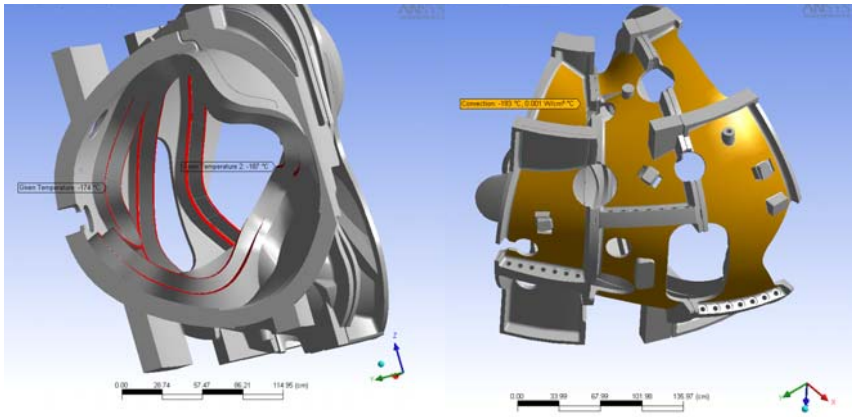

Approximate temperatures applied to edges of tee

Convection applied to outer shell surfaces.

Temperature values estimated from detailed thermal analysis of winding pack.

Fig 5: Thermal boundary conditions for modular coil analysis.

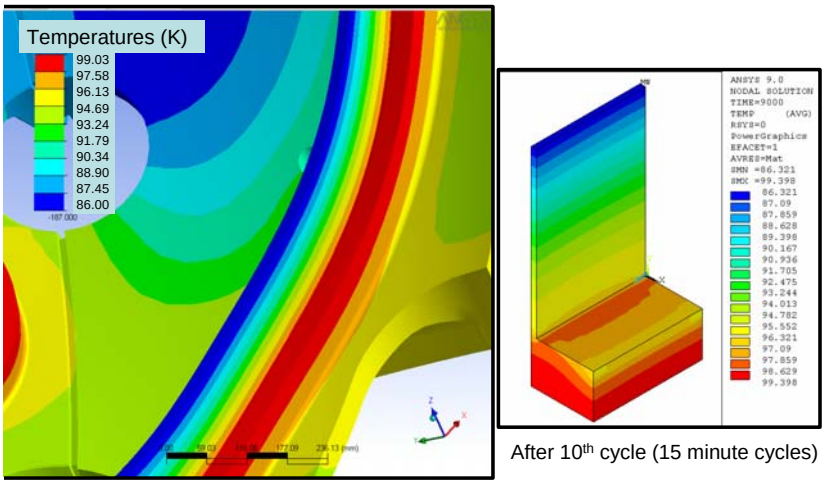

Fig 6: Variation of temperature distribution in the shell of the modular coil after the thermal profile (right image) is mapped onto the castings.

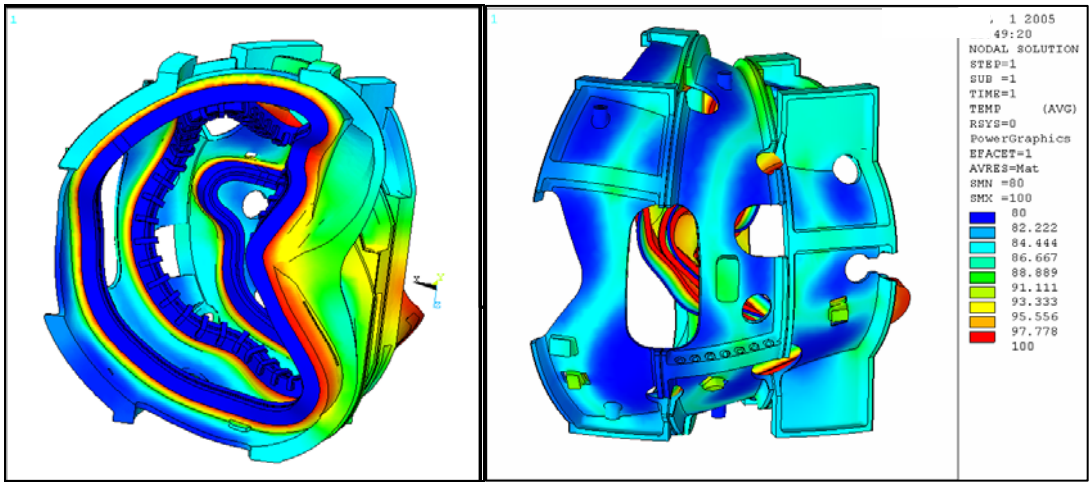

Fig 7: Castings and Windings (left image) Castings only Thermal variation. Reference temperature is 80 K.

Software and data files

The model is constructed in Ansys 9.0-11.0 and all of the preprocessing and post processing is done within the Ansys classic environment.

Drawings and models

No drawings have been referenced in this study. All models have been created as .cdb and .db files.

Material properties

The temperature dependent material properties are above listed in Table 1. For clarification, the insulation is the material that surrounds the winding cable and the glue is the material that is used to connect the copper cladding layers together and used in the "crimp" joints. Also, for modeling and meshing purposes it is necessary to model the glue as thicker than it is in reality, otherwise an extremely large mesh will result. The glue is 0.2" thick in the model and is approximately 0.05" in reality, thus the conductivity has been multiplied by 4 to account for this scaling factor.

III. RESULTS

Table 1 summarizes the stress results from both FEA programs (Ansys and Mechanica for each respective study. Initially, the analyst used Mechanica when first examining the structure in 2003. The Mechanica shell stress reported is for the supporting tee structure only as the entire shell was not able to be modeled in that program. The max stresses occur in relatively the same spots on the windings even though the two models are restrained differently. The lone max stress that exceeds 83 MPa is the coil C run on Mechanica. This stress, upon closer inspection, is more than likely an overestimate as the max stresses is due to the tee base being rigidly constrained at its base. Compared to the ANSYS analysis where the tee is attached directly to the shell and not rigidly fixed, the stress in the same region is 76 MPa.

TABLE III. Stress Results for both winding and shell for 2T case. (Von Mises Stress Reported in all cases)

Coil	Max Winding Stress (MPa)	Max Shell Stress (MPa)
Mechanica A	72	170 (Tee)
Mechanica B	79	269 (Tee)
Mechanica C	89	221 (Tee)
Ansys A	79	231
Ansys B	66	283
Ansys C	76	227

Table 3 summarizes the max gap deflections and strains that each model predicts. The gap indicated in the table is the predicted maximum separation that will occur between the winding and the tee based on the non linear contact algorithms. The shell deflection presented for the Mechanica runs only include the deflection on the web of the tee sine the model is restrained on the back of the tee, thus a direct comparison between the two models based on this criterion cannot be easily made. The trend for maximum gap deflection holds for booth the analysis programs as the gap increases from A to and B to C in both programs with coil C experiencing the largest gap of 0.6 -0.8 mm. The maximum gap for the non-linear ANSYS run of coil B is shown below in Fig. 8, which is indicative of how the gaps in the other models appeared near the extreme wing turns.

TABLE IV: Principle Strains and global deformations.

Case/Coil	Max Principal Strain (mm/mm)	Winding Shell Gap (mm)	Max Shell Deflection (mm)
Mechanica A	0.0011	0.09	0.24 (Tee)
Mechanica B	0.0012	0.58	0.76 (Tee)
Mechanica C	0.0015	0.8	0.36 (Tee)
Ansys A	0.0013	0.2	1.4
Ansys B	0.0010	0.5	2.6
Ansys C	0.0012	0.6	1.4

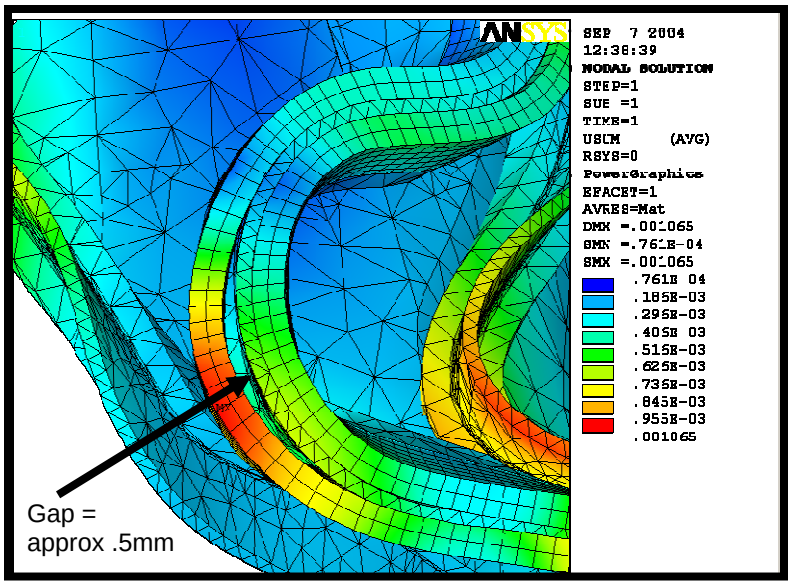

Fig. 8. Winding/shell Gap of approximately 0.5 mm located on the extreme turn of the wing of the modular coil B.

The maximum principle strains for the two B coil runs are compared in Figure 9. The maximum principle strain occurs on the extreme interior of the wing regions in both cases. The Ansys model has a higher average strain along its outboard edges as the coil is being moved by the shell which itself is deforming due to the magnetic loads.

The Von Mises Stress distribution for the shell structure is shown in Fig. 10. The max stress occurs near the wing interests between shells B and C. The peak stress on the tee structure of coil B is about 175 MPa. Fig. 11 indicates the degree of which the shell will globally deform due to the electromagnetic loads with a maximum deformation of 2.2 mm occurring on the web of the tee holding the slippery coil. The max deformation of all three non-linear models occurred on the tee of the coil that was free to move out and along the shell. Fig 12. shows the global deflection of the twelve coils (a half period) with a peak movement 2.18 mm occurring on the two B coils near the same location as the deflection on the B shell tee.

According to the specification of casting shell, Ref. [6], the minimum 0.2% yield strength and the tensile strength to be 496.4 GPa and 655 GPa, respectively. The allowable is the less of 1/2 tensile strength or 2/3 yield strength. Thus, the allowable stress would be 322.5 MPa, which is higher than the maximum von Mises stress of 283 Mpa listed in this report.

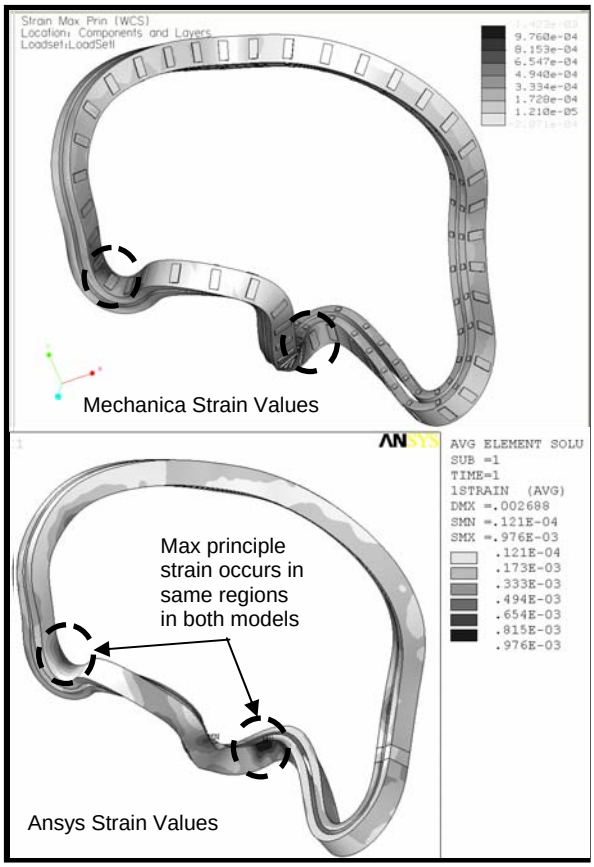

Fig. 9. Strain Values for winding pack B for both Mechanica and Ansys setups.

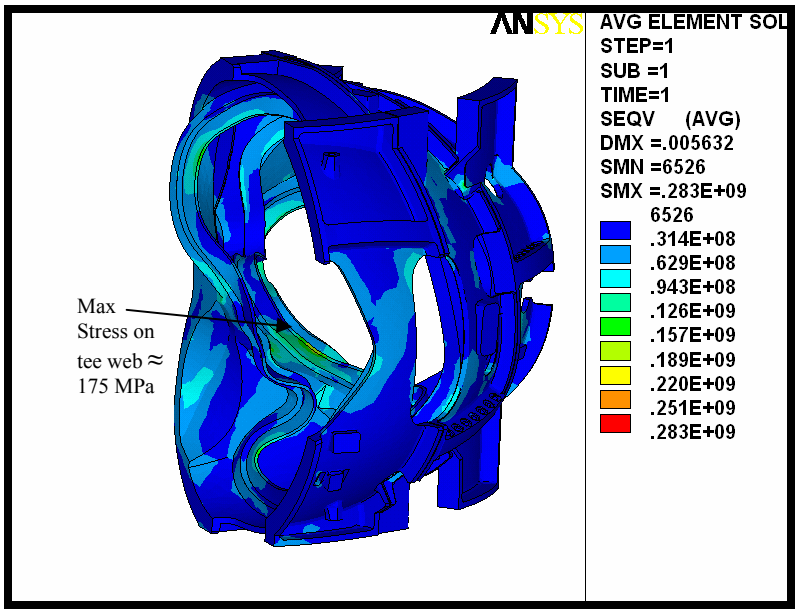

Fig. 10. Von Mises Stress Distribution for the shell structure. Max Stress (283 Mpa) occurs at joint region geometric discontinuity between shell flanges, Max Web tee stress ≈ 175 Mpa..

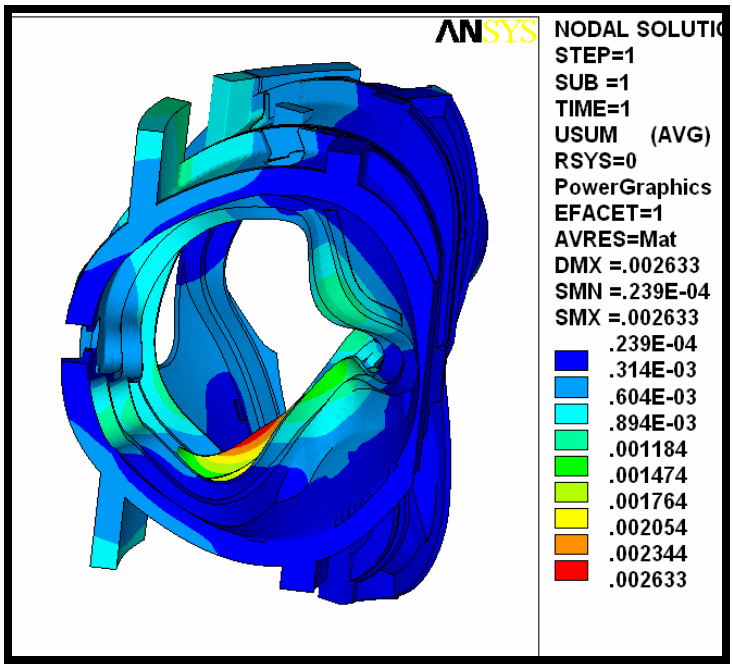

Fig. 11. Shell Deformation for a “slippery” coil B.

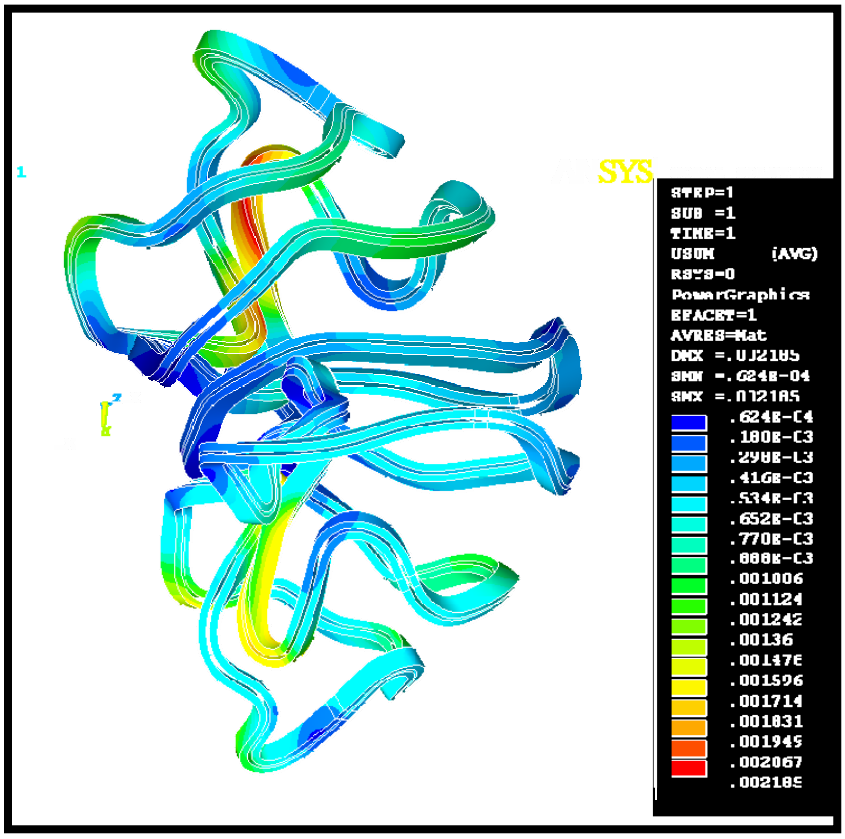

Fig 12: Deflections of coils for non-linear analysis

Clamp stresses

The clamps shown in this report are simplistic in that they do not model all of the connecting components in detail. The clamps are preloaded by applying a thermal expansion to the pads separating them from the winding forms. Figure 13 displays the Von Mises contour plot of the coil type B clamp pattern. High stresses are found at the interfaces of clamps and the tee because of the rigid bonded connection there. High stresses are primarily caused by the bending moments and the shear forces that are primarily induced by the lateral movement of the coils. The maximum Von Mises stress is 247 MPa at the clamp-tee interface. The actual stresses should be much smaller once sliding and rotational effects are allowed for in the model.

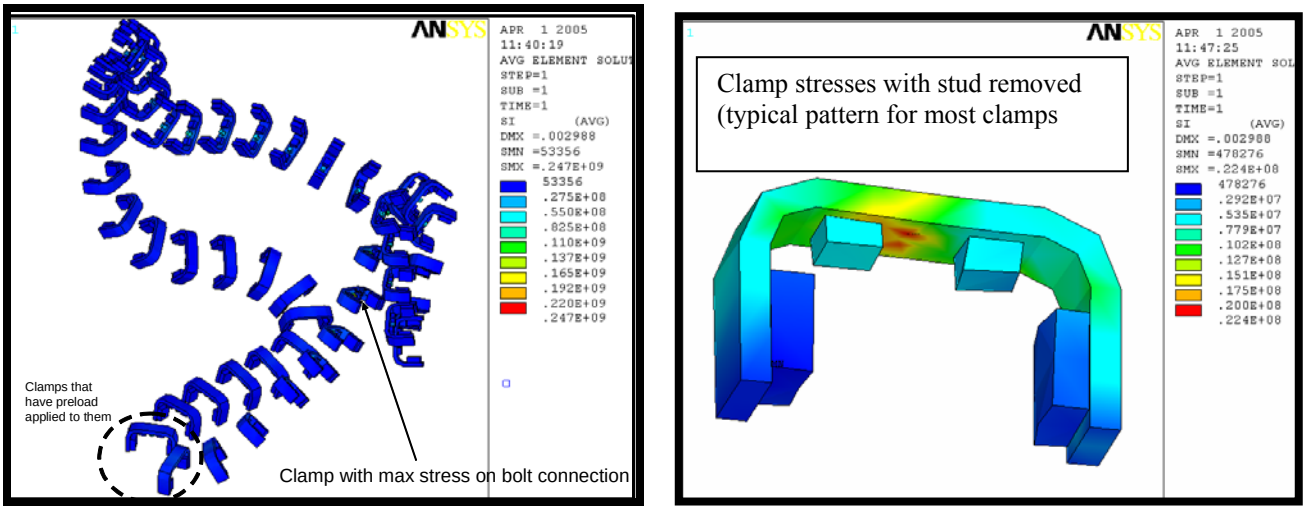

Fig 13: Stresses (Intensity) on clamps

III.c. High stress regions

Figure 14, Figure 15 , Figure 16,and Figure 17 identify the relative high stress areas on each coil type. They illustrate a numbering scheme for the 3/8-16UNC tapped holes in the tee. Per the proposal of Major Tool, every tenth hole shall be identified by etching. The high stress region shall be identified as the web of the “tee” cross-section.

Detailed stress plots have been produced at every clamp location, which helped to determine the exact location of the higher stress regions. A demo of the stress script is shown in Appendix C.

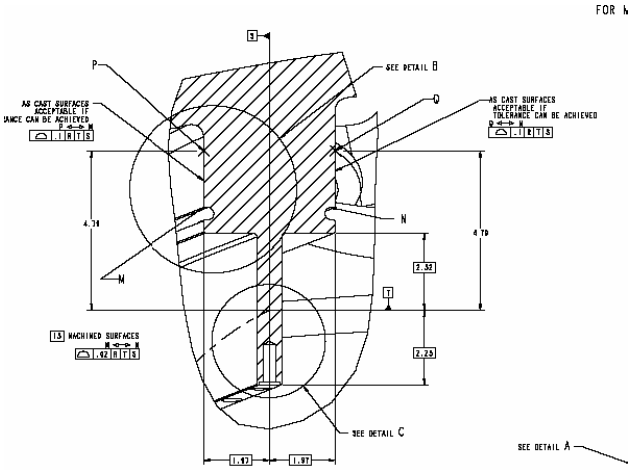

Fig. 14 Identification of High Stress Zones

The figures also show approximate dimensions, including ½-in. stock material allowance, from the flat surfaces of the casting to the start and end locations. These dimensions shall be used to identify the high stress regions prior to machining. Figure 15 (Type C), Figure 16 (Type B), and Figure 17 (Type A) depict the high stress region identification for each type casting.
The profile of the high stress region is shown in red. (Type C shown in illustration).

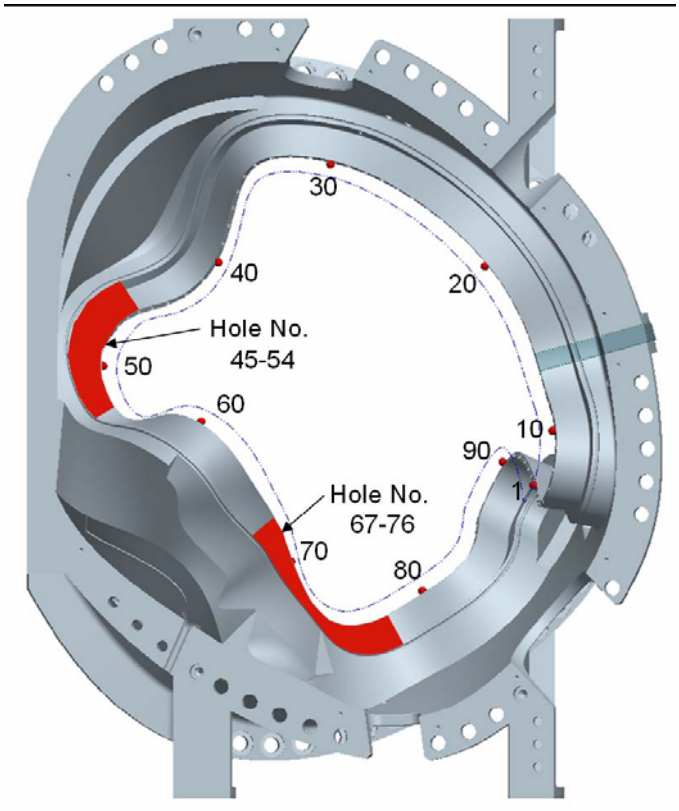

Fig. 15 High Stress Region Identification for Type-C MCWF

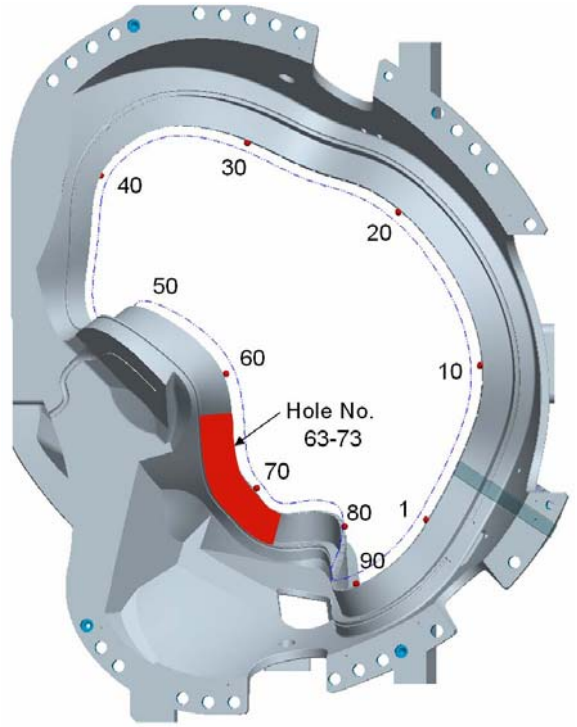

Fig. 16 High Stress Region Identification for Type-B MCWF

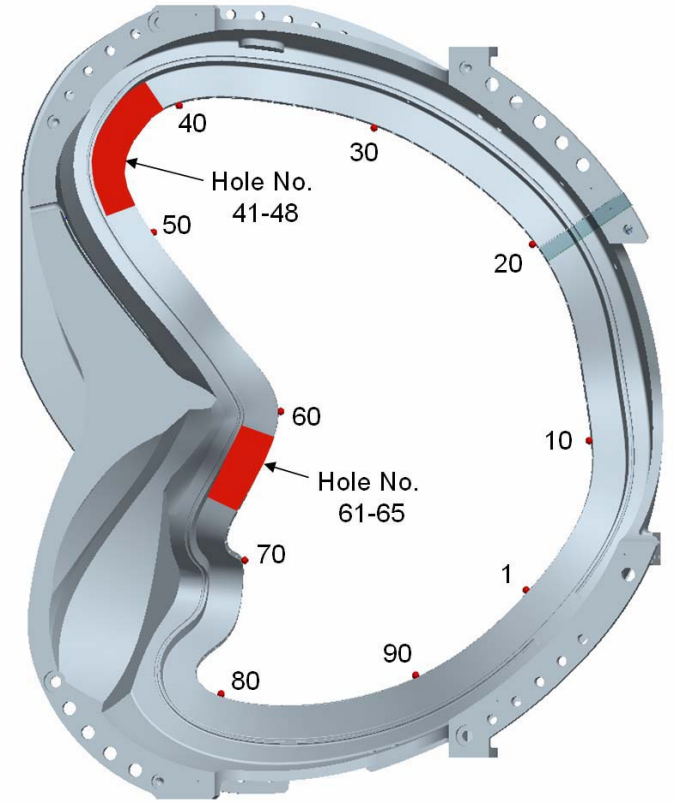

Fig. 17 High Stress Region Identification for Type-A MCWF

III.d. Mod Coil Toroidal Flange Connections

This model does not include any bolt or bolt preloads on the toroidal flange joints. This will be covered in a future analysis report where we will include the bolt, preload and friction on each of these joints. Here, all coils and shims are boned/glued together. Fig 14 - Fig. 17 show the shear and normal stresses for each of the interfaces. The top set of pictures is the PPPL Fan [7] images of the their NCSX global analysis. There is quite good agreement between the two models on these comparison figures. The same contour scales have been used for direct comparison. Looking at the normal compression plots below, one can see that the flange is in both compression and tension and that there is no clear compressional force on the inboard leg that could restrain it by friction alone. Thus, of particular concern, is the area that is unbolted on each of the flanges as it experiences a large amount of shear with no preload/ bolt connection to react it. After a considerable amount of discussion and an exhaustive study of inboard restraint options, it was decided to weld the inboard legs together for the AA, AB and BC joints. Further, additional inner leg bolts will be added to the CC interface. The weld analysis and the CC inner leg bolt analysis are essentially spin offs of this analysis as they use the same magnetic forces, TF coil loading, and restraints as this model. These separate spin-offs will show that the welds and bolts do adequately address the shear problem over the entire flanges face of the toroidal shims. Thus, the issue of slippage and shear loads on the inner leg has been resolved.

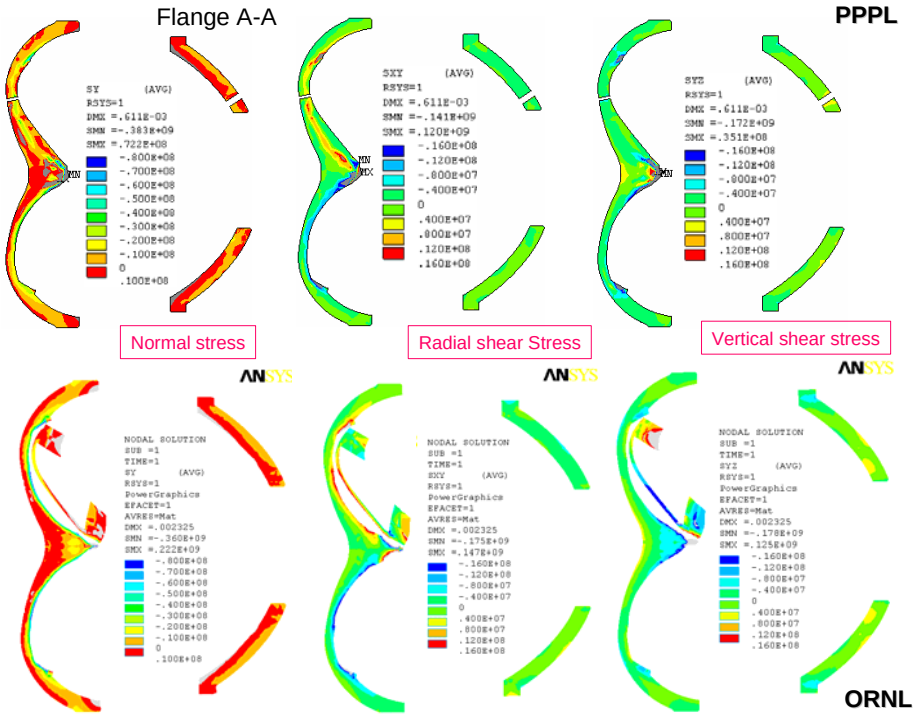

Fig 14: Normal Stresses and Shear Stresses for the Flange Spacer Elements at 0°

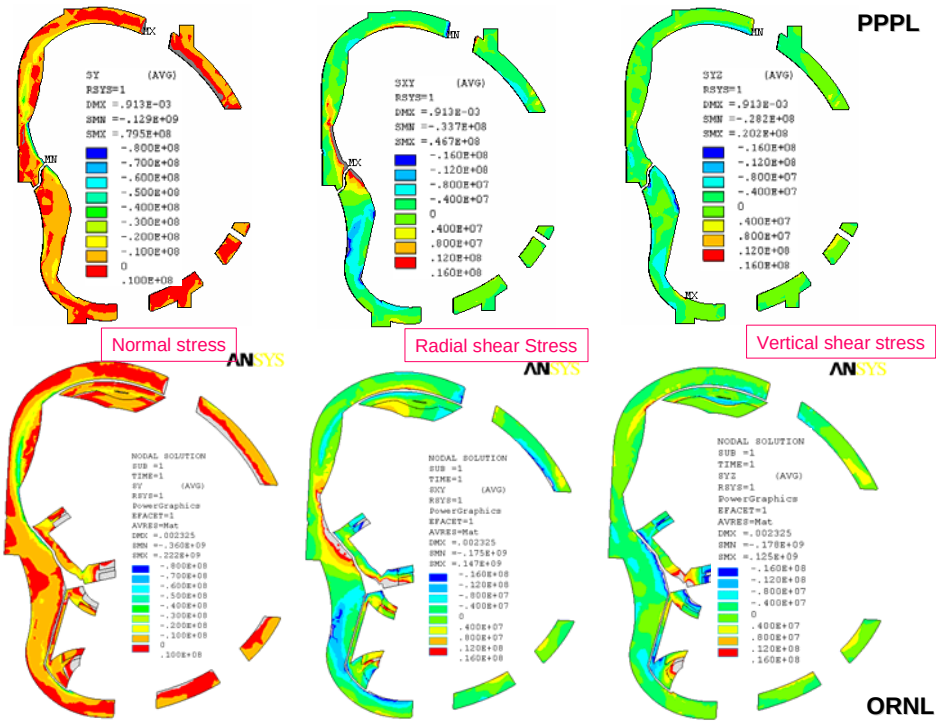

Fig 15: Normal Stresses and Shear Stresses for the Flange Spacer Elements at 20°

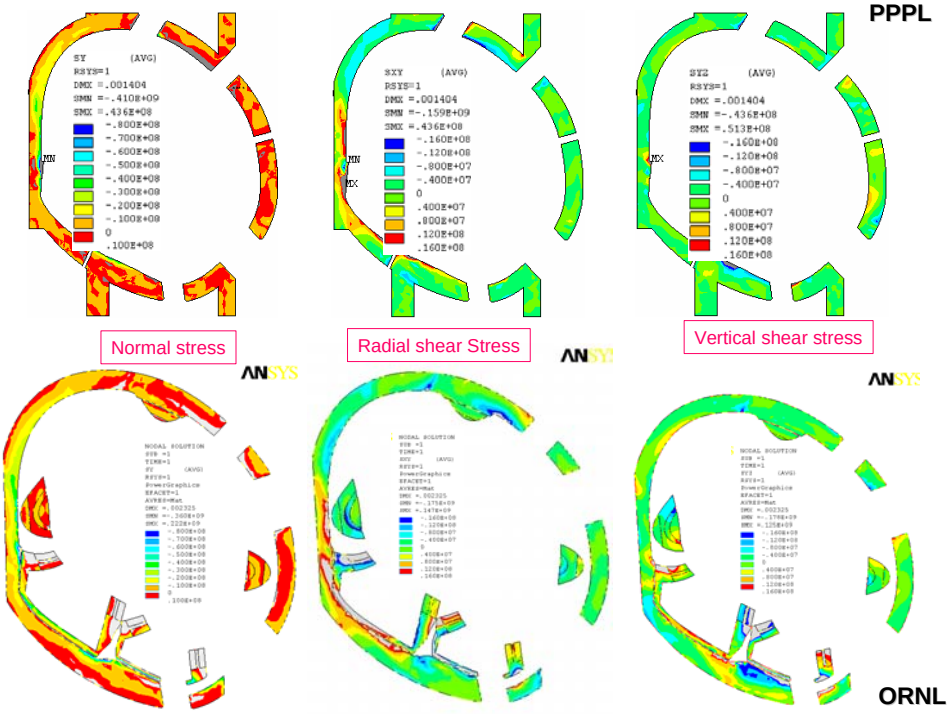

Fig 16. Normal Stresses and Shear Stresses for the Flange Spacer Elements at 40°

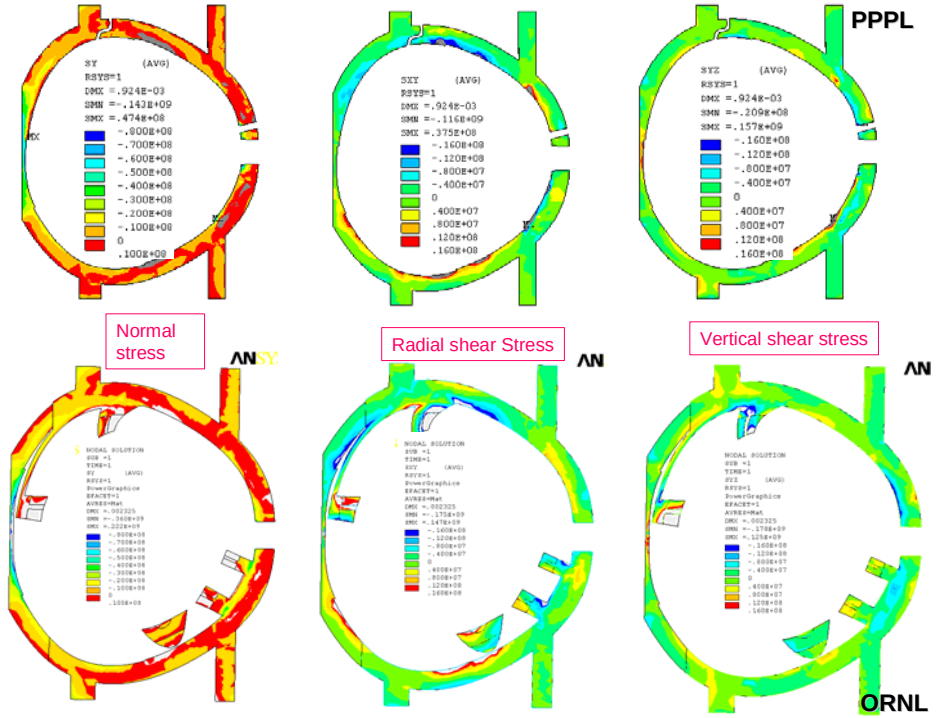

Fig. 17. Normal Stresses and Shear Stresses for the Flange Spacer Elements at 60°

IV. CONCLUSIONS AND FUTURE WORK

The following Conclusions are made based on the results of these two separate independent finite element analysis studies (Mechanica and ANSYS).

1. The allowable stress for the membrane plus bending will be 322.5 MPa, which is larger than the maximum stress of 283 which occurs on the BC interface near a geometric discontinuity. The peak stress on the tee structure, which occurs on the B coil shell, is about 175 MPa.
2. The maximum gap between the coil and the shell structure reported is 0.8 and occurred in the Mechanica study of coil C. The corresponding ANSYS value for the same coil was 0.6.
3. The Ansys models provide a great more detail into the behavior of the shell structure and yields an accurate deformed coil shape that does not rely on artificial constraints on the tee, which will be used by a physics code to predict the doing pulse plasma shape.
4. The stresses in the Mechanica runs are slightly higher than those from ANSYS. This is most likely due to the normal constraints placed on the clamps pads which help apply the preload to the clamps. Ansys ties the clamps directly to the shell instead of fixing them in a specific direction.
5. The maximum deflection in the shell is 2.6 mm which occurs on the type B on the leading edge of the tee near a wing transition.
6. The max winding stresses (Von Mises) are generally quite low ranging from 66 top 79 Mpa between the three coil types.

This analysis report serves as a check on the previously non-linear report produced by PPPL on the modular coil assembly. The two analysis utilize similar analysis paths and properties with the main difference being that PPPL choose to solve a 6 coil courser model with cyclic symmetric conditions and ORNL choose to analyze a 3 coil model with a finer mesh. The main difference between the two analysis result summaries is that PPPL shows somewhat larger peak stresses in the windings than the ORNL model. This is most likely due to the course 3X1 mesh of the mold coil (PPPL version) versus the 6X2 mesh of the ORNL analysis. The finer mesh allows for the peak stresses to be distrusted more evenly and accurately. The shell and flange interface stresses are in good agreement between the two models.

This analysis only documents one load scenario to be used on the NCSX machine. Further analysis should be performed on the others for verification purposes. Further, the weld analysis and the analysis of the bolted joints between the modular coils are not considered here. They will be addressed in separate Dacs in the near future.

REFERENCES

[1] L. MYATT, D. E. WILLIAMSON and H.M. FAN, "Electromagnetic Linear Structural Analysis of the National Compact Stellarator Experiment (NCSX) Modular Coil System," 16th ANS Topical Meeting on the Technology of Fusion Energy, Madison WI, September 12-14, 2004.

[2] W. REIERSEN, Modular Coils (WBS14) System Design Description, NCSX FDR, May 2004

[3] ANSYS Inc, 275 Technology Drive, Canonsburg, PA 15317

[4] W.D. CAIN, "MAGFOR: A Magnetics Code to Calculate Field and Forces in Twisted Helical Coils of Constant Cross-Section", 10th IEEE/NPSS Symposium on Fusion Engineering, 1983

[5] PTC, 140 Kendrick Street, Needham, MA 02494

[6] NCSX Product Specification, "Modular Coil Windings Forms", NCSX-CSPEC-141-03-10, November 15, 2005

[7] H.M. Fan. "Nonlinear Analysis of Modular Coil and Shell Structure" NCSX-CALC-14-001-001, February 2006

Appendix A: Reaction Forces on MCWF from TF-Induced Loads

To: Michael Kalish (PPPL)
From: Leonard Myatt (Myatt Consulting, Inc.)
Date: 2 June 2005
Subject: Reaction Forces on MCWF from TF-Induced Loads

1.0 Executive Summary

Two existing ANSYS[1] models are used to determine the forces which must be carried by the Modular Coil Winding Form (MCWF) as a result of the loads developed by TF coil system. The hybrid model[2] is used to determine the vertical forces which develop when the TF support structure restrains the vertical displacements from cooldown (85K) and max-current operation (0.5 T). This is expected to be 18.2 kN/TF coil (top and bottom).

The global model[3] is then used to determine the reaction force distribution as the applied load enters the TF coil superstructure and enters the MCWF support points. This analysis shows that the four inboard support points per 120˚ sector carry 60% of the TF coil vertical load: ~17 kN each. The 12 outboard support points per 120˚ sector carry the remaining 40% of the vertical load, with maximum value of ~4 kN.

These forces can be used by to determine the impact of restraining vertical displacements at the top and bottom of the TF coils through structural attachments on the MCWF.

[1] ANSYS Release 9.0, UP20041104, INTEL NT, ANSYS, Inc., Canonsburg, PA.
[2] Leonard Myatt, "Stress Analysis of the 3x4 Slip-Plane TF Coil with Cast SS Wedges," 16-May-05.
[3] Leonard Myatt, "Effects of Coil Support Concepts on TF WP Stresses,"16-May-05.

2.0 Analysis

The vertical forces developed by the vertical restraint of the TF coil are quantified by the hybrid model. Fig. 2.0-1 is a plot of the vertical displacement of TF winding pack (wedges excluded from plot) when the coil is cooled to 85K and energized to 0.5 T. So-called reaction force vectors are superimposed on the greatly deformed plot. Querying the database indicates that these vertical reaction forces sum to 18.2 kN on the top and bottom of each coil. It should be noted that some of the vectors point in the opposite direction compared to the majority. This is because the radial extent of the applied UZ boundary condition is slightly too big. However, it is reasonable to believe that the net vertical load is correct. This represents the most significant load which must ultimately be carried by the MCWF.

Fig. 2.0-1 Vertical Displacements and Reaction forces on the Hybrid Model WP (85K, 0.5 T)

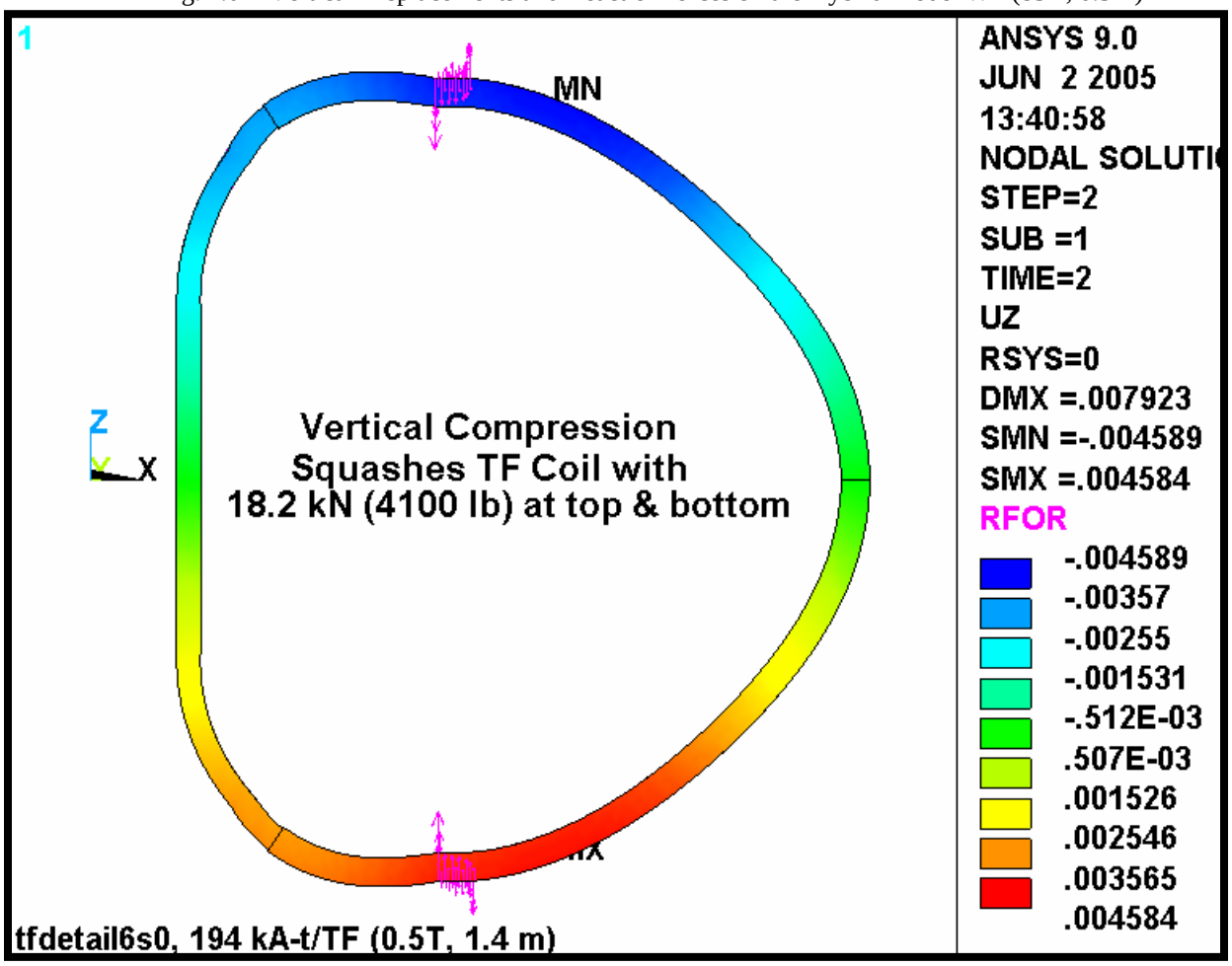

The vertical forces developed in the TF coil from 85k/0.5T operation must be transmitted through the coil support structure and into the MCWF. The global model has this load path fairly well defined, with the exception of the MCWF. The global model assumes that the MCWF provides a rigid restraint for the TF support structure.

Fig. 2.0-2 provides a graphical representation of the load distribution. The stress intensity in the support structure is contoured. Red vectors represent the 18.2 kN/TF applied load which is developed when the coils are restrained vertically at 85K and 0.5T. These come from the hybrid model as indicated in Fig. 2.0-1. The black vectors represent the reaction forces which are determined by this global model. They are simple representations of the more complex force distribution which is developed from anchoring nodal displacements in the bolting regions. Structural reaction forces are summed at each anchor point. On the inboard side, the distribution is rather uniform: 15.6+17.1+17.0+15.9 kN at the four anchor points in this 120˚ sector. These account for ~60% of the applied load. The outboard forces are much smaller and a bit more varied: 2.1+4.8+3.7+3.4+3.9+3.9+4.0+3.9+3.4+3.6+4.9+2.1 kN. These account for ~40% of the applied load.

Fig. 2.0-2 TF Loads from Hybrid Model Distribute to MCWF through TF Support Structure

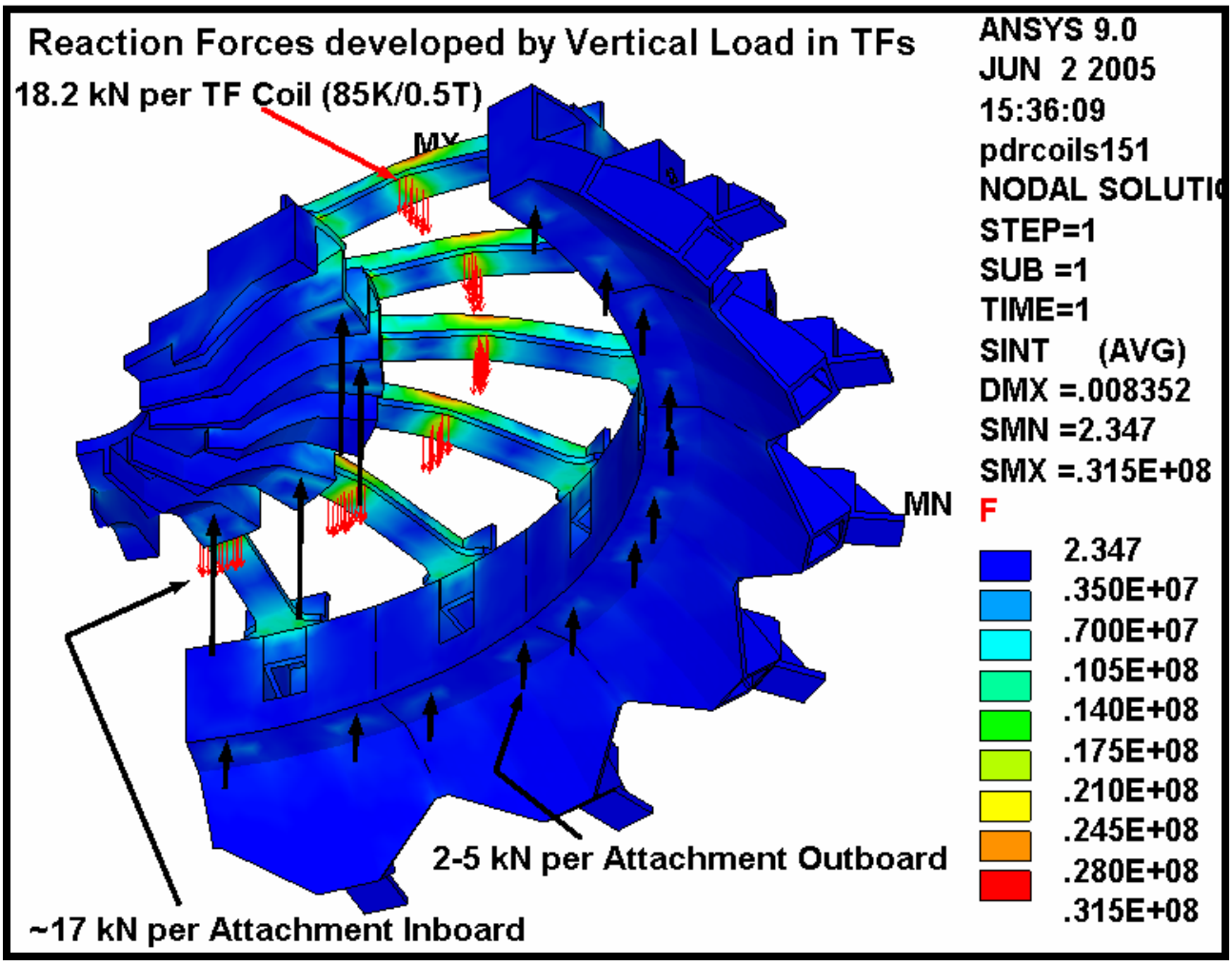

Appendix B: Consideration of using one bolt on inner leg to get total shear load:

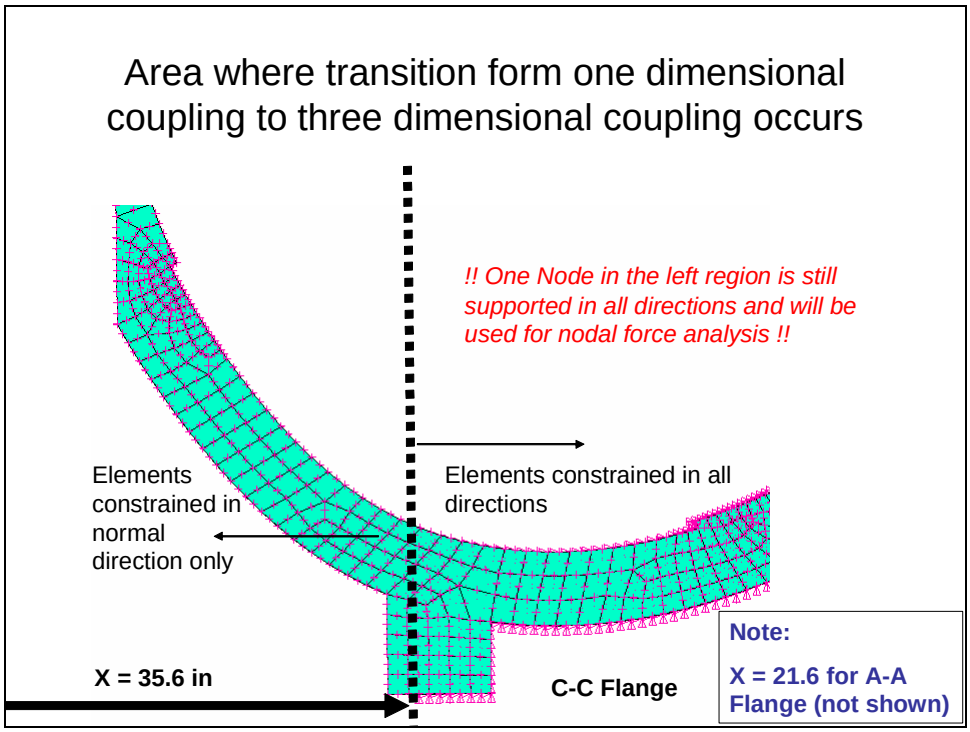

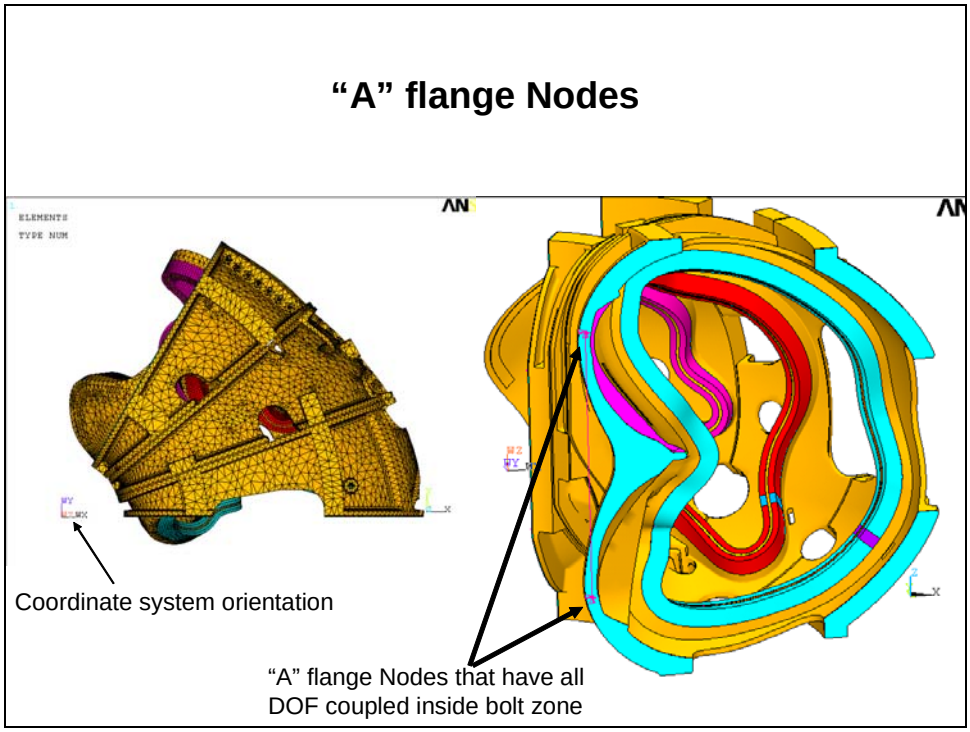

“C” flange Nodes

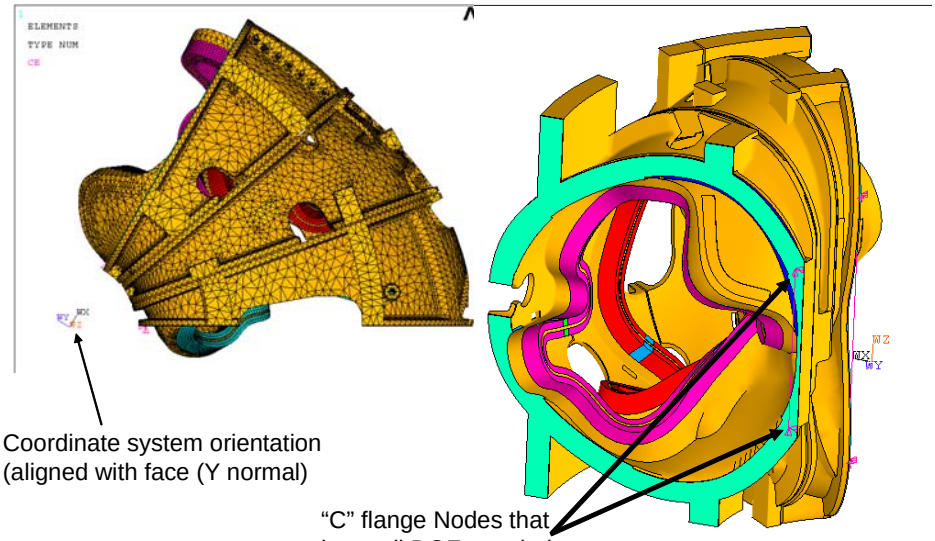

Coordinate system orientation
(aligned with face (Y normal)

“C” flange Nodes that
have all DOF coupled

Flange A: Force Results for the node pair

Force are in Newtons

- **THE FOLLOWING X,Y,Z SOLUTIONS ARE IN THE GLOBAL COORDINATE SYSTEM**
-
- **NODE FX FY FZ**
- **513516 -34636. 667.35 -10916.**
- **524077 34636. 667.35 -10916.**

- **TOTAL VALUES**
- **VALUE 0.66264E-03 1334.7 -21831.**

Note:

! Asymmetric nodes move in X together
! Asymmetric nodes move in opposite Y
! Asymmetric nodes move in opposite Z

Flange C: Force Results for the node pair

Force are in Newtons

- THE FOLLOWING X,Y,Z SOLUTIONS ARE IN COORDINATE SYSTEM 11
-
- NODE FX FY FZ
- 511246 -0.18868E+06 7753.9 -34450.
- 521807 0.18868E+06 7753.9 -34450.

- TOTAL VALUES
- VALUE 0.58263E-03 15508. -68901.

Rather Large X force .18868e6 N = 42,416 lbs

Note:

! Asymmetric nodes move in X together
! Asymmetric nodes move in opposite Y
! Asymmetric nodes move in opposite Z

Nodal Stress Intensity on Flange C-C

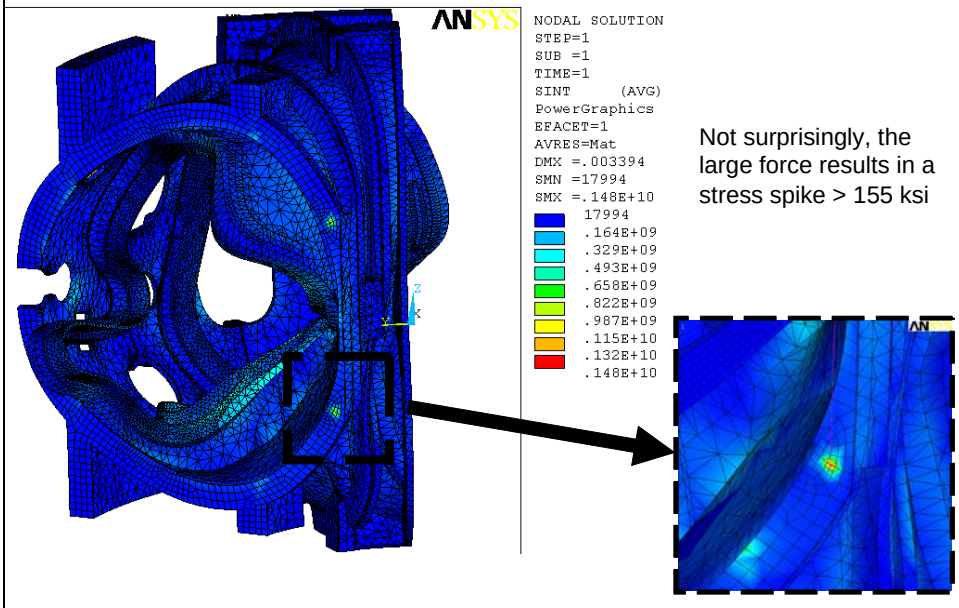

Not surprisingly, the large force results in a stress spike > 155 ksi

Element Stress Intensity on Flange C-C (Average)

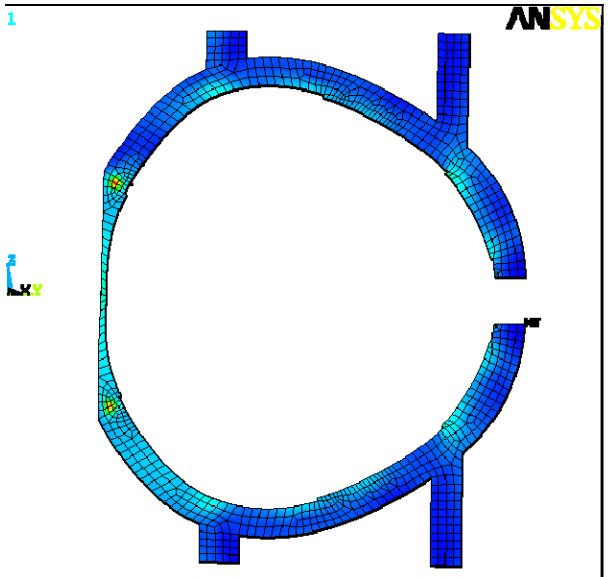

When looking at the element stress, the max value drops to around 32 ksi (clearly centered around the constrained nodes)

Global Deflection of Flange C-C

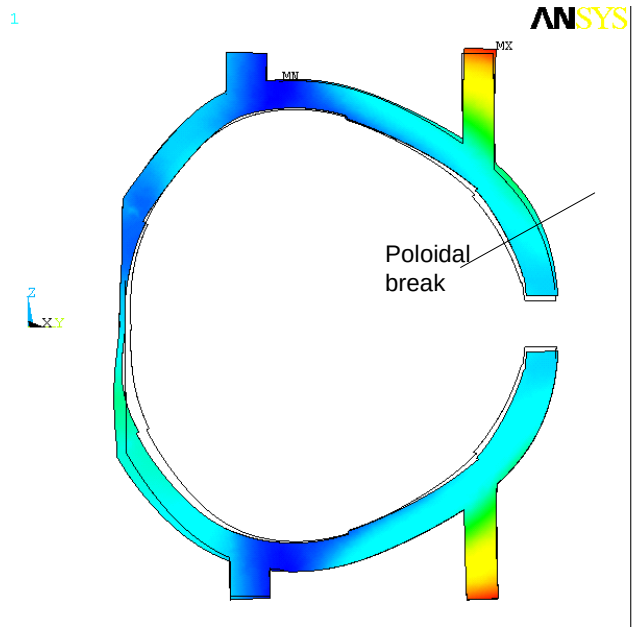

Element Stress Intensity on Flange A-A Average)

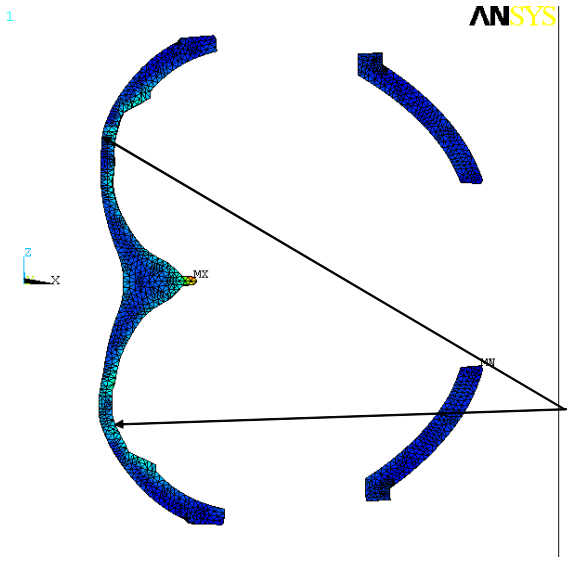

The nodal loads are not as obvious on this flange

max stress is dominated by the midsection protrusion.

Appendix C Stresses Near Area of Clamp 63 on C Coil (DEMO of stress plots at every clamp.)

Location of Clamp

Clamp 63

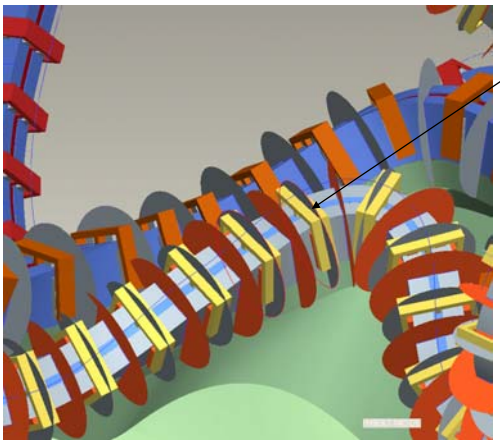

PROE

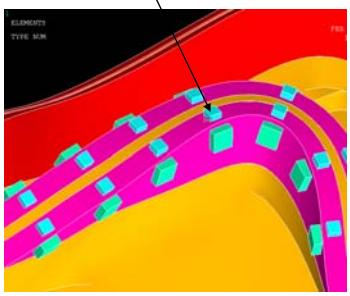

ANSYS

X (Normal) Stress (Pa), though Clamp 63

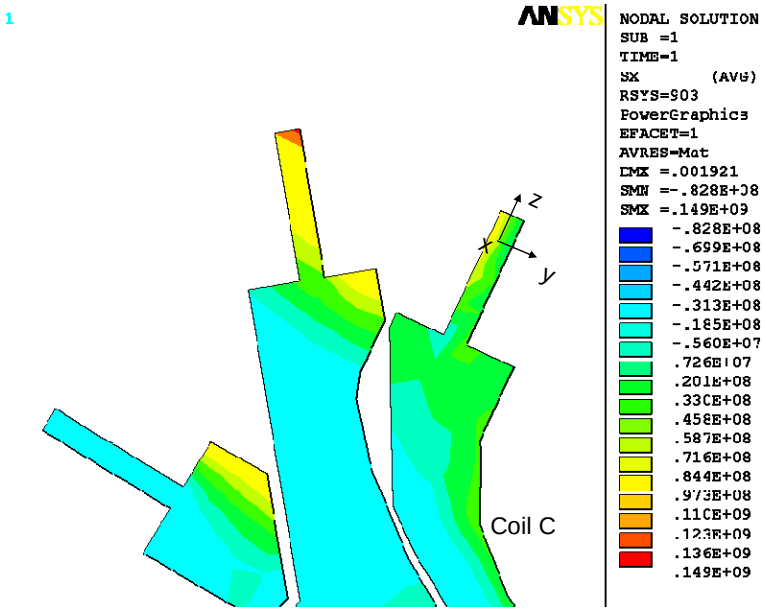

Y Stress (Pa), though Clamp 63

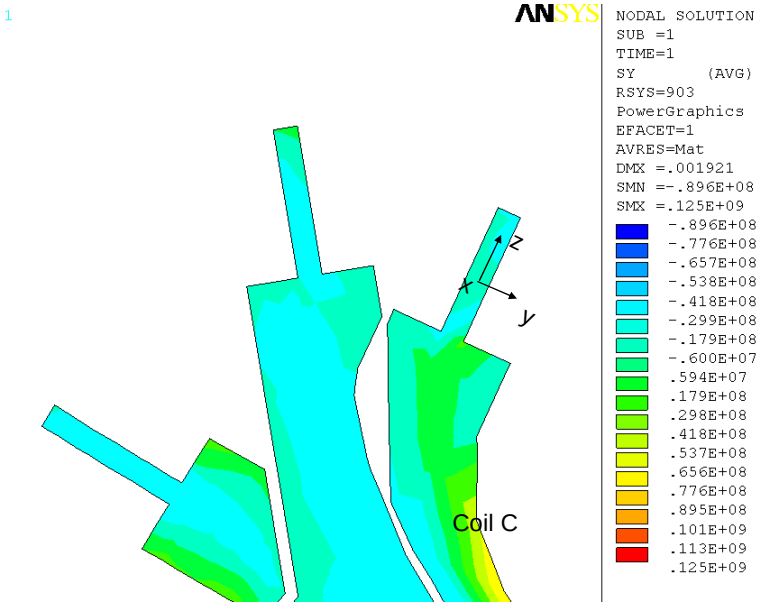

Z Stress (Pa), though Clamp 63

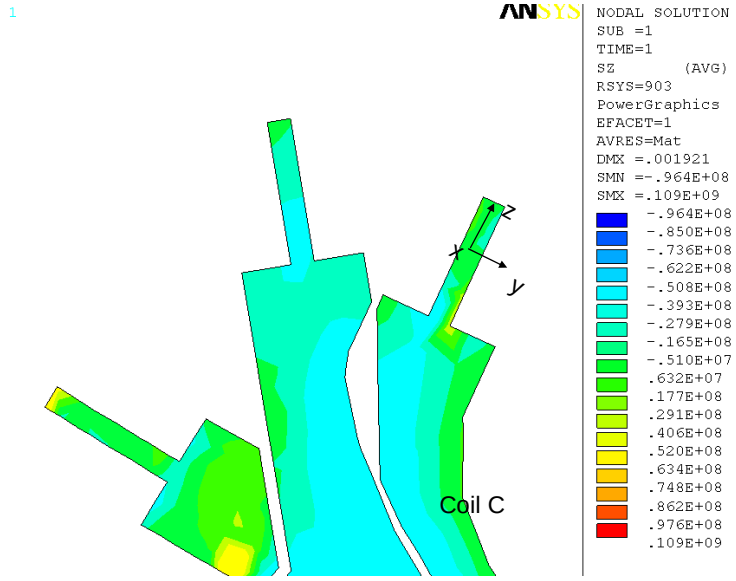

Shear Stress Clamp 63

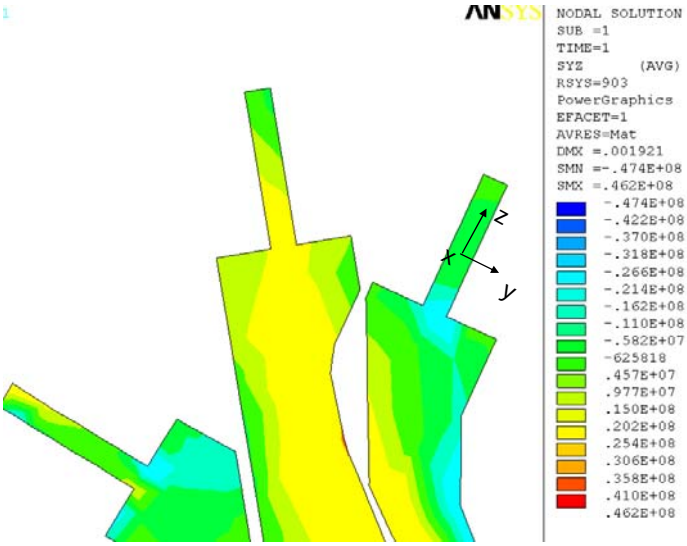

NCSX MODULAR COILS

Failure Mode and Effect Analysis (FMEA)

NCSX-FMEA-140-01

Prepared by: _____
D. Williamson, NCSX WBS 14 Manager

Concur: _____
B. Nelson, Project Engineer for Stellarator Core Systems (WBS 1)

Concur: _____
R. Simmons, Systems Engineering Support Manager

Approved by: _____
W. Reiersen, NCSX Engineering Manager

Table of Contents

1 Introduction and Scope

The National Compact Stellarator Experiment (NCSX) is an experimental research facility that is to be constructed at the Department of Energy's Princeton Plasma Physics Laboratory (PPPL). Its mission is to acquire the physics knowledge needed to evaluate compact stellarators as a fusion concept, and to advance the understanding of three-dimensional plasma physics for fusion and basic science.

A primary component of the facility is the stellarator core, an assembly of four magnet systems that surround a highly shaped plasma and vacuum chamber. The coils provide the magnetic field required for plasma shaping and position control, inductive current drive, and error field correction.

This document, the Modular Coil (MC) Failure Mode and Effect Analysis (FMEA), is used to identify possible failure modes, their causes, and the effects of these failures on coil performance. It is hoped that the process of identifying potential failures will lead to design solutions that increase the overall reliability and safety of the modular coil system.

2 Applicable Documents

PPPL Procedure ENG-008, "Failure Modes and Effects Analysis"

3 System Description and Functions

The modular coil set consists of three field periods with 6 coils per period, for a total of 18 coils. Due to symmetry, only three different coil shapes are needed to make up the complete assembly. The coils are connected electrically with three circuits in groups of six coils, according to type. Figure 1 show the general arrangement of the coils and structure.

The primary function of the modular coil system is to provide a quasi-axisymmetric magnetic field configuration with up to 2-T on axis for 1-s with a 15-min repetition rate. Additional functions may be categorized according to coil subsystem:

Winding Forms –

- Provide an accurate means of positioning the conductor during the winding and vacuum-pressure impregnation (VPI) process.

- Support the windings during operation with symmetric and minimal deflection.
- Provide segmentation for assembly purposes and to prevent circulation of eddy currents.
- Support the vacuum vessel and internals.

Coil Winding Assembly –

- Provide up to 2-T magnetic field configuration for reference scenarios.
- Maintain current center within 1.5-mm (0.060-in) of theoretical position during operation.
- Incorporate independent control of each coil type for flexibility.
- Provide capability to monitor field, current, voltage, and temperature.
- Cool the windings back to operating temperature (80K) between pulses

Bag Mold and Structural Clamps –

- Provide a mold structure that supports VPI process requirements
- Provide clamping system that is generic in design, but capable of adapting to coil curvature
- Provide clamping force sufficient to pre-load windings against the winding form.

The level of resolution of this FMEA is indicated in Figure 2, a block diagram of the modular coil system.

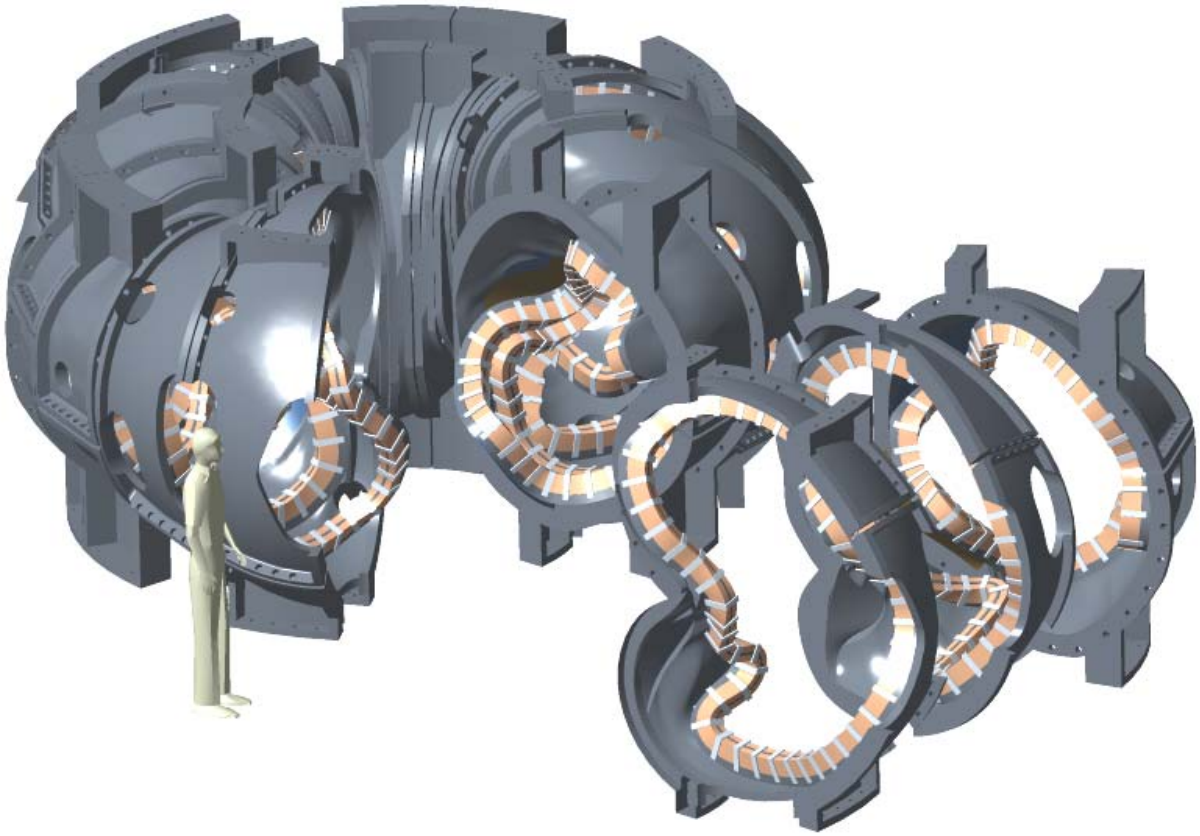

Figure 1 - Modular Coil General Arrangement

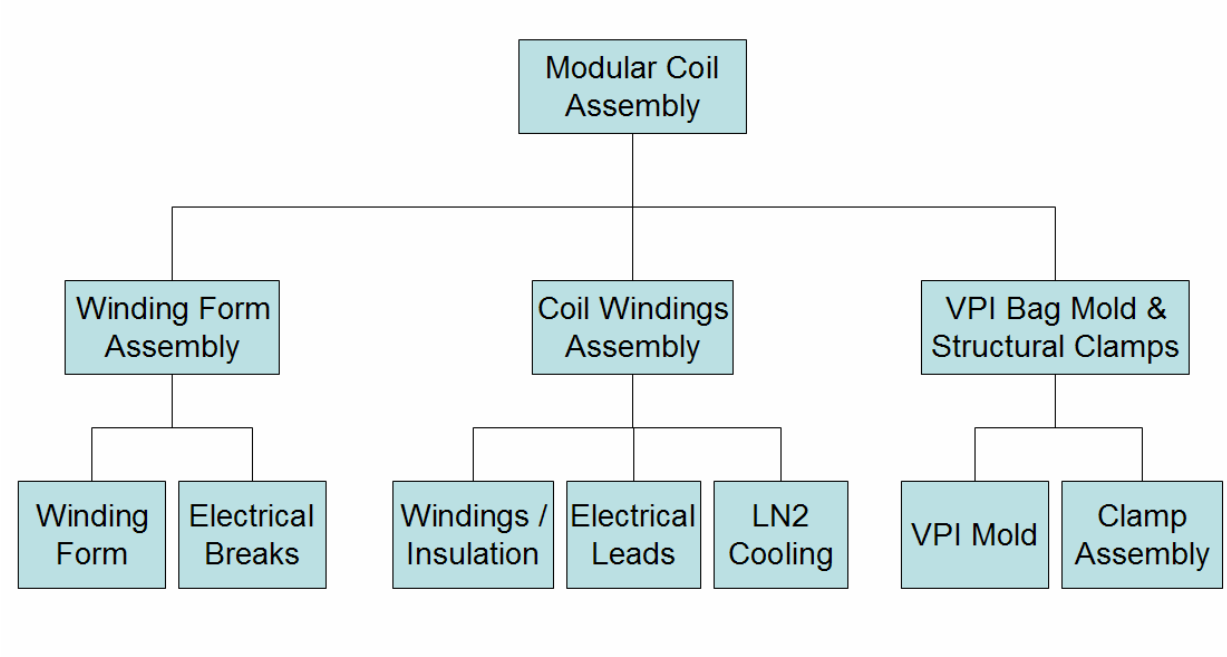

Figure 2 - Modular Coil System Block Diagram

4 FMEA Worksheets

Project: NCSX FAILURE MODE AND EFFECT ANALYSIS Page: 1 of

WBS Element: 14 Modular Coils Performed By: D. Williamson Date: 4/28/04

Component: Winding Forms Reviewed By: Date:

Function:

- Provide an accurate means of positioning the conductor during the winding and vacuum-pressure impregnation (VPI) process.
- Support the windings during operation with symmetric and minimal deflection.
- Provide segmentation for assembly purposes and to prevent circulation of eddy currents.
- Support the vacuum vessel and internals.

Operating Mode	Failure Mode /Cause	System Effect	Fault Detection /Isolation	Compensating Provisions	Remarks
Fabrication	Components do not meet specification for casting / machining.	Limited coil performance, field errors, etc.	QA provisions of specification, vendor surveillance.	Re-work components if necessary.	
Field period assembly	Incorrect alignment of coils to each other.	Magnetic field errors, loss of field symmetry.	Independent metrology assessment during all phases of assembly.	Re-assemble.	
Field period assembly	Coils do not fit over vacuum vessel.	Delay in schedule, increased costs.	Simulate assembly using metrology of as-fabricated components.	Modify components during construction or prior to field period assembly.	
Cool-down	Structure does not behave as expected structurally.	Magnetic field errors, loss of field symmetry.	Manufacturing and assembly QA.		
Operation	Structure does not behave as expected electrically.	Induced currents, field errors.	None.	None.	
Operation	Structure experiences excessive or non-symmetric deformation.	Magnetic field errors, loss of field symmetry.	None.	None.	

Project: NCSX

FAILURE MODE AND EFFECT ANALYSIS

WBS Element: 14 Modular Coils

Performed By: D. Williamson

Date: 4/28/04

Component: Coil Windings Assembly

Reviewed By:

Date:

Function:

- Provide up to 2-T magnetic field configuration for reference scenarios.
- Maintain current center within 1.5-mm (0.060-in) of theoretical position during operation.
- Incorporate independent control of each coil type for flexibility.
- Provide capability to monitor field, current, voltage, and temperature.
- Cool the windings back to operating temperature (80K) between pulses

Operating Mode	**Failure Mode /Cause**	**System Effect**	**Fault Detection /Isolation**	**Compensating Provisions**	**Remarks**
Fabrication	Windings have incorrect geometry due to fabrication errors, tolerance build-up.	Magnetic field errors, loss of field symmetry.	In-process measurement of winding pack to identify deviation.	Adjust thickness and placement of winding pack shims.	
Operation	Failure of turn-to-turn insulation.	Possible motion of conductors under load, abrasion, electrical failure.	Magnetic diagnostics, electrical impedance.	Shutdown, repair if accessible.	
Operation	Local failure of ground insulation.	Leakage current to ground, electrical failure.	Power supply system ground fault detector.	Shutdown, repair if accessible.	
Operation	Excessive motion of electrical leads under load.	Abrasion, shorts, electrical failure.	Power supply response, visual inspection.	Shutdown and repair.	
Operation	Local heating due to failure of vessel insulation during bakeout.	Possible damage to coil insulation.	None.	Shutdown, repair if accessible.	
Operation	Local heating due to contact resistance between chill plate and winding pack.	Change in coil resistance, possible damage to coil insulation.	None.	Shutdown, repair if accessible.	
Operation	Local heating due to blockage of cooling circuit.	Change in coil resistance, possible damage to coil insulation.	Flow switches.	Shutdown, repair if accessible.	

Project: NCSX

FAILURE MODES AND EFFECTS ANALYSIS

WBS Element: 14 Modular Coils

Performed By: D. Williamson

Date: 4/28/04

Component: Bag Mold and Structural Clamps

Reviewed By:

Date:

Function:

- Provide a mold structure that supports VPI process requirements
- Provide clamping system that is generic in design, but capable of adapting to coil curvature
- Provide clamping force sufficient to pre-load windings against the winding form.

Operating Mode	**Failure Mode /Cause**	**System Effect**	**Fault Detection /Isolation**	**Compensating Provisions**	**Remarks**
Fabrication	Voids due to failure of bag mold / VPI process.	Coil electrical, thermal, structural performance is limited.	None.	Remove windings and re-install.	
Fabrication	Improper installation of structural clamps.	Excessive coil deflection under load, field errors.	Magnetic diagnostics.	Shutdown, repair if accessible.	
Operation	Loss of clamp pre-load.	Excessive coil deflection under load, field errors.	Magnetic diagnostics.	Shutdown, repair if accessible.	
Operation	Relative motion between clamps and windings.	Possible wear, failure of coil insulation.	None.	None.	

5 Risk Mitigation

The analysis indicates that the most serious potential failures involve misalignment and/or excessive motion of winding pack during operation. This is being addressed in the design phase through design, analysis, R&D, and fabrication and assembly planning:

Design: The coils are designed around a cast and machined winding form that is very accurate, with the winding surfaces and mounting features integrated into a single unit. The coils are wound directly onto this form and vacuum pressure impregnated with epoxy. The casting is massive (just like the frame of a high precision machine tool) and deflections due to the winding and assembly process should be negligible. Since the windings are not removed from the winding form, the distortions that would normally occur during this operation are avoided.

Analysis: Nonlinear structural analysis has been performed to determine the behavior of the winding and clamps during cool-down and operation. Using conservative material properties assumptions, coil deflection due to thermal and electromagnetic loads has been determined and found not to have a significant impact on the magnetic field configuration. The analysis will continue to be refined as material tests and prototype fabrication and testing is completed.

R&D: Significant R&D is being performed in order to determine the material properties of the composite winding pack. This includes the tensile, compressive, and flexural modulus at operating temperature, orthotropic effects, and the fatigue characteristics of the material.

Fabrication and Assembly: The coil forms are wound at PPPL with total control over all processes by NCSX personnel. The use of a laser tracker or multi-link coordinate measuring system will allow the conductor placement to be continuously measured and corrections made throughout the winding process. Once the coils are completed, additional measurements of the as-built geometry can be entered into codes and the relative placement of each coil can be optimized, if necessary, for best control of error fields. Continuous measurements will be made during the assembly process to ensure that the coils are aligned correctly. Each coil will be located to a global reference frame that is continuously updated for the best fit to the coil array.

6 Recommendations

TBD, or omit.